1998

The migration of fines from contaminated sediment through geosynthetic fabric containers ulitized in dredging operations

Charles E. Ochola
Lehigh University

Ochola, Charles E.

The Migration of Fines From Contaminated Sediment Through Geosynthetic Fabric...

May 13, 1998

THE MIGRATION OF FINES FROM CONTAMINATED SEDIMENT THROUGH GEOSYNTHETIC FABRIC CONTAINERS UTILIZED IN DREDGING OPERATIONS

By

Charles. E. Ochola

A Thesis

Presented to the Graduate and Research Committee

Of Lehigh University

In Candidacy for the Degree of

Master of Science

In

Civil and Environmental Engineering

Lehigh University

5-4-1998

This thesis is accepted and approved in partial fulfillment of the requirements for the Master of Science.

5-4-98
Date

Horace Moo-Young
Thesis Advisor

Horace Moo-Young
Research Advisor

Le Wu-Lu
Chairperson of Department

ACKNOWLEDGEMENTS

First and foremost, I would like to express my sincerest thanks to my advisor Dr Horace Moo-Young for his unwavering support and guidance especially during those frustrating times when nothing seemed to be working as expected. I would also like to thank Tommy Myers and Dan Townsend of Waterways Experiments Station for all their help in the analysis and interpretation of the data. I also extend my thanks to all my fellow graduate students Marc Gallagher, Antoinette Weeks, Yue Xu and anyone else I may have left out for all their help. Special thanks go out to Dr Henry Odi for all his support throughout my stay at Lehigh. I am also indebted to Christine Martey for her support, encouragement, and proofreading of my thesis. Finally, I would like to thank the following organizations for supporting this research: Army Research Office, Battelle, and Waterways Experiments Station. I would also like to thank T.C. Mirafi for providing the samples utilized in our tests, and Brian Tomlinson of BT Technology for his contribution to the project.

Charles. E. Ochola

To Mom, Dad, Isaac, Donald,

Edward, Ruth, and Peter.

TABLE OF CONTENTS

LIST OF SYMBOLS

A	=	GT1000 Woven geotextile (Strength layer)
B	=	S400 Non-woven needle punched geotextile (filter layer)
C	=	S800 Non-woven needle punched geotextile (filter layer)
D	=	S1200 Non-woven needle punched geotextile (filter layer)
E	=	S1600 Non-woven needle punched geotextile (filter layer)
C_t	=	Total contaminant Concentration (M/L^3)
${}^{o}C_t$	=	Observed total contaminant concentration (M/L^3)
${}^{e}C_p$	=	Estimated particulate-bound contaminant concentration (M/L^3)
C_d	=	Dissolved contaminant concentration (M/L^3)
q	=	sediment contaminant concentration (M/M)
CH	=	Sandy Clay
d_{85}	=	Diameter through which 85% will pass (L)
MDL	=	Minimum detection limit for instrument

LIST OF TABLES

LIST OF FIGURES

Abstract

Environmental regulations to protect ocean water have prohibited the practice of disposing dredged sediment into open waters. Because of these restrictions on dredging and disposal of contaminated dredged materials, alternative methods of dredging and disposal of the sediments are needed. Containing the contaminated sediment in a Geosynthetic Fabric Container (GFCs) for placement from split hull barges is one alternative that can reduce the movement of contaminated sediments outside of the boundary of the disposal site and decrease the impact on the water column. This research looked at the contaminant migration through these GFCs, and how this migration was affected by changes in the container. A combination of various fabrics used in the manufacturing of the GFCs were tested in conjunction with contaminated sediment from the New York harbor. To determine the contaminant migration through the GFC, the following tests were conducted:

1. Material characterization of geotextiles and dredged sediment
2. Pressure filtration tests
3. Hanging bag tests
4. Barge simulation tests
5. Fabric stress analysis tests
6. Filtration test with varying strain

Test results and subsequent analysis from this study show that GFCs are a viable alternative to the open water disposal of these contaminated sediments, since it reduces the migration of contaminants and fines into the water column.

Chapter 1

Introduction

1.1 Background

New York Harbor is a major industrial port on the East Coast of U.S. where 4,500 ships carry $60 billion year worth of goods and generates tens of thousands of jobs. River borne silts sift into the harbor's shipping channels and reduce the depth of the harbor. New York and New Jersey Port Authority must be continuously dredged to maintain channel depths for cargo ships and tankers. From 1990-1994, the average amount of dredged material was approximately 4.3 million cubic yards. Dredged material is disposed in the Atlantic Ocean a few miles east of the Jersey Shore at the New York Bight Dredged Material Disposal Site. Recent changes in environmental regulations have restricted open water disposal of the New York Harbor dredged material due to contamination. These restrictions on dredging have decreased the average amount of sediment by 70% to 1.3 million cubic yards for 1996. As a result, New York Harbor will lose about a foot of depth each year if contaminated sediments are not dredged. Decreases in the harbor depth will have a severe impact, as larger cargo ships will dock at deeper ports.

Capping, the placement of a barrier layer over dredged material, is one possible option that can be applied to contaminated dredged material problem. The major drawbacks to capping are as follows: cost of placing the material, location of sufficient volumes of capping material, impact of the dredging material on the water column, and the spread of the contaminated dredged material beyond the boundary of the disposal site.

Because of the restrictions on dredging and disposal of contaminated dredged materials, limited upland disposal sites, and perceived political problems, alternative methods of dredging and disposal of the sediments are being evaluated by the New York and New Jersey Port Authority and the Corp of Engineers. Containing the contaminated sediment in a Geosynthetic Fabric Container (GFCs) for placement in split hull barges is one alternative that can reduce the movement of contaminated sediments outside the boundary of the disposal site and decrease the impact on the water column. GFCs are constructed from synthetic fibers that are made into a flexible porous fabric by weaving, knitting, or matting, and act to filter the dredged sediment. During the dredging operation, the barge is lined with the appropriate GFC (see Figure 1.1). The dredged sediment is mechanically or hydraulically placed into the barge. After placement of the sediment, the opening of the GFC is closed and the GFC is released from the barge after transport to an aquatic disposal site as shown in Figure 1.2.

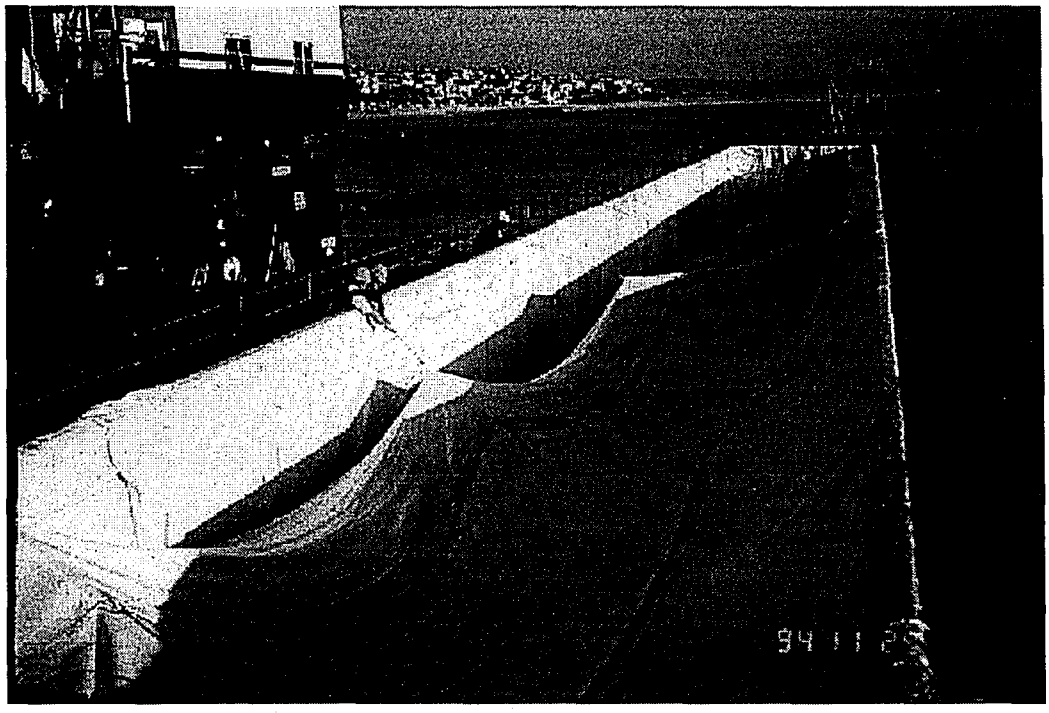

Figure 1.1 Barge Lined with Geosynthetic Fabric Container (GFC).

Figure 1.1 Barge Lined with Geosynthetic Fabric Container (GFC).

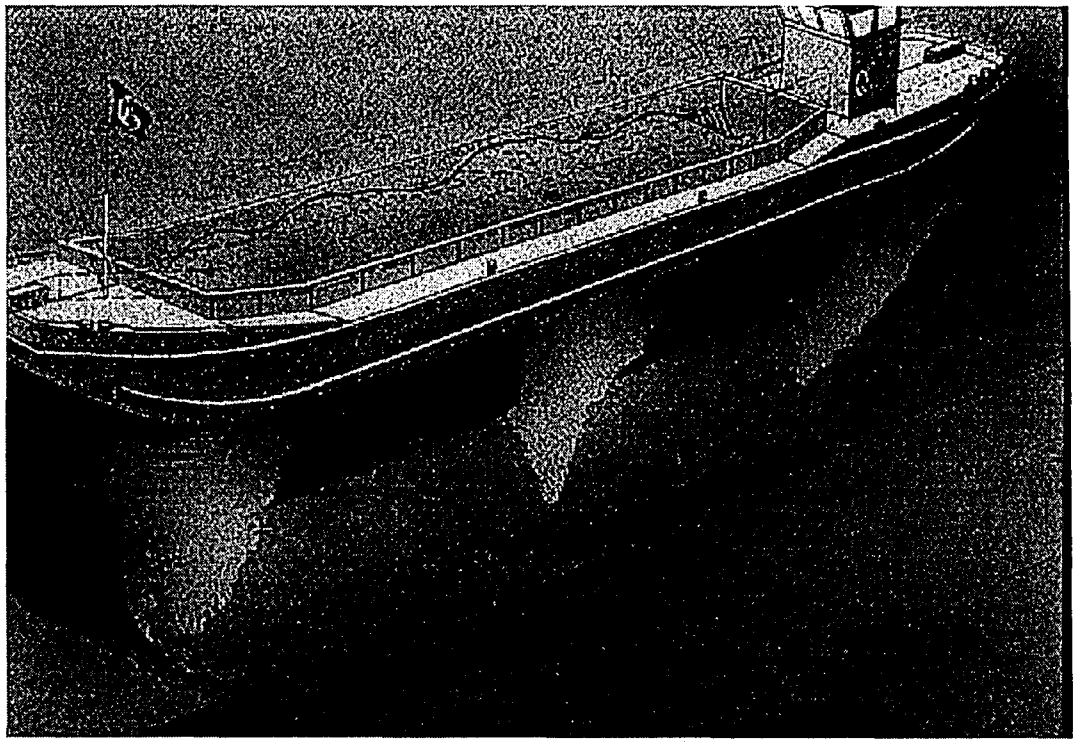

Figure 1.2 GFC Being Deployed From Barge at Aquatic Disposal Site.

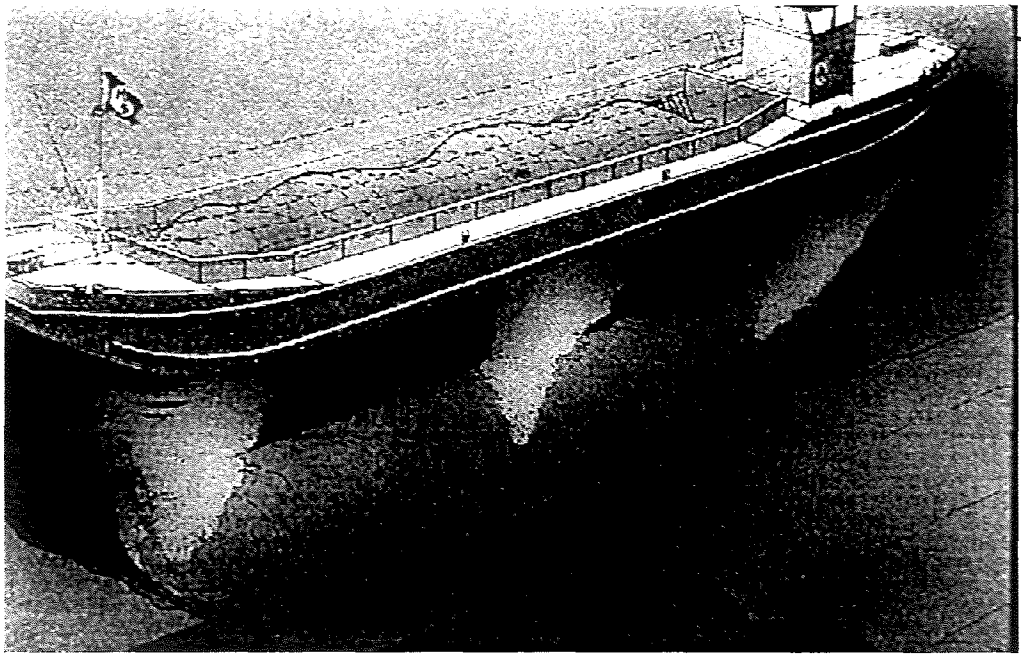

Figure 1.2 GFC Being Deployed From Barge at Aquatic Disposal Site.

1.2 Previous Application of Geosynthetics to Dredging

Applications of geosynthetics in civil engineering construction have grown rapidly over the past two decades (Koerner, 1998). Geosynthetics, synthetic materials (usually made from hydrocarbons) used in geotechnical engineering and heavy construction, have four general classification areas: geotextiles, geogrids, geomembranes, and geocomposites. Geotextiles are synthetic fibers that are woven, knitted, or pressed into a permeable fabric and that perform at least one of five functions: separation, reinforcement, filtration, drainage, or as a moisture barrier. Geogrids are plastics that are formed into open net configurations and primarily function to reinforce and separate. Geomembranes are impervious thin sheets of plastic or rubber used primarily for solid and liquid storage. Geocomposites consist of a combination of geotextiles, geogrids, or geomembranes. Geocomposites can function in separation, reinforcement, filtration, drainage, and as moisture barriers.

In confined disposal facilities (CDFs), geosynthetics are sometimes used for the stabilization of dikes. Dredged material filled tubes have been used as containment dikes in Brazil and France (Bogossian et al 1982, Perrier 1986). In the Netherlands geotextile containers were utilized to fill scour holes (Jagt, 1988). Sand filled geosynthetic fabric containers (GFCs) comprise a newly emerging technology for construction of submerged structures such as stability berms, groins, and sill structures. GFCs are geocomposites that are formed by sewing together long sheets of geosynthetic fabrics. For dredged

material, GFCs consist of an inner non-woven geotextile to reduce the migration of clay and silt sized and of an outer woven polypropylene or polyester geotextile for strength particles to increase the resistance to rupture. When properly constructed, GFCs have performed well as hydraulic and geotechnical structures. Numerous projects have shown the beneficial uses of GFCs for dikes in shallow and deep-water energy (Fowler and Sprague, 1993; Pilarczyk, 1994; Landin et al., 1994; Garbarino et al., 1994; Fowler et al., 1995). At Red Eye Crossing on the Mississippi River near Baton Rouge, Louisiana, for example, GFCs were filled with clean sand to create a small dike to improve navigation along the river (Duarte et al., 1995).

Aquatic disposal of contaminated dredged material presents a new application for GFCs. GFCs can reduce the water column impact, bottom foot print, and resuspension of sediment after aquatic disposal of dredged material. GFCs reduce the dispersion of dredged material to the water column, since the fabric filters the solids from the water. Reduction in the spread of material at the bottom occurs, since the spread of the sediment is limited to the shape of the bag. In the Port of Los Angeles, GFCs were used to contain contaminated dredged sediment from Marina Del Ray in Venice, California (Fowler et al., 1995; Mesa, 1995; Risko, 1995).

1.3 Objectives

The objectives of the study were to provide information on the GFC performance with respect to the migration of contaminants and fines. To meet these objectives, the following tasks were conducted:

- Physical and chemical characterization of New York Harbor sediments.
- Bench top filtration test to provide information on the release of fines from GFCs
- Laboratory determinations of the flow rate of suspended solids from a GFC system following the proposed ASTM procedure (D18.13.05) (i.e. Hanging bag test).
- . Laboratory barge simulation tests to estimate the release of particulate bound and dissolved contaminants as a result of dredged material reworking (i.e., cake deformation during GFC deployment).
- Fabric analysis Stress tests to determine the variation in the apparent opening size (AOS) with strain.
- Filtration tests with varying strain to investigate the release of fines with variations in geotextile strain.

Chapter 2

Materials

2.1 Geosynthetics

A geosynthetic fabric container (GFC) is constructed by sewing one or more layers of geotextiles together to form a container that will support and contain a measured amount of saturated material. Filtration properties of geotextiles are a function of their retention, permeability, and ability not to clog.

Woven geotextiles are fibers or yarns of a polymer oriented in perpendicular directions, while non-woven geotextiles consist of randomly oriented and distributed discrete fibers. Figure 3 illustrates SEM micrographs for various woven and non-woven fabrics. There are variations in the physical properties of the geotextiles shown in Figure 3, and this is attributed to the differences in the manufacturing processes. The processes and types of material used to construct the geotextiles are what differentiate them from each other.

Geotextiles are manufactured from polymers such as polypropylene (PP), polyester (PET), polyamide (nylon), and polyethylene (PE). These polymers are utilized in the manufacturing process of geotextile fibers of which there are four main types:

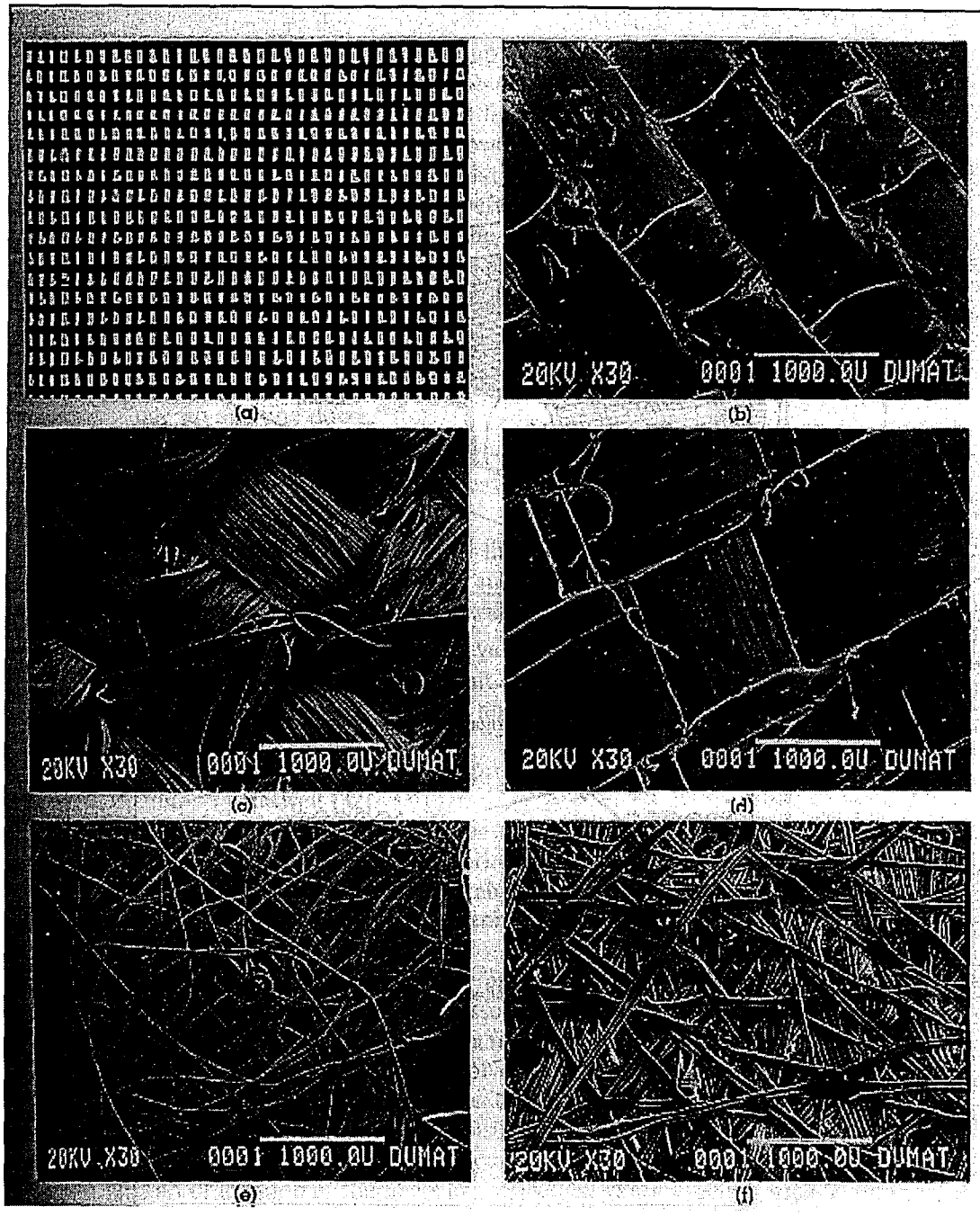

Figure 2.1 Micrograph of geotextiles: (a) woven monofilament; (b) woven monofilament calendered; (c) woven multifilament; (d) woven slit (split) film; (e) nonwoven needle punched; (f) nonwoven heat bonded.

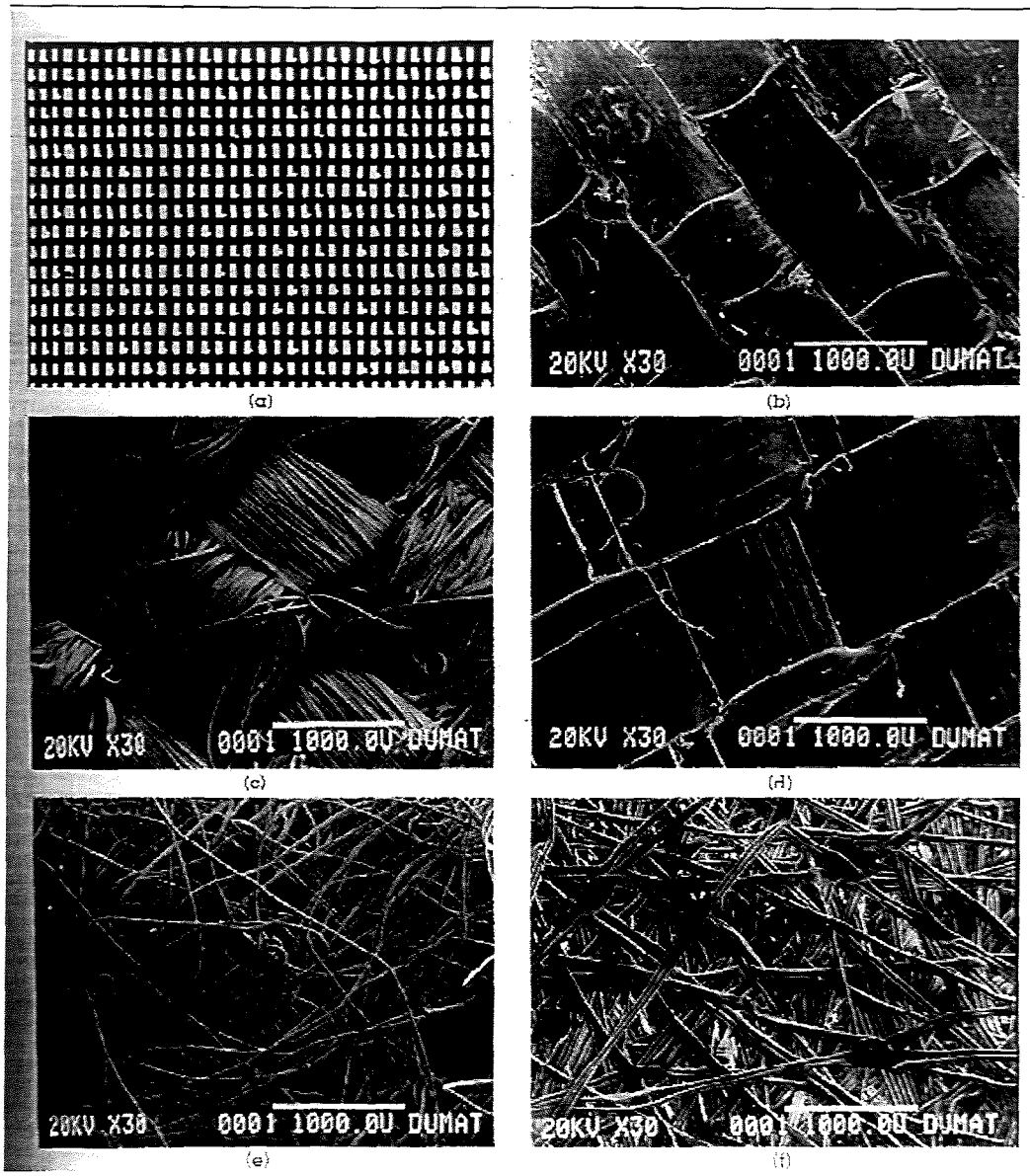

Figure 2.1 Micrograph of geotextiles: (a) woven monofilament; (b) woven monofilament calendered; (c) woven multifilament; (d) woven slit (split) film; (e) nonwoven needle punched; (f) nonwoven heat bonded.

monofilament, multifilament, slit film, and filbrated fibers. These four fibers are the primary fibers used in the manufacture of woven geotextiles, and pore size distribution is influenced by the diameter of the fibers, the spacing between them, and the type of weave used. Fibers used in the manufacturing of non-woven geotextiles include continuous filament, and staple fibers. The major difference between these two types of fibers is their length, and as the name implies continuous fibers are long while staple fibers are very short.

Woven geotextiles are manufactured on looms. The thread which runs along the length of the loom are known as warp threads, while the threads which intercept these warp threads at right angles are known as weft threads. Plain and twill weaves are utilized to manufacture woven geotextiles. In the plain weave the warp and weft threads are alternated throughout the geotextile and may be packed loosely or tightly. Due to these intersections, the parallel threads are placed further apart resulting in a loose structure and consequently larger pore sizes. The twill weave has fewer intersections than the plain weave resulting in a much tighter weave. The drawback to this type of weave is a tendency for the threads to twist and increase the pore spaces. Pore size in woven geotextiles is a function of the number of warp and weft threads, the weight of the fibers, and the type of weave. (Koerner, 1998)

Non-woven geotextiles are made from a spunbounding process that consists of four steps; fiber preparation, web formation, web bonding, and winding into rolls. This loose web is

then bonded by one of three techniques; mechanical bonding, thermal bonding, or chemical bonding. In mechanical bonding, a needle punch is utilized to mechanically entangle the fibers together. This process causes the geotextiles to have an uneven surface, and the opening size will vary depending on which surface is tested. Some manufacturers needle punch both sides of the textile while others do not. This difference also causes variations in the pore size. Thermal bonding utilizes heat in the form of either pressurized steam or hot air to fuse the fibers at cross over points. The parameters that affect pore size distribution for this type of process are the degree of fusion, line speed, engraved pattern, fiber type, and fiber density. (Koerner, 1988) The third method is by chemical bonding where a chemical binder is applied on the web before it is placed in an oven or subjected to a hot roller for curing of the binder. Another chemical bonding process utilizes hydrogen chloride gas to break the hydrogen bonds between polymer chains and, upon reversal by desorption, form new hydrogen bonds between polymer chains in different fibers.(Koerner, 1988)

The Nicolon Corporation in Norcross, Georgia manufactured the GFCs used in the New York Harbor demonstration project and provided the geosynthetic fabrics for fine migration analysis. Geotextile A ,was used as the strength layer in the GFC. Four polypropylene non-woven needle punched geotextiles were tested as potential filter layers for the GFC: Geotextile B, Geotextile C, Geotextile D, and Geotextile E. Physical properties of the geotextiles were determined according to American Society of Testing and Materials (ASTM) procedures and are shown in Table 1.

Table 2.1 Geotextile Properties

Fabric Properties	Test Method *	Units	Fabric				
			A	B	C	D	E
Weight	D-5261	g/m^2 (oz/yd^2)	NP	136 4.0	272 8.0	480 12	544 16
Thickness	D-5199	mm (mils)	NP	1.8 70	2.7 105	3.7 145	4.7 185
Grab Tensile Strength	D-4632 D-4595*	KN (lb)	6900 kPa* 1000 psi*	0.47 105	1.0 225	1.56 350	2.23 500
Grab Elongation	D4632 D-4595*	%	10*	50	50	50	60
Trapezoid Tear Strength	D-4533	kN (lb)	3.6 800	0.20 45	0.38 85	0.57 125	0.68 150
Puncture Resistance	D-4833	kN (lb)	1.8 400	0.29 65	0.58 130	0.87 190	1.07 240
Mullen Burst Strength	D-3786	kPa (psi)	NP	1585 230	3101 450	4479 650	5512 800
Water Flow Rate	D-4491	1/min/m2 (pm/ft2)	NP	6518 160	4072 100	2443 60	1832 45
Permeability	D-4491	cm/sec	NP	0.54	0.44	0.33	0.28
Permittivity	D-4491	sec-1	NP	2.0	1.26	0.75	0.571
U.V. Resistance	D-4355	%	NP	70	70	70	70
Apparent Opening Size	D-4751	mm (US Sieve)	0.250 60	0.212 70	0.212 70	0.15 100	0.15 100

Nicolon provided the values in this table.
NP – Not provided by manufacturer
* - Properties for the D-4595 test method

2.2 Contaminated Dredged Sediment

Contaminated sediment (Category III by U.S. Army Corps of Engineers, New York District (CENAN) classification) from New York Harbor was used in this study. The sediment was mixed in a 250-gallon (946.35-liter) tank for three hours. Samples of the mixed sediment were collected for geotechnical and chemical analysis.

Particle-size distributions were obtained using ASTM procedures E-11 for grain size analysis and D-422 for hydrometer analysis and are shown in Figure 2.2. According to ASTM designation D-2487, the sediment classifies as sandy clay (CH). Geotextiles in this study meet the recommended soil retention criteria, which requires the AOS to be less than two to three times the soil particle size for which 85% of the total soil is finer. (AOS <2 or 3 d_{85}) (See Table 1 for AOS# and d_{85} = 0.19 mm from Figure 2.2).

The initial water content (ASTM procedure D-2974) of the sediment was 207%, and the specific gravity (ASTM procedure D-854) of the sediment was 2.57. Consolidation tests were performed on sediment according to ASTM procedure D-2435 method A, and the void ratio and effective stress relationship is shown in Figure 2.3. Consolidation test results show that the sediment is highly compressible. Hydraulic conductivity tests were conducted on the dredged sediment in the consolidometer. Figure 2.4 plots the hydraulic conductivity and void ratio relationship for the sediment. As the void ratio decreases which corresponds to an increase in the applied stress, the hydraulic conductivity of the sediment decreases.

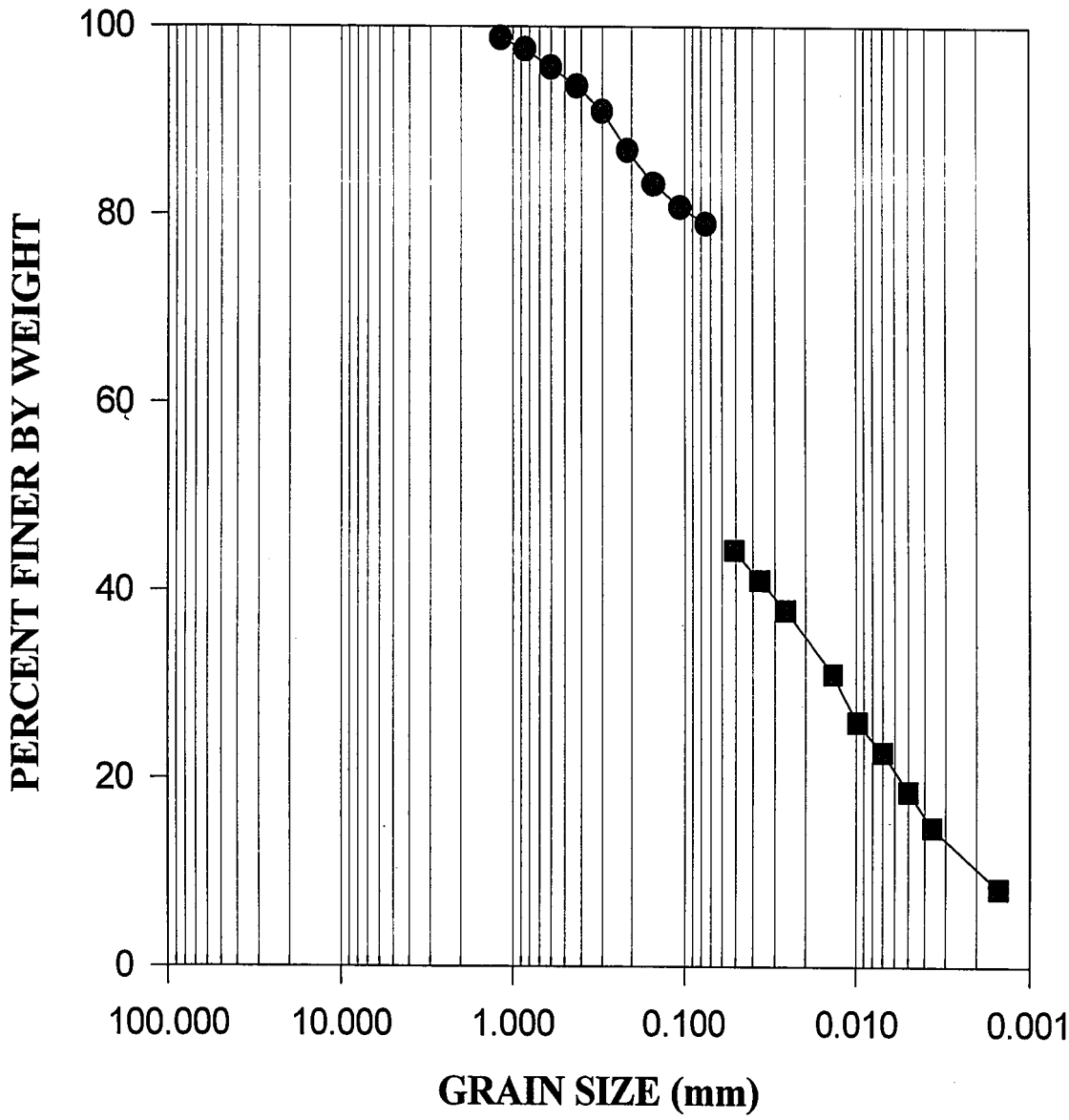

Figure 2.2 Particle Size Analysis of the Sediment

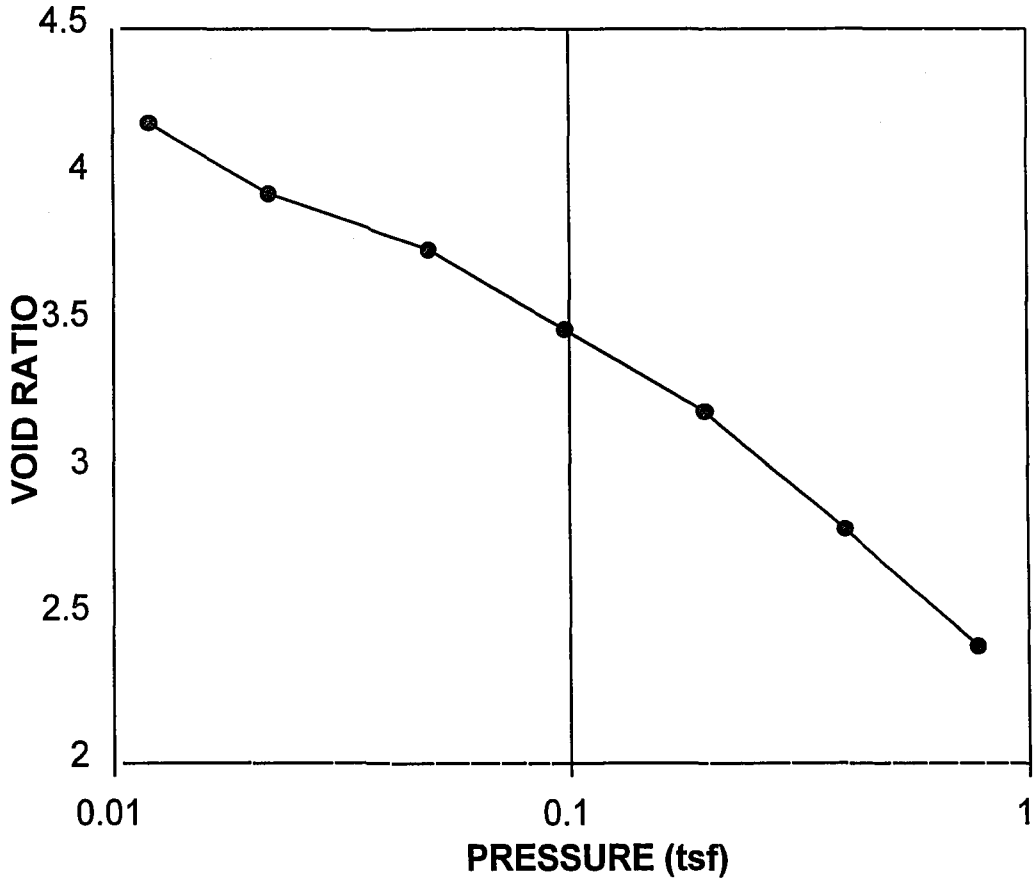

Figure 2.3 One-Dimensional Consolidation Curve

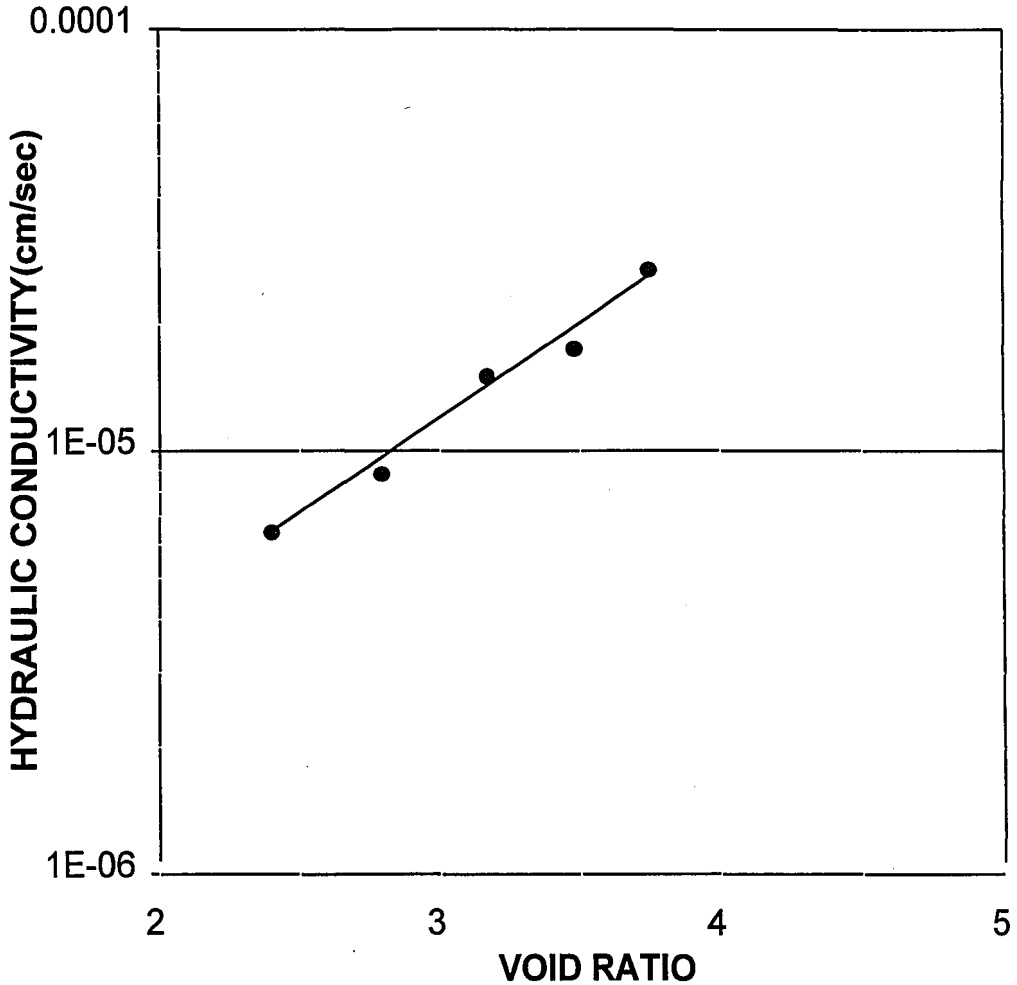

Figure 2.4 Hydraulic Conductivity and Void Ratio Relationship

Six samples of the contaminated dredged sediment were analyzed for polychlorinated biphenyls (PCBs), polychlorinated dibenzo-p-dioxins (Dioxins) and polychlorinated dibenzo-p-furans (Furans), polycyclic aromatic hydrocarbons (PAHs), NH_4, Total Organic Carbon, Arsenic, Cadmium, Chromium, Copper, Iron, Manganese, Lead, Mercury and Zinc. Table 2.2 summarizes the standard procedures, detection limits, and chemical analysis on the sediment. Appendix A provides the detailed analysis for the PAH, PCB, and Dioxin and Furan analysis of the sediment (Tables A.1-A.3).

Table 2.2 Chemical and Metal Analysis of Sediment

Chemical /Metal	Procedure	Detection Limits		Replicates in mg/kg						Avg.
		water mg/l	sediment mg/kg	1	2	3	4	5	6	
NH_3-N	EPA-600-350.1 EPA-CRL #324	0.01		177	185	232	143	117	129	164
TOC	SM-5310 EPA-CE-81-1	1.0	1.0	49,000	54,000	56,000	63000	133000	56000	68500
Chromium	SW-846-6020 SW-846-6010	0.0003	0.2	184	186	175	191	211	209	193
Copper	SW-846-6020 SW-846-6010	0.001	0.1	621	668	633	604	616	578	620
Iron	SW-846-6020 SW-846-6010	.005	2.0	36600	36200	33500	42700	427003	34300	36217
Manganese	SW-846-6020 SW-846-6010	0.00002	0.1	340	335	316	356	397	341	348
Mercury	SW-846-7470A SW-846-7471A	0.000004	0.04	2.01	1.95	2.20	3.41	2.34	2.37	2.38
Lead	SW-846-6020 SW-846-6010	0.00002	1.0	415	471	402	424	408	403	420.5
Arsenic	SW-846-7060A SW-846-6010	0.001	2.0	20.4	20.9	19.6	19.7	21.7	19.1	20.2
Cadmium	SW-846-6020 SW-846-6010	0.000008	0.1	12.1	13.1	12.1	14.7	14.9	14.7	13.6
Zinc	SW-846-6020 SW-846-6010	0.0006	1.0	925	958	910	977	973	940	947
Nickel	SW-846-6020 SW-846-6010	0.0001	2.0	104.4	105	102	112	112	118	108.9
Silver	SW-846-7761 SW-846-7761	0.00010	0.10	11.0	4.48	5.04	11.7	11.6	11.2	9.17
PAH	SW-846-8270B			95.52	86.2	92.32	94.54	83.35	87.05	89.08
PCB	SW-846-8081			8.65	7.72	10.32	9.42	9.56	12.95	9.77
Dioxins	EPA-8290 SOP-CS152			0.0206	0.0205	0.0186	0.0173	0.0187	0.0279	0.0261
Furans	EPA-8290 SOP-CS152			0.0150	0.0150	0.0129	0.0126	0.0147	0.0128	0.0138

Chapter 3

Pressure Filtration Test

3.1 Background

Bench top filtration tests were conducted to obtain information on the release of fines from geosynthetic fabrics of varying apparent opening sizes (AOS). The filtration procedure described in this method simulates the migration of fines through a GFC. Cake formation results from the application of an applied load. During a dredging operation, cake formation occurs after the GFC is filled with the sediment and is caused by self-weight consolidation. Cake formation also occurs after placement of the GFC in the disposal facility and is caused by consolidation under a hydrostatic pressure.

Pressure filtration is commonly used to dewater slurries and sludge. A vacuum is applied to a filter media to separate liquids from solids. The filtering capacity of the sludge solids and the porosity of the solid cake formed are directly related to the quantity of de-watered solids per unit time and the moisture in the cake. From Poiseuille's and Darcy's laws, the rate of filtration was derived (Eckenfelder, 1966):

$$\frac{dV}{dt} = \frac{PA^2}{\mu(rcV + R_m A)} \qquad (3.1)$$

Where V = Volume of filtration

t = Cycle time

P= Vacuum Pressure

A = Filtration Area

μ = Filtrate Viscosity

r = Specific Resistance

R_m = initial resistance of the filter media and is usually neglected since it is low compared to the resistance developed by the filter cake.

c = Weight of Solids per Unit Volume of Filtrate

$$= \frac{1}{c_i/(100-c_i) - c_f/(100-c_f)}$$

c_i and c_f = initial, and final weight of solids per unit volume of filtrate.

The specific resistance measures the filterability and is equivalent to the pressure difference required to produce a unit rate of filtrate flow through a unit weight of cake. Integration of equation (3.1) and rearrangement of the terms yield the following relationship:

$$r = \frac{2bPA^2}{\mu c} \qquad (3.2)$$

Where b is the slope of the plot of t/V versus V. Specific resistance measures the compressibility of the material. To minimize the effect of the initial resistance, the filtration pressure is raised gradually. When the specific resistance is equal to zero, the specific resistance is independent of pressure, and the material is incompressible.

3.2 Apparatus

A Millipore Hazardous Waste Filtration System (Millipore Corporation, Bedford Ma) was used to conduct the pressure filtration tests as shown in Figure 3.1. This pressure filtration device is used for the Toxicity Characteristic Leaching Procedure (TCLP) in hazardous waste testing (U.S. Environmental Protection Agency (EPA), 1982; Bricka et al., 1992). The filtration device is made of stainless steel and is coated with Teflon to eliminate heavy metal contamination. The filtration device is 184 mm in diameter and 422 mm in height, and has a filter area of 97 cm^2. The geosynthetic fabric was placed on a filter holder that was able to withstand pressures up to 100 psi (690 kPa). Five GFC configurations were tested: A, A+B, A+C, A+D, and A+E. Three filtration tests were conducted on each fabric configuration at applied pressures of 5 psi (34.5 kPa) and 10 psi (69 kPa). Thus a total of thirty tests were conducted.

Pressure was applied to the inlet of the filtration device using a compressed nitrogen cylinder. A relief valve on top of the chamber was used to adjust the pressure. A 250 ml graduated cylinder was used to measure the volume of filtrate as a function of time.

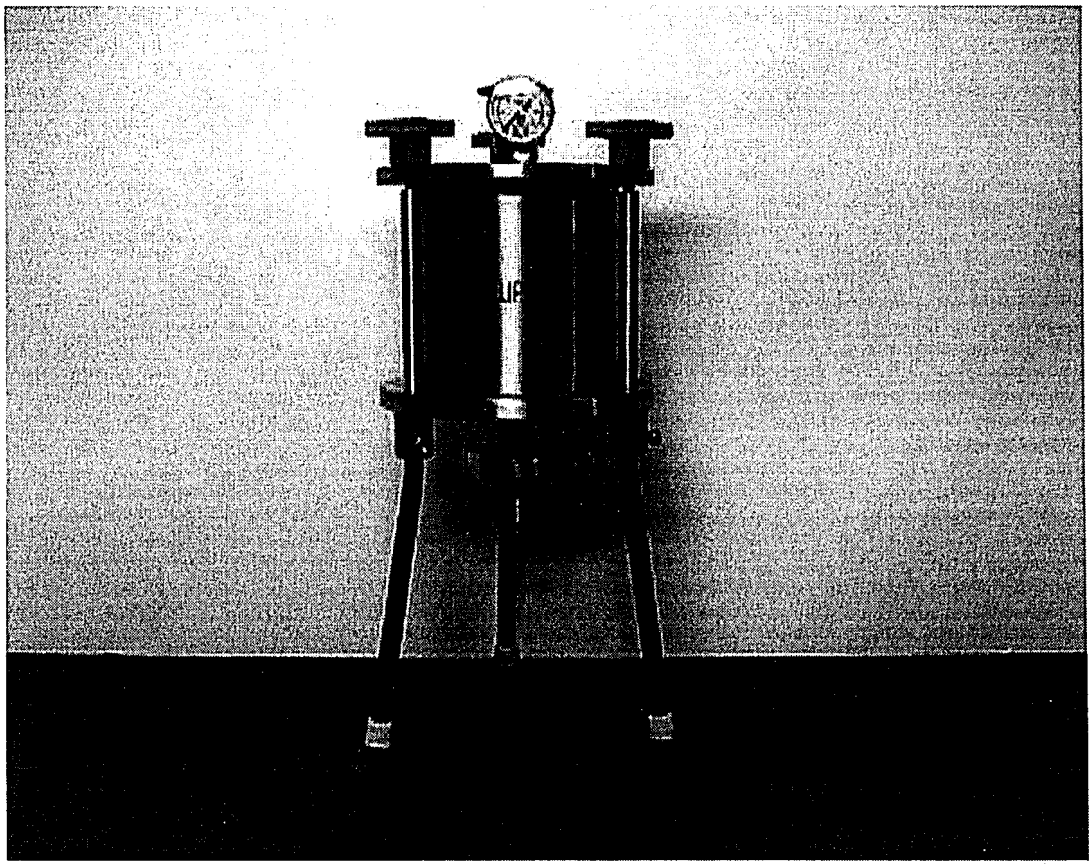

Figure 3.1 Pressure Filtration System

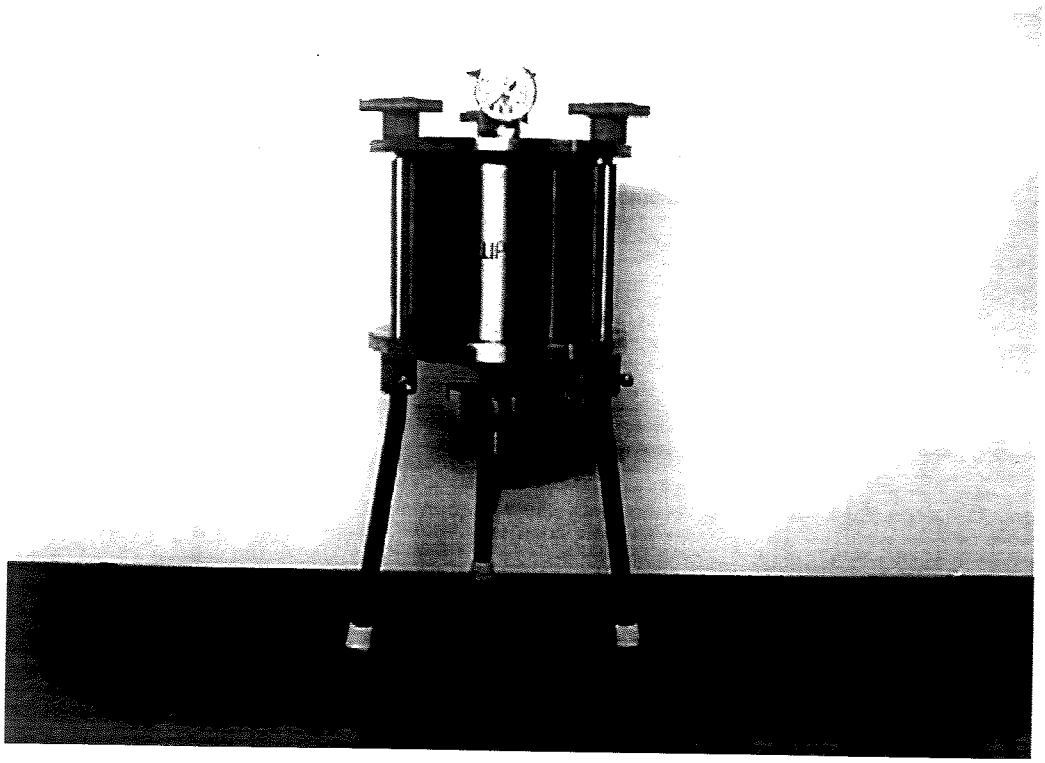

Figure 3.1 Pressure Filtration System

3.3 Procedure

1. The lower portion of the filtration apparatus was assembled. The geosynthetic fabric and the filtration chamber were weighed.
2. The geosynthetic fabric was soaked in simulated seawater manufactured by Instant Ocean (Aquarium Systems, Mentor, OH), allowed to drip dry, and placed on the filter holder. To reduce the potential for migration of fines at the edges, the filter fabric slightly overlapped the filter holder.
3. Approximately 500 grams of the sediment was weighed and placed into the filtration device. The slurry was allowed to settle before running the test.
4. The top plate was placed on top of the chamber and sealed. Silicone grease was used to reduce the loss of pressure between the chamber and the upper and lower plates.(Figure 3.1 Filtration System)
5. Pressure from the nitrogen cylinder was gradually applied on top of the sample, until the desired pressure was achieved.
6. The volume of the filtrate was measured using a 250-ml beaker and recorded with respect to time.
7. Tests were conducted until the pressure began to decrease, and no more filtrate passed through the filter. When consolidation of the sediment at the applied pressure was completed, the filter cake ruptured which caused a decrease in the applied pressure.
8. The filtration apparatus was disassembled, and the final water content of the filtered cake was obtained using ASTM procedure D-2216.

9. Total suspended solids (TSS) tests (Standard Methods for the Examination of Water and Wastewater method 2540D) were conducted on the collected filtrate.

3.4 Results

Thirty filtration tests were conducted on the contaminated sediment from the New York Harbor; three replications were conducted for the five fabric configurations at filtration pressures of 5 psi (34.5 kPa) and 10 psi (69 kPa). Tables 3.1 and 3.2 summarize the results for filtration tests conducted at 5 and 10 psi (34.5 and 69 kPa), respectively and show the initial and final water content, initial and final TSS, specific resistance, and filtering efficiency.

Initial and final TSS data in Tables 3.1 and 3.2 indicate that there was low migration of the fines through the various filter configurations. The filtering efficiency was determined by comparing the final TSS of the filtrate to the initial TSS of the contaminated sediment as shown in equation 3.

$$FE = \frac{TSS_{initial} - TSS_{final}}{TSS_{initial}} \times 100 \tag{3.3}$$

Where FE = Filtering Efficiency, %

$TSS_{initial}$ = initial TSS, mg/l

TSS_{final} = final TSS, mg/l

Table 3.1 Results from Filtration Tests at 5 psi (34.5 kPA)

Test	Initial Water Content (%)	Final Water Content (%)	Initial TSS (mg/l)	Filtrate TSS (mg/l)	Specific Resistance (sec^2/g)	Average Flow (ml/min)	TSS Filtering Efficiency (%)
A							
1	196.5	121.8	428122.9	81	9.17×10^9	0.78	99.98
2	199	125.4	423757.3	68.3	8.60×10^9	0.95	99.98
3	186	115.2	447907.7	44.4	1.37×10^{10}	0.84	99.99
A+B							
1	199.6	130.3	422113.6	56	2.45×10^9	0.67	99.99
2	202.6	140.8	417368.9	35.3	1.19×10^9	0.83	99.99
3	191.4	126.7	437771.1	42.3	1.78×10^9	0.70	99.99
A+C							
1	181.1	124.3	458415.8	39.6	2.29×10^9	0.69	99.99
2	196	130.9	429110.8	35.5	2.40×10^9	0.85	99.99
3	195.9	124.5	429293.1	26.1	2.29×10^9	0.79	99.99
A+D							
1	176.1	111.5	469139	32.5	1.00×10^{10}	0.61	99.99
2	196.9	129.2	427402.2	18.4	1.57×10^9	0.62	99.99
3	194.2	124.3	432199.8	34.5	3.26×10^9	0.81	99.99
A+E							
1	187.4	112.7	445555.1	60.7	7.2×10^9	0.79	99.98
2	202.4	123.8	417685.7	66.9	3.9×10^9	0.96	99.98
3	170.9	101.0	481013.3	77.5	1.00×10^{11}	0.87	99.98

A = strength layer, B = 4 oz/yd^2 fabric, C = 8 oz/yd^2 fabric, D = 12 oz/yd^2 fabric, E = 16 oz/yd^2 fabric

Table 3.2 Results From Filtration Tests at 10 psi (69 kPA)

Test	Initial Water Content (%)	Final Water Content (%)	Initial TSS (mg/l)	Final TSS (mg/l)	Specific Resistance (sec^2/g)	Average Flow (ml/min	TSS Filtering Efficiency (%)
A							
1	198.4	120.9	424650.6	214.6	2.49×10^9	1.32	99.95
2	178.8	115.3	463226.6	178.9	4.57×10^9	1.03	99.96
3	192.2	110.2	436222.5	104.3	6.71×10^9	1.00	99.97
A+B							
1	200.1	134.8	402513.9	102.4	1.19×10^9	1.085	99.97
2	208.9	131.1	421564.6	76.5	1.44×10^9	1.08	99.98
3	208.9	138.5	406483.6	43	1.15×10^9	1.00	99.98
A+C							
1	182.5	121.5	455410.6	31.5	2.62×10^9	0.89	99.99
2	175.4	115.9	470767	22.2	2.59×10^9	0.71	99.99
3	183.4	112	453685.1	18.3	5.96×10^9	0.98	99.99
A+D							
1	174	123.7	473554.1	20.7	1.70×10^9	0.87	99.99
2	171	115.1	479190.4	29.8	3.61×10^9	0.94	99.99
3	175.3	118.6	471031.8	20.4	2.79×10^9	0.76	99.99
A+E							
1	193.9	117.5	432927.8	50.5	3.44×10^9	1.16	99.99
2	214.7	135.4	397253.7	40.5	1.08×10^9	1.23	99.99
3	188.2	114.9	444035.4	37.5	3.23×10^9	1.10	99.99

A = strength layer, B = 4 oz/yd^2 fabric, C = 8 oz/yd^2 fabric, D = 12 oz/yd^2 fabric, E = 16 oz/yd^2 fabric

At 5 psi (34.5 kPA) and 10 psi (69 kPA), the various geosynthetic fabric configurations have a minimum filtering efficiency of 99.9%. Christopher and Holtz (1985) recommend a minimum filtering efficiency for silt fence applications of 75%. The fabric configurations reduced the TSS migrating to the water column by an average factor of 1000 under the conditions tested.

Figure 3.2 shows an example of the flow and time relationships for the filtration test for the A+B fabrics at 10-psi (69 kPA). In all tests, the water flow through the fabric and sediment slowed with time. The reduced flow is probably caused by the formation of a filter cake on the geotextile fabric (Henry and Hunnewell, 1995).

The specific resistance was computed by obtaining the slope of the filtrate curve, b, by plotting the t/V vs. V where V is the filtrate volume collected in time, t. Figure 3.3 displays the filtrate curves for the A+B fabrics at 10 psi (69 kPA). Specific resistance values shown in Tables 3.1 and 3.2 compare favorably to the values obtained for water and wastewater treatment sludge (Eckenfelder, 1966). The sediment is highly compressible, and the specific resistance is dependent on pressure.

Figures 3.4 and 3.5 plot the TSS and fabric weight relationships for the filtration tests conducted at 5 and 10 psi (34.5 and 69 kPA), respectively. In Figure 3.4, the TSS and fabric weight relationship follows a third order linear regression with a minimum TSS

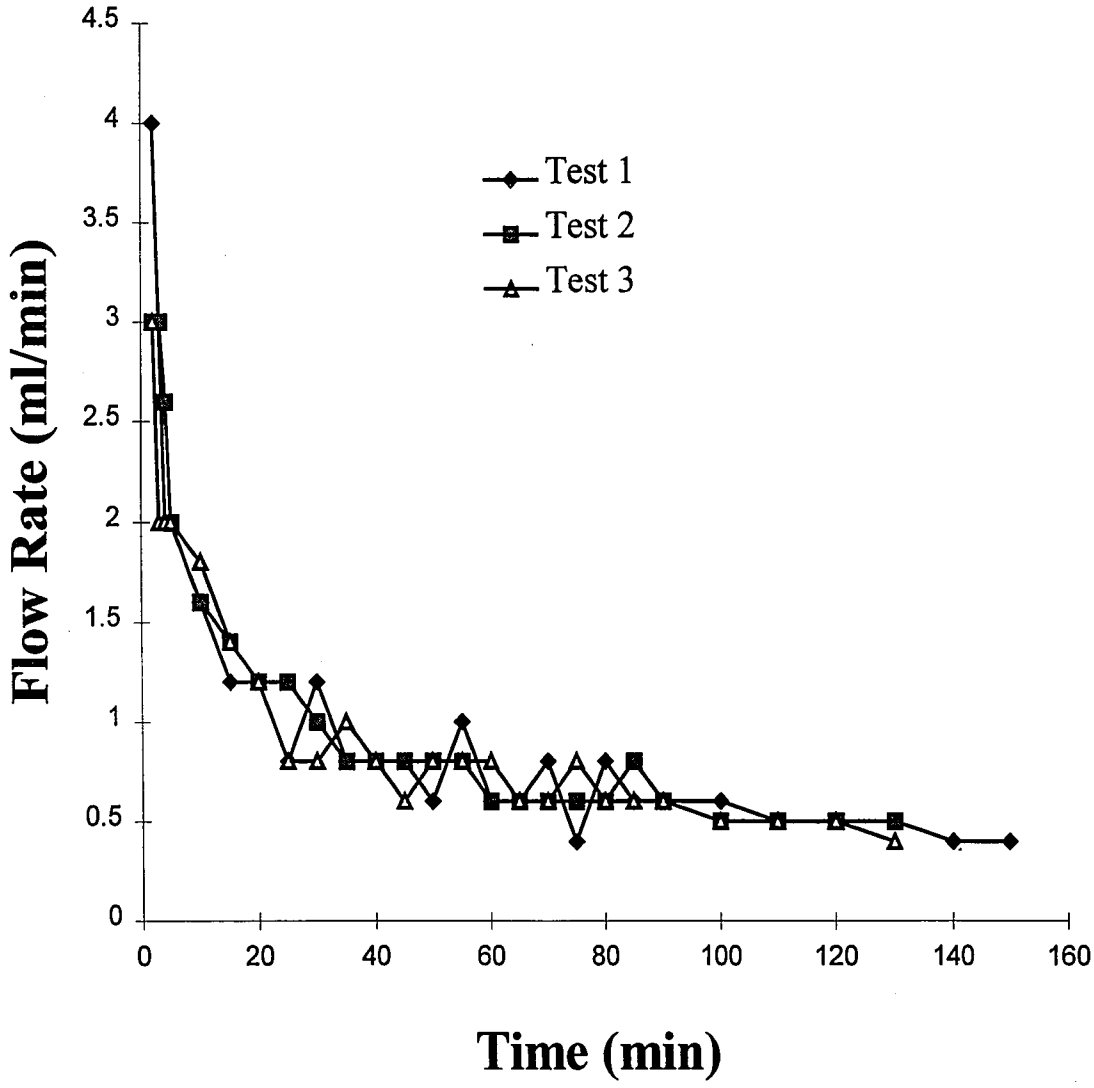

Figure 3.2 Flow Rate vs. Time Relationship for A+B fabric at 10 psi (69 kPA)

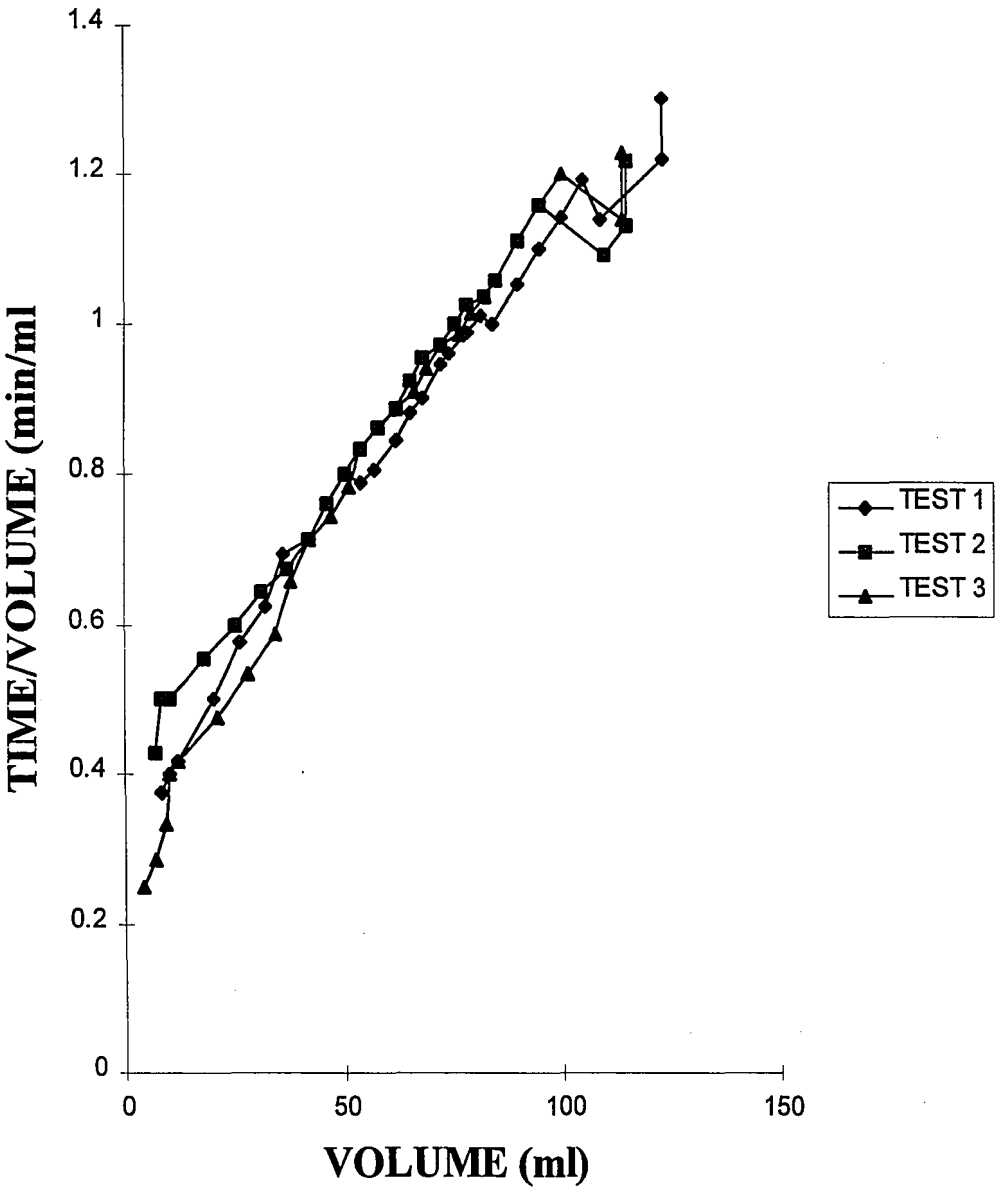

Figure 3.3 Filtration Curve for A+B fabric at 10 psi (69 kPA)

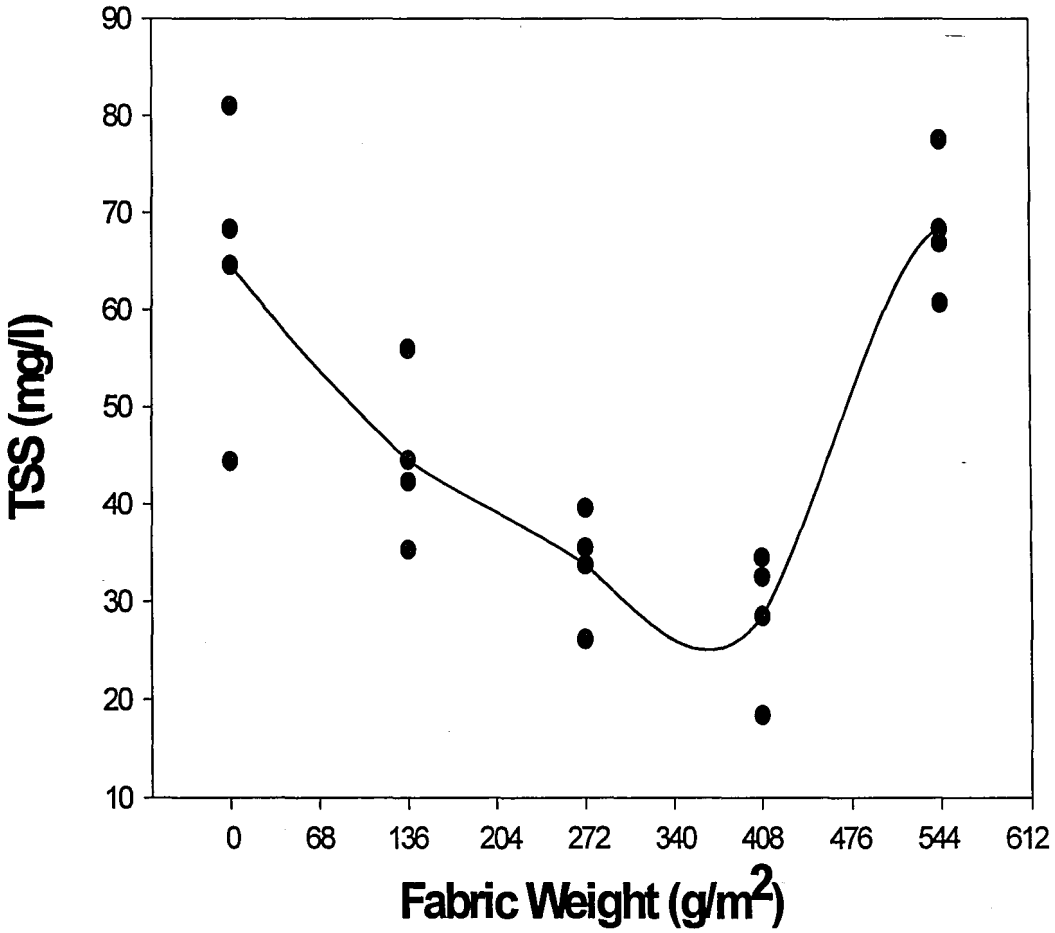

Figure 3.4 TSS vs. Fabric Weight for Filtration Tests at 5 psi (34.5 kPA)

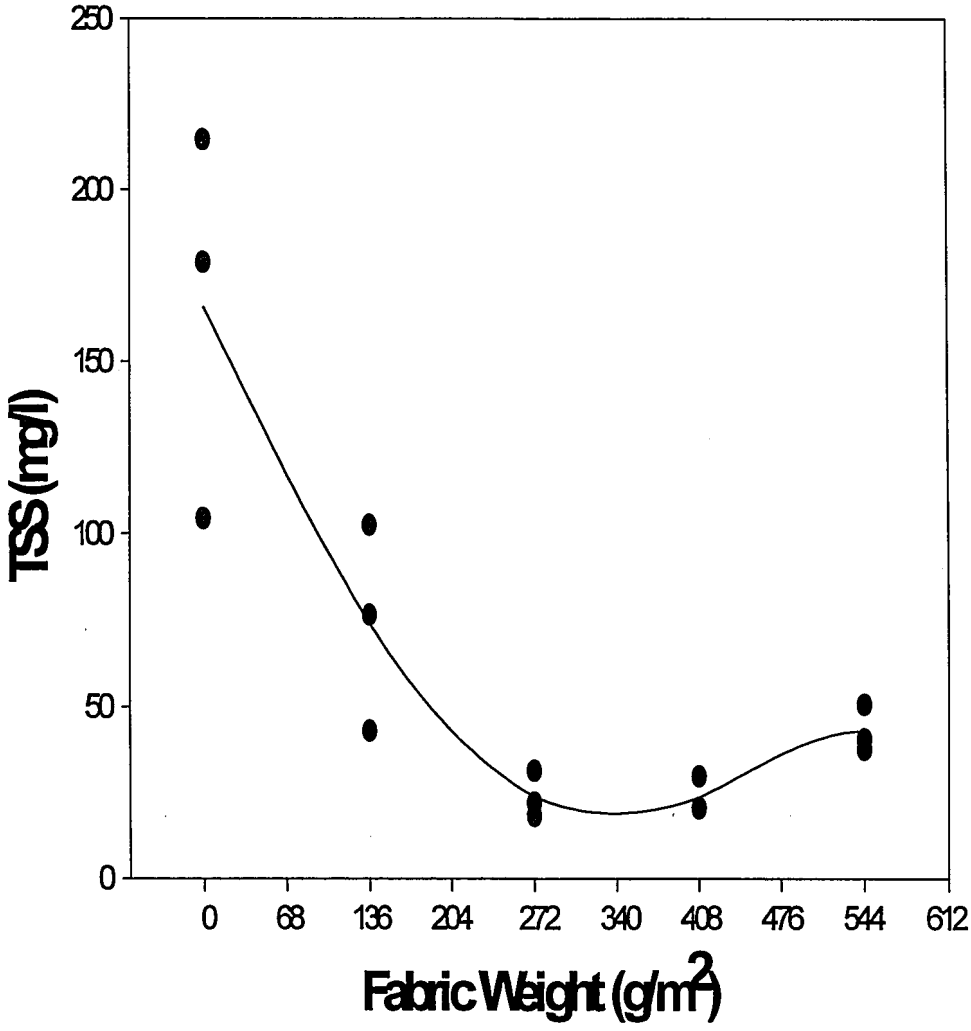

Figure 3.5 TSS vs. Fabric Weight for Filtration Tests at 10 psi (69 kPA)

concentration occurring at the (12 oz/yd^2) fabric geotextile D. The (16-oz/yd^2)-fabric geotextile E showed a sharp increase in TSS compared to the (12-oz/yd^2)-fabric geotextile D. In figure 3.5, the TSS and fabric weight relationship follows a second order linear regression with the minimum TSS also occurring at the (12-oz/yd^2) fabric geotextile D. These data indicate that geotextile D has the lowest TSS concentration passing through the material.

Figure 3.6 plots the apparent opening size and total suspended solids relationship for tests conducted at 5 psi (34.5 kPA) and 10 psi (69 kPA). As the apparent opening size decreases, the total suspended solids concentration decreases. Although geotextiles D and E have the same AOS, geotextile D performs more efficiently as a filter at 5 psi (34.5 kPa) and 10 psi (69 kPa) than geotextile E.

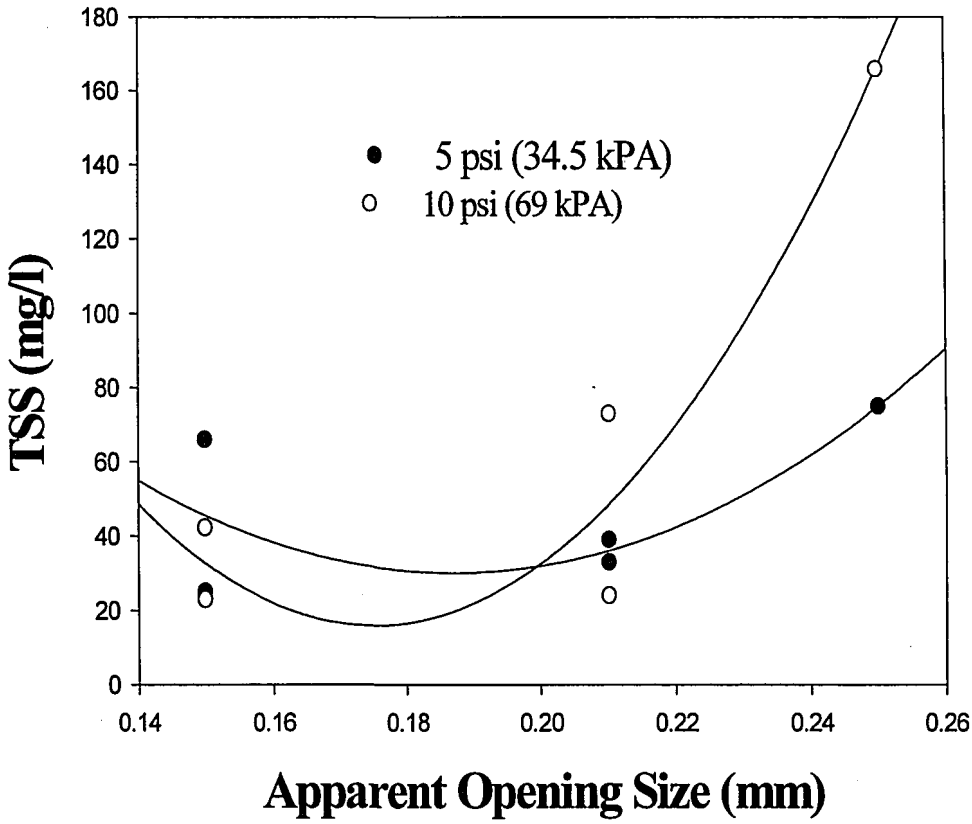

Figure 3.6 TSS and AOS Relationship

Chapter 4

Hanging Bag Tests

4.1 Background

Laboratory tests were conducted on GFCs according to the proposed ASTM (Section D18.13.05 on Navigation Dredging) standard method. The hanging bag test is used to determine the rate of suspended solids migration through a geotextile container used to contain dredged material.. Total Suspended Solids and chemical analysis are conducted to determine the amount of fine and contaminant migration through the container. Hanging bag tests represent the self-weight consolidation that occurs in the GFCs after loading. This proposed test is intended to be used to design geotextile containers that meet environmental regulations and reduce the impact of the sediment on the water column at open water dredging disposal facilities. Hanging bag tests were conducted on the geotextile fabrics described in chapter 2 using sediment from the site.

4.2 Apparatus

A wooden frame with a length of 27 inches (68.6 cm), width of 24 inches (61 cm), and height of 80 inches (203.2 cm) was used to support the GFC during the test. Figure 4.1 displays the hanging bag apparatus. An aluminum pipe with a diameter of 15 inches (38.1

cm) and a length of 9 inches (22.9 cm) was used to connect the GFC to the wooden frame. The GFC had eight evenly spaced metal grommets to connect to the aluminum flange and had a length of 65 inches (165.1 cm) and a circumference of 45 inches (114.3 cm). A 24-inch (61-cm) diameter funnel was placed on the bottom of the wooden frame to collect the filtrate during the test and was connected to 1-liter amber glass jars for sample collection. A trash can with the bottom cut out was placed around the GFC to guide water flow into the funnel. Three GFC configurations were tested: geotextiles A+B, A+D, and A.

4.3 Procedure

1. The geotextile containers were provided by the manufacturer and were connected to the flange pipe on the wooden frame by connecting the metal grommets to the metal pipe with a 3/8 inch (0.925 cm) galvanized bolts. As shown in Figure 4.1.
2. Geotextile containers were pre-wetted by soaking the geotextile in artificial seawater and were allowed to drain the free water.

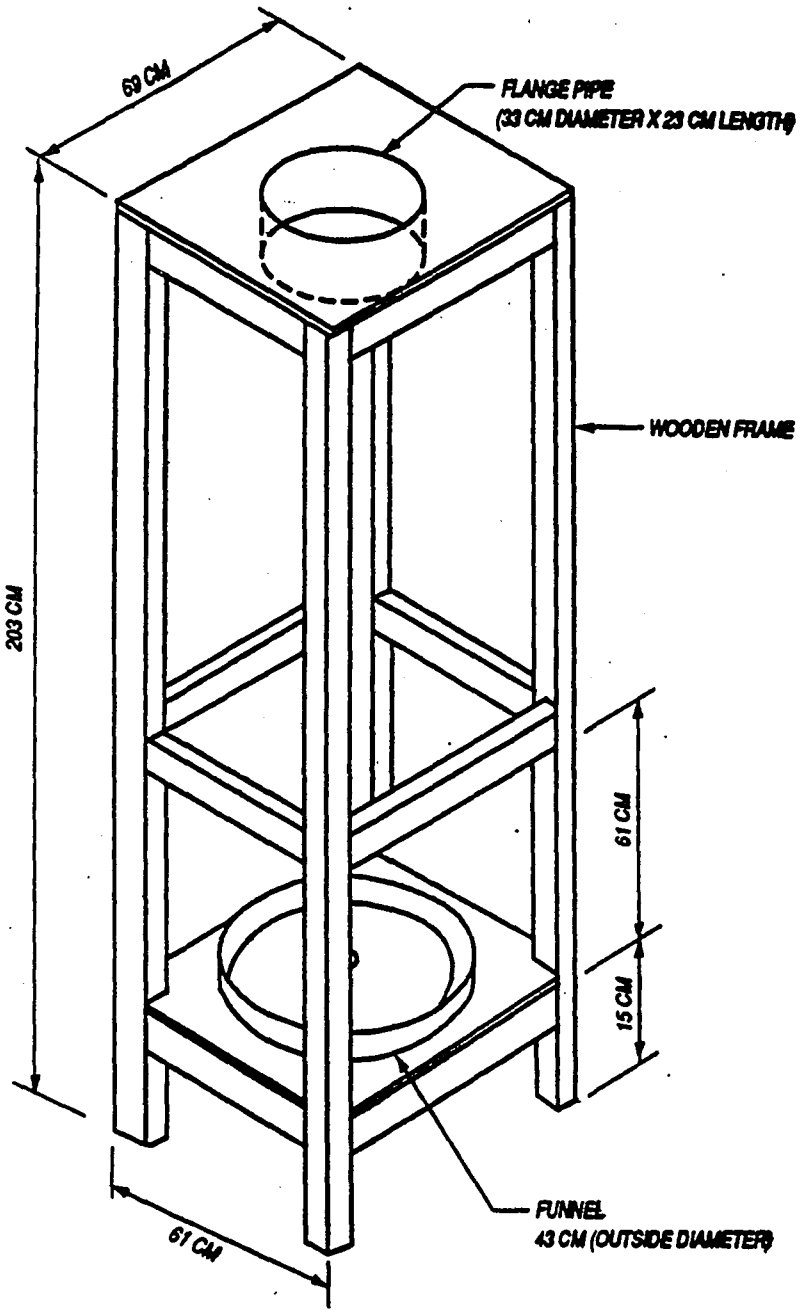

Figure 4.1 Hanging Bag Apparatus

3. Contaminated sediment was mixed in a 55-gallon (208.2-liter) drum and was loaded into the GFCs with a 5-gallon (18.9-liter) bucket. The weight of the sediment placed into the GFCs was recorded, and the initial distance from the top of the sediment to the top of the GFC was recorded.
4. A funnel connected to a 1-liter amber glass jar was placed at the bottom of the wooden frame to collect the filtrate through the GFC. Filtrate volumes and distances from the top of the sediment to the top of the GFC were recorded with time.
5. An aliquot from each collected sample was placed into a 2 gallon (7.571 liter) jar for chemical analysis for Dioxin, PAH, PCB, TOC, and Metals. The remainder of each sample was used for TSS analysis.

4.4 Results

4.4.1 Solids Release and Consolidation

Hanging bag tests were conducted using three geotextile fabric configurations: A, A+B, and A+D. Each test was conducted for three days. Figure 4.2 displays the TSS versus time relationship for the three hanging bag tests. For the geotextile A, high initial TSS concentrations occurred. TSS concentrations decreased significantly with time, which is expected, since the fabric meets the soil retention criteria with an AOS less than 2 to 3 times the d_{85}. For geotextile A+B and A+D configurations, the initial TSS was

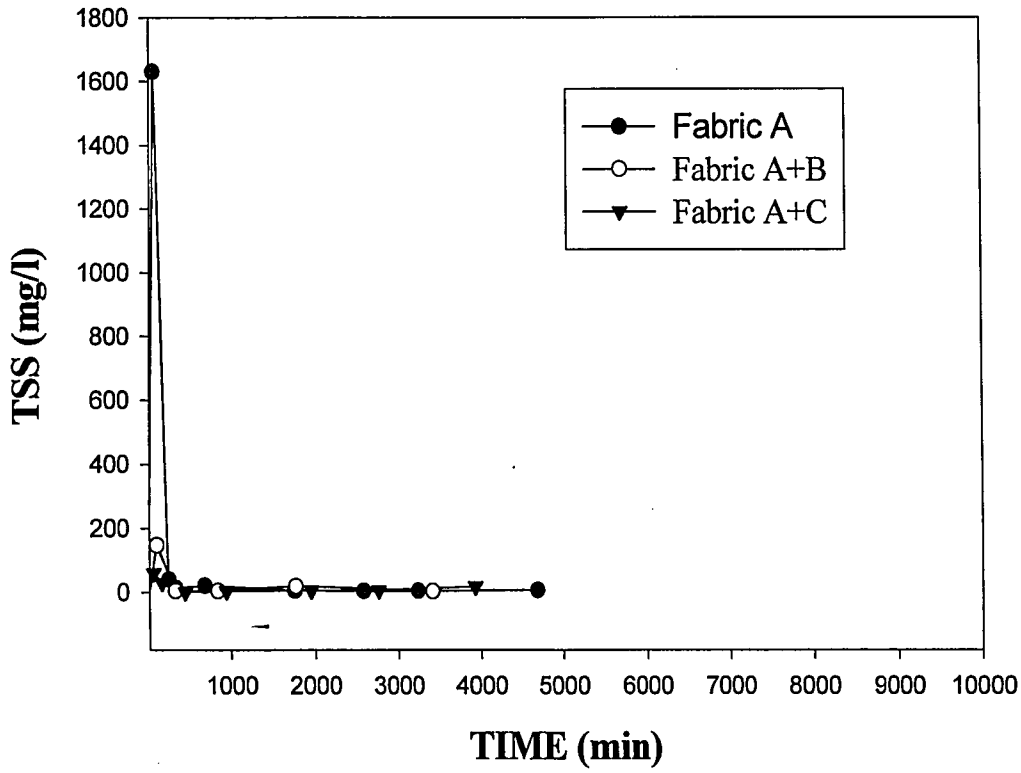

Figure 4.2 TSS Concentrations for Hanging Bag Tests

significantly lower than the TSS for A. TSS concentrations for geotextiles A+B and A+D configurations decreased with time. TSS concentrations for each configuration reach a steady state condition after 3 to 4 hours.

The steady state TSS concentrations provide estimates of the long-term solids retention properties of the various GFC configurations. First, there is no substantial difference in the long term TSS release properties of the three GFC configurations tested. Second, the steady state TSS values indicate a very small potential for long term solids release from the GFCs tested. In the field, TSS concentrations (initial and steady state) and the small volume of water released from the GFCs would be significantly diluted in the immediate vicinity of the GFC. TSS concentrations greater than the field TSS would not be expected in the field unless the GFC ruptures or is torn.

Figure 4.3 plots the settlement and time relationship using a semi-logarithmic scale for the three hanging bag tests. Settlement measurements were taken by measuring the depth of self-weight consolidation occurring at various times. For each fabric configuration, there were considerable amounts of self-weight consolidation. For the various fabrics configurations, the average final void ratio and water content of the sediment were 4.08 and 160%. The average final void ratio for the sediment corresponds to an effective stress of 0.014 tsf (1.3 kPA) from one-dimensional consolidation tests as shown in Figure 2.3.

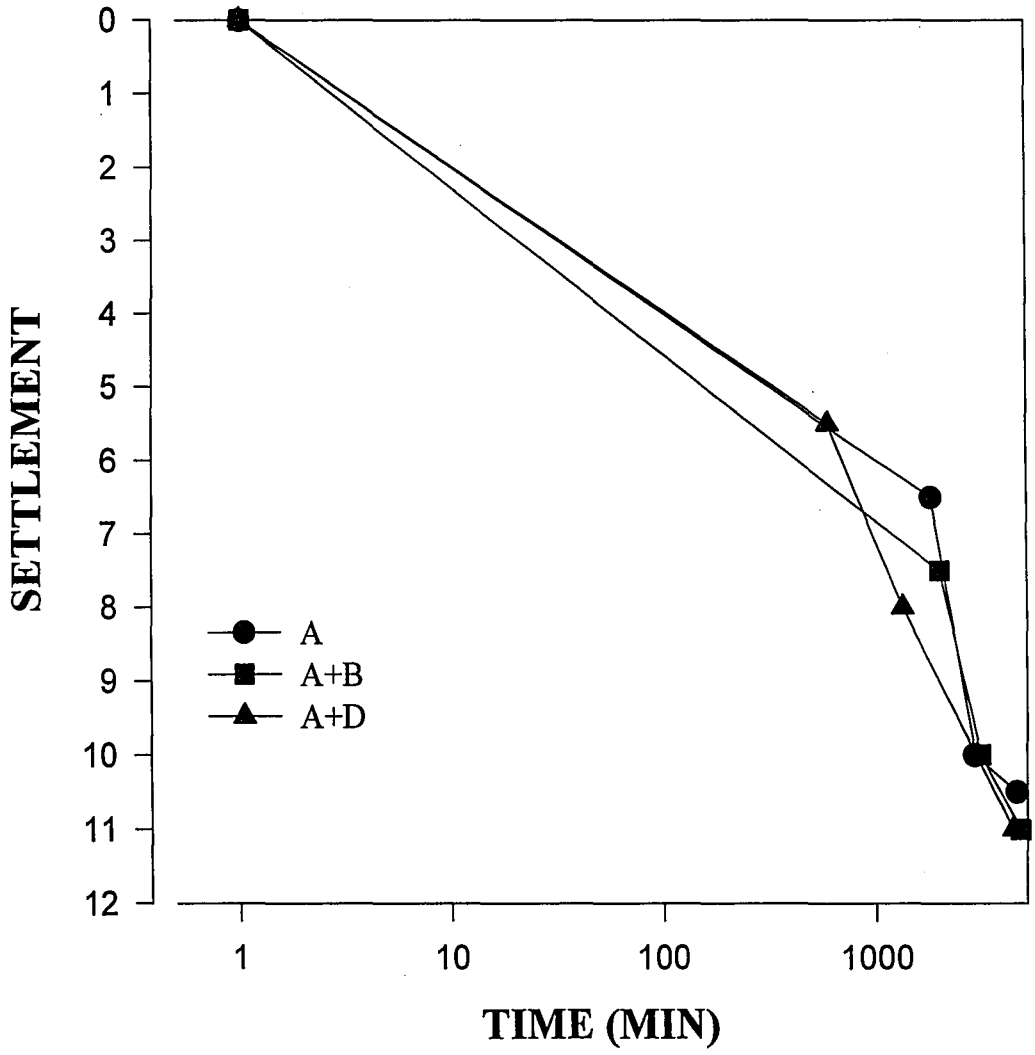

Figure 4.3 Settlement Relationships for Hanging Bag Tests

The volume of leachate produced during the hanging bag tests decreased exponentially with time. Leachate production in hanging bag tests is due to self-weight consolidation as indicated by the settlement curves in graph 10-appendix b. Thus, reduction in leachate production with time is due to sediment consolidation properties and does not reflect clogging of the GFCs.

4.4.2 Chemical Releases

4.4.2a METALS

Leachate metal concentrations in the hanging bag tests were low (Table 4.1) in comparison to metals concentration in the sediment as shown in Table 2.2, and all with the exception of silver were above the minimum detection limit (MDL). The general trend was that the A configuration had the highest concentration of metals followed by the A+B and finally the A+D configurations. The only exceptions to this trend were for Chromium, Lead, and Zinc where there was an increase in concentration between the A+B configuration, and the A+D configuration, and also for Nickel where there was an increase in concentration between the A and the A+B configurations.

4.4.2b TOC

The first line of Table 4.1 gives the various leachate concentrations of TOC determined in the hanging bag tests, and in all three configurations the concentrations are well above the minimum detection limit (MDL). Interestingly enough the concentrations tend to be lowest for the A configuration

Table 4.1 Chemical and Metal Analysis for Hanging Bag Tests

Chemical/Metal	**A** mg/l	**A+B** mg/l	**A+D** mg/l
TOC	41.8	51	61.3
Chromium	0.0461	0.0301	0.0307
Copper	0.0308	0.00869	0.00834
Iron	0.375	0.162	0.0905
Manganese	0.139	0.132	0.129
Mercury	0.000070	0.000038	0.000020
Lead	0.00779	0.00237	0.00266
Arsenic	0.0250	0.0229	0.0201
Cadmium	0.00116	0.001107	0.0011021
Zinc	0.0336	0.00144	0.00585
Nickel	0.0239	0.0265	0.0237
Silver	0.00010	<0.00010	<0.00010
PAH	0.03624	0.02074	0.00536
PCB	<0.0128	<0.0128	<0.0128
Dioxins	$<9.0x10^{-6}$	$<7.0x10^{-6}$	$<7.0x10^{-6}$
Furans	$<8.0x10^{-6}$	$<8.0x10^{-6}$	$<8.0x10^{-6}$

slightly higher for the A+B configuration and highest for the A+D configuration. This in itself is an indication that the TOC is mostly in the dissolved form.

4.4.2c PAHs

Table 4.1 summarizes the concentrations of the PAHs from samples collected, and the mass fraction retained in the GFCs during the hanging bag tests. PAH concentrations for the hanging bag tests are much lower than the initial PAH concentrations in the sediment (Table A-1). Table B-1 in appendix B shows the complete chemical analysis for PAH. This suggests that pore water concentrations of PAH in the sediment are also very low. Concentrations of naphthalene, acenaphthylene, dibenzo(a,h)anthracene, and benzo(g,h,i)perylene were less than MDL (0.0003 mg/l) in all the hanging bag test filtrate. The largest observed PAH concentration that was observed was for fluoranthene (0.00208 mg/l) in the A configuration test. Leachate PAH concentrations were generally greatest in the A configuration test followed by the A+B and A+D tests. Exceptions to this trend were acenaphthene, fluorene, benzo(b)fluoranthene, and benzo(k)fluoranthene.

4.4.2d PCBs

PCB concentrations in the filtrate from the hanging bag tests were lower than the concentration in the leachate as shown in Table 4.1. Table B-2 shows the complete analysis for PCBs For the A configuration test, observed leachate PCB congener concentrations were below MDL (0.00003 mg/l), with the exception of PCB 54, which was slightly above MDL. For the A+B test, concentrations were below MDL with the

exception of PCB 77, which was slightly above MDL. For the A+D test concentrations were below MDL, with the exception of PCB 54, PCB 66, and PCB 155. Thus, few PCB congener concentrations greater than MDL were measured for any of the GFC configurations. The absence of measurable PCB concentrations in hanging bag filtrate reflects the low PCB concentrations in the sediment inside the GFC and does not necessarily imply PCB sorption by the GFCs.

4.4.2e DIOXINS and FURANS

Filtrate Dioxin and Furan concentrations are shown in Table 4.1, and the complete analysis is shown in Table B-3 in appendix B. Most of the isomers were undetectable for all three configurations with the exceptions of 1,2,3,6,7,8-HxCDF, 1,2,3,4,6,7,8-HpCDF, OCDF, OCDD, PECDF, HXCDF, HPCDF, and HPCDD. For 1,2,3,6,7,8-HxCDF, 1,2,3,4,6,7,8-HpCDF, OCDF, OCDD, HPCDF, and HPCDD, the lowest concentrations were detected in the A+B configuration. The concentration of PECDF, and HXCDF were highest in the A configuration followed by the A+B and finally the A+D configurations.

4.5 Analysis

The purpose of this section is to indicate how much of the observed total contaminant concentration was probably particulate bound (in particle and not dissolved form). If

most of the contaminant mass in the hanging bag leachates were particulate bound, then additional solids removal with heavier weight liners would be beneficial in reducing contaminant transport through the GFC. On the other hand, if most of the contaminant mass was dissolved, additional solids removal will not be effective in reducing contaminant transport through the GFC.

In general, contaminant concentrations are given by

$$C_t = C_p + C_d \tag{4.1}$$

Where

C_t = total contaminant concentration, mg/l

C_p = particulate-bound contaminant concentration, mg/l

C_d = dissolved contaminant concentration, mg/l

Ratios of particulate-bound contaminant concentration, C_p, and dissolved contaminant concentration, C_d, to total contaminant concentration, C_t, are, the mass fractions, C_p/C_t, particulate-bound and C_d/C_t dissolved, respectively. The available hanging bag leachate data, however are for total contaminant concentration only, that is, there was no separate analysis of dissolved or particulate-bound contaminant concentrations. The volume of sample from the hanging bag tests was too small for analysis of either dissolved or particulate phase concentrations. To evaluate the significance of particulate bound

contaminant, it was therefore necessary to estimate the particulate bound contaminant concentrations. Particulate-contaminant concentrations were estimated using the following equation:

$$^{e}C_p = q\,(TSS) \qquad (4.2)$$

Where

$^{e}C_p$ = estimated particulate-bound contaminant concentration, mg/l

q = sediment contaminant concentration, mg/kg

TSS = observed total suspended solids concentration, kg/l

This equation assumes that contaminant concentrations in the sediment solids and the leachate TSS are the same. Ratios of estimated particulate-bound to observed total contaminant concentrations ($^{e}C_p$ / $^{o}C_t$) where $^{o}C_t$ is the total contaminant concentration were calculated using mean values (n=6) of the measured sediment contaminant concentrations for q and observed total contaminant concentrations.

Various processes may affect the estimated particulate-bound contaminant mass fraction and complicate interpretation of the ratios calculated. This includes sorption of dissolved phase contaminant by the GFC and enrichment of the solid phase contaminant concentration, q. If dissolved contaminant is sorbed by the GFC, then the fraction that is

particulate bound depends on how much dissolved contaminant is sorbed by the GFC and how rapidly equilibrium is reached in the filtrate.

The GFC can affect the solid phase contaminant concentration, q, through an enrichment process. GFCs tend to transmit fines (silts and clays) and retain coarse grain materials (sands and gravel's). Since the fines are usually enriched in contaminant concentrations relative to the coarse grain materials, the removal of coarse grain material by the GFC can enrich the contaminant concentration in the TSS in the leachate relative to the solids inside the GFCs.

The available data are not sufficient to evaluate sorption of dissolved contaminant or enrichment of the particulate phase contaminant concentrations by GFCs. Table 4.2 summarizes the interpretation that can be made of estimated particulate-bound contaminant mass fractions for contaminant partitioning in the leachate and contaminant transport through GFCs. Ratios of estimated particulate to observed total concentrations less than 0.5 indicate that dissolved concentrations are probably significant and that additional solids removal may not significantly improve leachate quality. Ratios of estimated particulate-bound to the observed total concentrations greater than 0.5 indicate that the particulate bound-fraction is significant and solids removal may improve leachate quality.

Table 4.2 Interpretation of Mass Fraction Ratios from Hanging Bag Tests

$\frac{{}^{e}C_p}{{}^{0}C_t}$	**Contaminant Partitioning in sample**	**Contaminant Transport through GFC**
< 0.5	most of the contaminant mass is in dissolved form	additional solids retention by GFC not likely to improve leachate quality
> 0.5	most of the contaminant mass is particulate-bound	additional solids retention by GFC may improve leachate quality

$^{e}C_p$ = particulate bound contaminant concentration, mg/l
$^{0}C_t$ = total contaminant concentration, mg/l

4.5.1 METALS

Ratios of estimated particulate to observed total heavy metal concentrations are shown in Figure 4.4. Appendix C (Figures C.6-8) details each heavy metal. Here, a general trend with the exception of chromium is the reduction in particulate transport in the lined as opposed to the unlined GFC. The ratios of estimated particulate to observed total concentration for the various metals range from 20 to nearly 0. On the assumption that no other processes affect particulate distribution, it can be said that with the exception of very few metals namely Arsenic, Nickel, and Manganese the other metals (Cadmium, Chromium, Copper, Lead, Mercury, Silver, Zinc, and Iron) are in particulate form. In the case of the metals in particulate form the use of a heavier weight liner may help in reducing their concentrations in the filtrate.

4.5.2 TOC

Figure 4.5 shows ratios of estimated particulate to observed TOC concentrations. In this case, there is a dramatic reduction in particulate transport from an unlined to a lined GFC and a further reduction with the usage of a heavier weight liner. In all three cases the ratios are below 0.5, which would indicate that most of the TOC, is in dissolved form. However, if this is the case then lining the GFC alone should not affect leachate TOC concentration but it obviously does. The process that may be responsible for this particular phenomenon is sorption of TOC by the GFC, but until further studies are carried out on this particular transport mechanism it can only be hypothesized that this is indeed a contributing factor in the reduction of TOC in the filtrate.

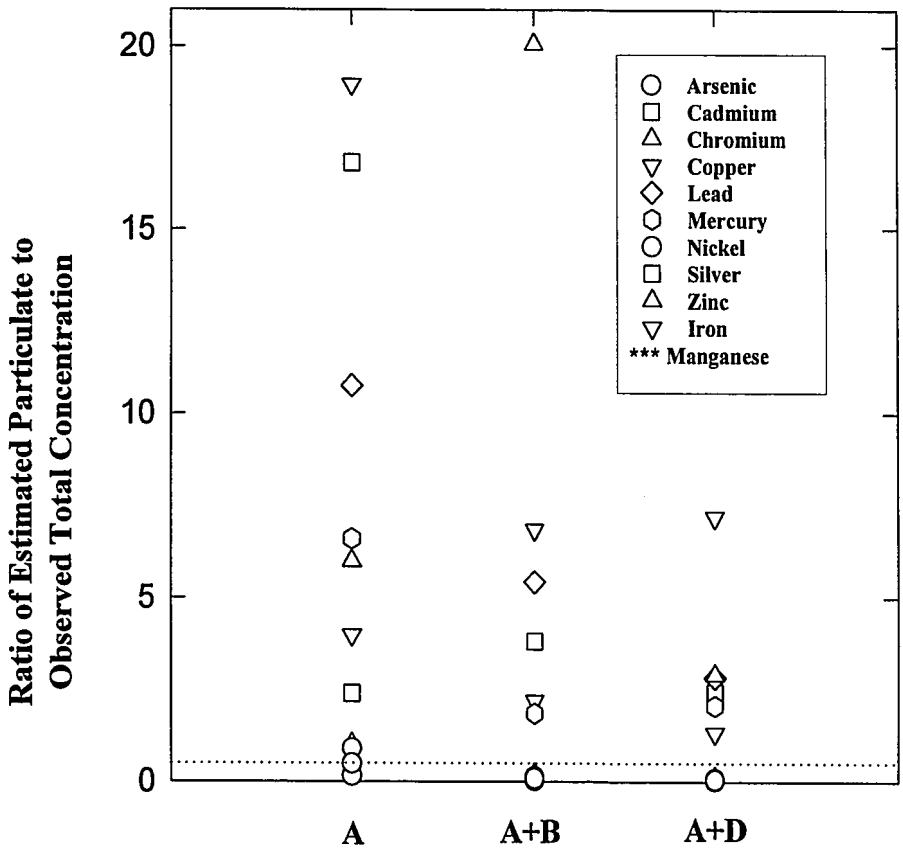

Figure 4.4 Ratios of Estimated Particulate to Observed Heavy Metal (As, Cd, Cr, Cu, Pb, Hg, Ag, Zn, Fe, and Mn) Concentrations

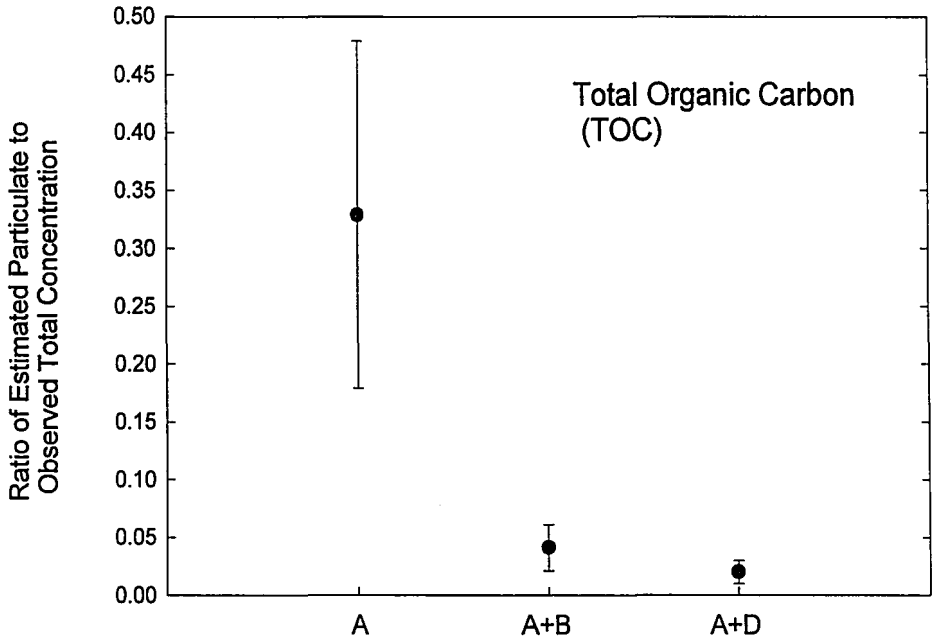

Figure 4.5 Ratios of Estimated Particulate to Observed Total TOC concentrations

4.5.3 PAHs

Ratios of estimated particulate to the observed total PAH concentrations are shown in Figure 4.6. Figures C.1-4 in appendix C details the analysis for each of the estimated particulate to observed PAH concentrations. For the A configuration test, ratios of estimated particulate-phase PAH concentrations to observed total PAH concentrations were generally greater than 1, indicating that the entire observed total was probably particulate-bound. For the A+B and A+D configuration tests, ratios of particulate-bound to the observed total PAH concentrations ranged from 0.07 to 0.75 and 0.08 to 0.93, respectively. These data show that the liners had a dramatic effect on PAH distribution between particulate bound and dissolved phases. Differences between the liners were small, but differences between lined and unlined were large.

The ratios tended to increase with PAH molecular weight in the A configuration test. The tendency for ratios to increase with molecular weight (MW) was not as significant for the lined GFCs as for the unlined GFC. This difference between unlined and lined is expected since the higher TSS in unlined filtrate provides more particulate mass for sorption, and high molecular weight PAHs have higher sorption coefficients than low molecular weight PAHs.

These data also show that the liners reduced the contaminant transport by reducing the transport of particulate bound contaminant. Although the heavier weight liner provided

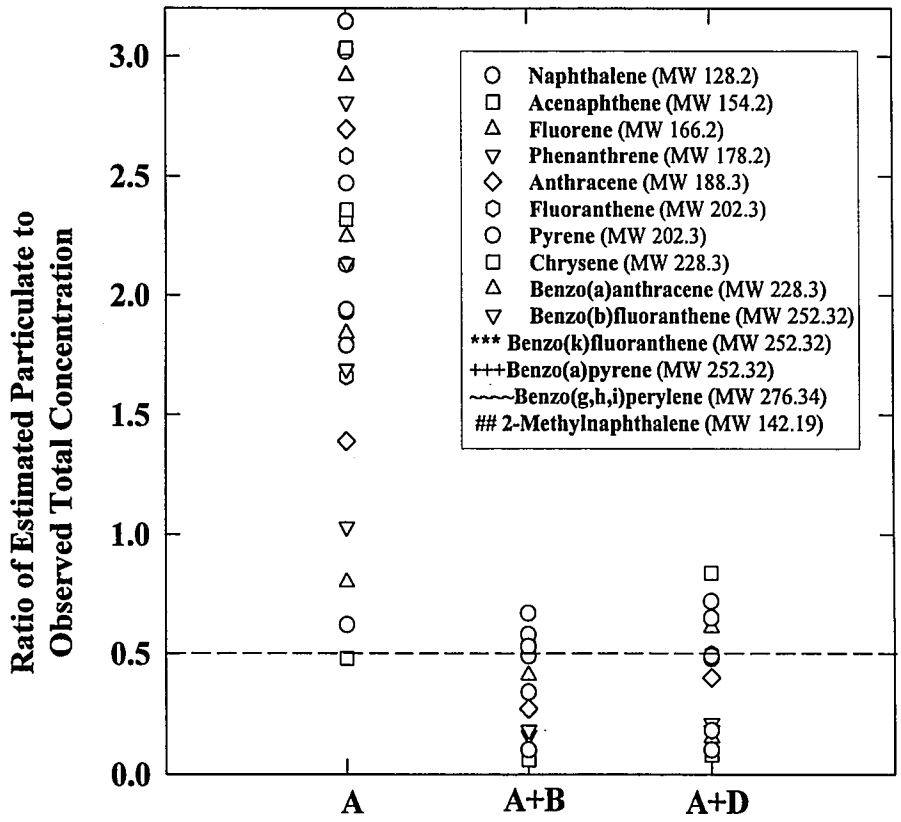

Figure 4.6 Ratios of Estimated Particulate to Observed PAH Concentrations

more resistance to transport of some PAHs, in general the two lined configurations A+B and A+D provided about the same level of resistance to PAH transport.

4.5.4 PCBs

Total PCB concentrations in hanging bag leachates were mostly below the detection limit, and the estimated particulate bound concentrations were also below the detection limit for most of the PCBs. For this reason, ratios of estimated particulate-bound to observed PCB concentrations provide limited insight to PCB transport Through GFCs. However concentrations of PCB 28, PCB 44, PCB 138, and PCB 66 were detectable in all the configurations. Figure 4.7 plots the estimated particulate to the observed PCB concentration. Figure C.5 appendix C plots these results for each PCB. The unlined GFC offered the least resistance to the transport of particulate PCB's, and there was an increase in resistance to particulate transport for the two lined configurations where the heavier weight liner has the greatest resistance. Another noticeable trend is the reduction in the difference in ratios of the four PCB's whereby the unlined GFC has the highest difference followed by the A+B configuration and finally in the A+D configuration the ratios are almost all the same. This means that the A+D configuration has the greatest retention of PCB followed by the A+B configuration and finally the unlined A configuration.

A limited interpretation that may be made from this data is that the lining of the GFC's, is very effective in the reduction of particulate matter, such that most of the PCB's being transported through the configuration are in the dissolved form.

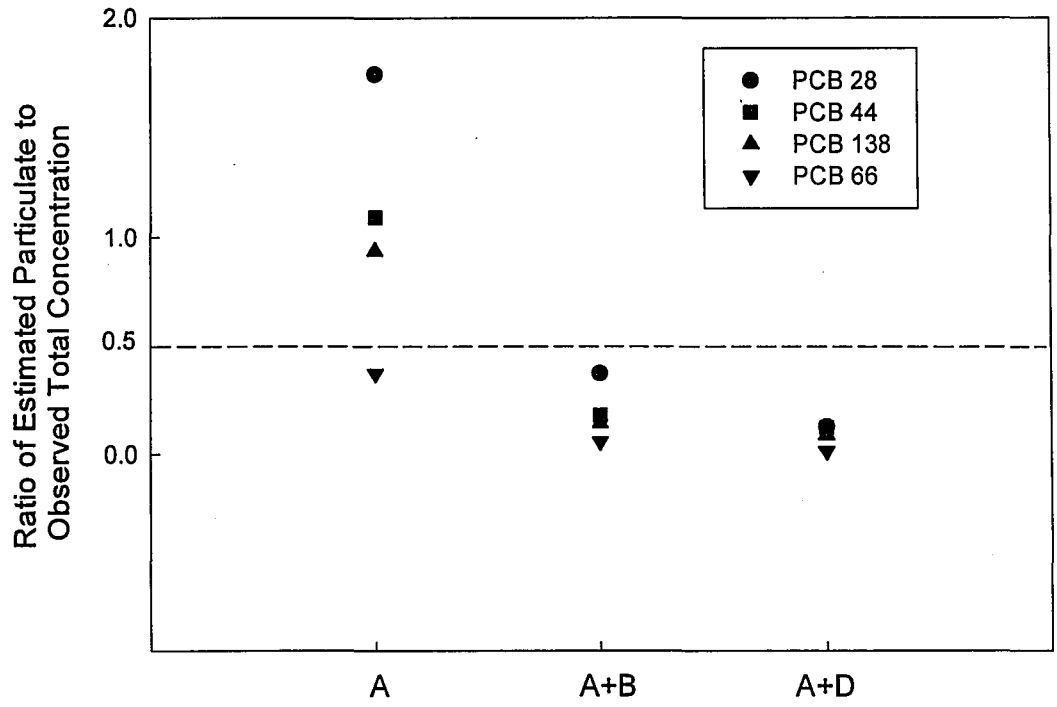

Figure 4.7 Ratios of Estimated Particulate to Observed (PCB 28, PCB 44, PCB 138, and PCB 66) Concentrations

4.5.5 DIOXINS and FURANS

Ratios of estimated particulate to the observed Dioxin and Furan concentrations for the ones that were detectable are plotted in Figure 4.7. Figure C.9-10 in appendix C plots these results for each of the detectable Dioxins and Furans. There is a noticeable general reduction in particulate transport from the unlined GFC to the first lined GFC, and finally the greatest reduction occurs with the use of the heavier weight liner. It is important to realize that these contaminants being organic may be affected by the sorption process, and whatever interpretations are drawn from this figure are limited. Nevertheless, despite whatever processes and or mechanisms are at play, it is fairly safe to say that for the Dioxin and Furan contaminants the use of lined GFC's are beneficial with the A+D configuration being the most adequate.

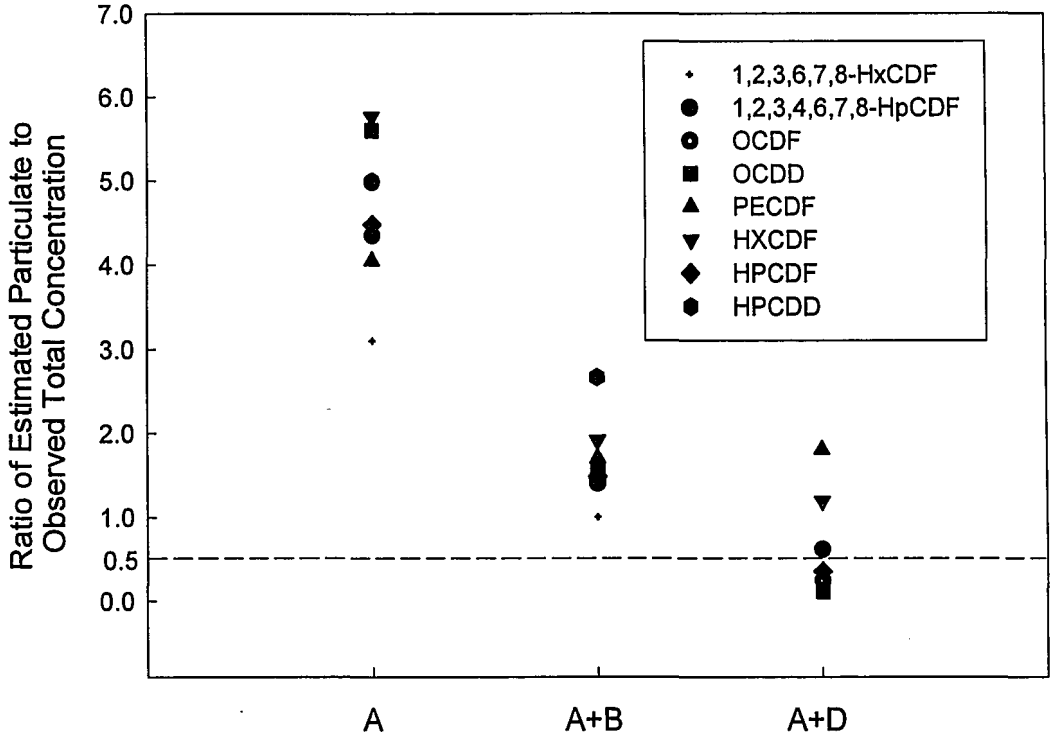

Figure 4.8 Ratios of Estimated Particulate to Observed Dioxin and Furan Concentrations

Chapter 5

Barge Simulation Test

5.1 Background

The purpose of this experiment was to simulate the stresses that a GFC undergoes during deployment and to evaluate the release of contaminants and solid into the water column as a result of these stresses. Figure 5.1 shows the release of a GFC into the water column. Neither pressure filtration tests nor hanging bag tests take into account the changes in the geometry and stress in the GFC caused by the opening of the barge as the container is released to the water column. During a dredging operation, self-weight consolidation will occur during the loading of the bag. When the GFC is deployed, it is anticipated that the dredged material will be deformed as the GFC exits the barge.

5.2 Apparatus

1. The GFCs were 5 feet (1.52 meters) in length with an inside diameter of 12 inches (30.5 centimeters). Three GFC configurations were tested: A, A+B, and A+D

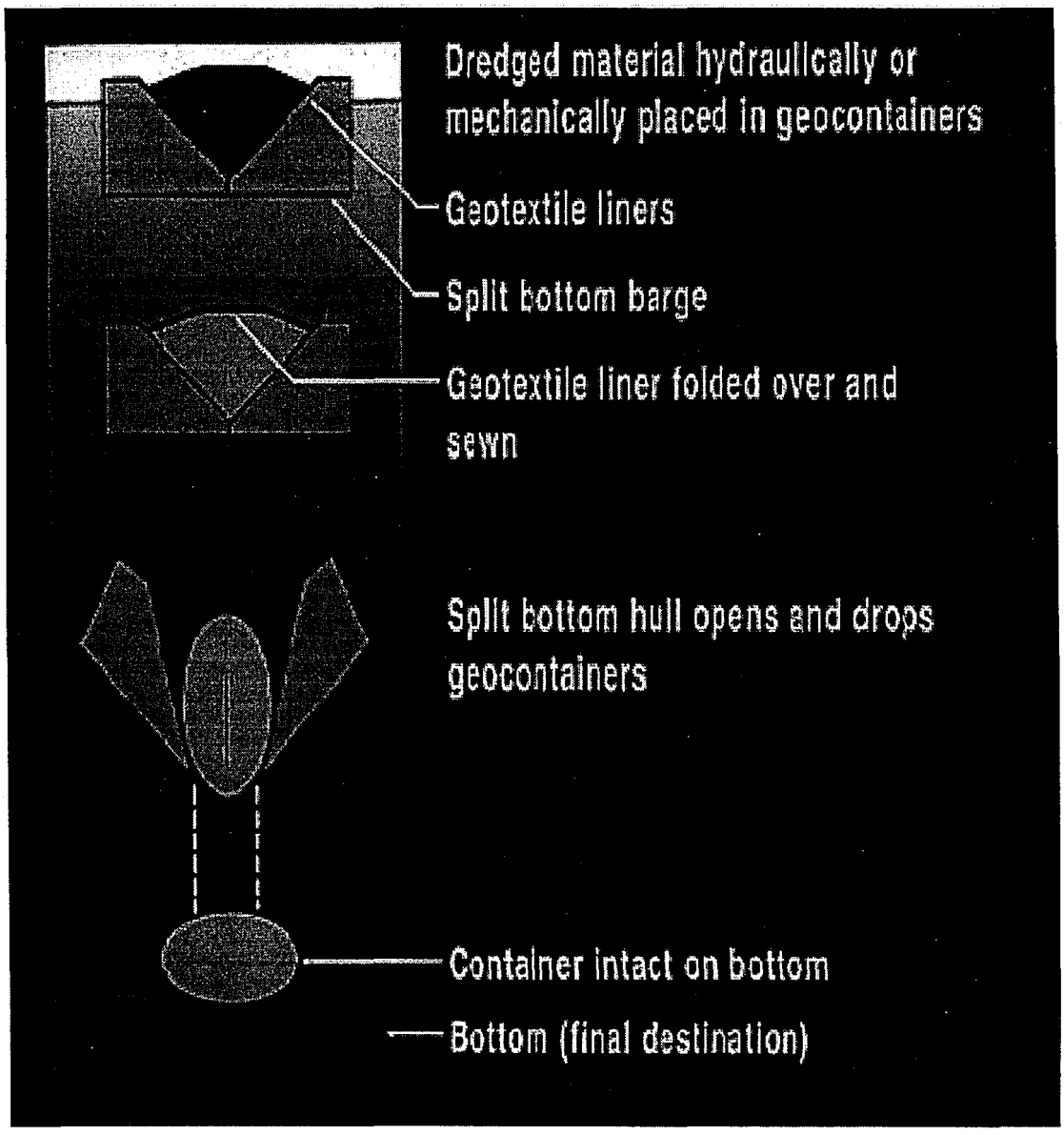

Figure 5.1 GFC Being Released from a Split Hull Barge

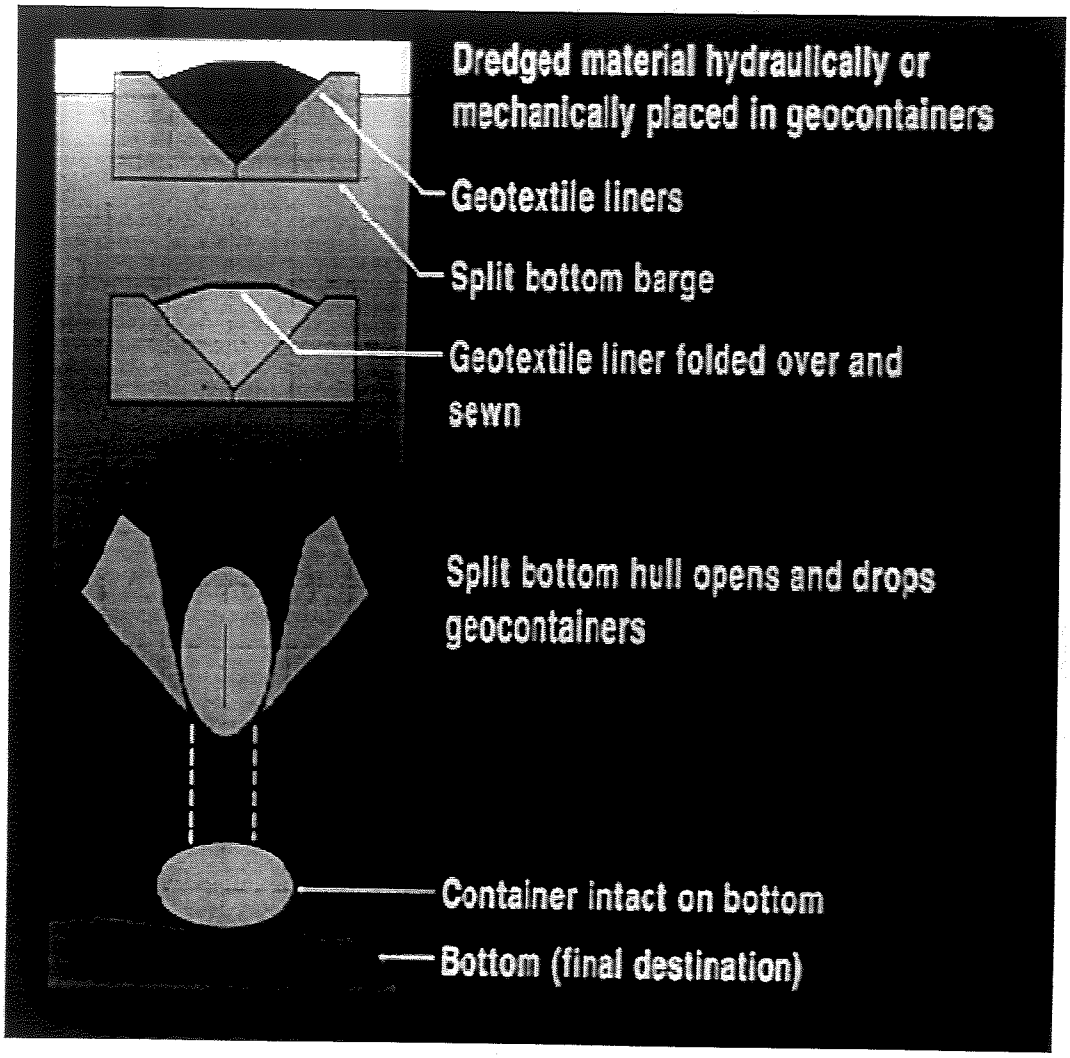

Figure 5.1 GFC Being Released from a Split Hull Barge

configurations. GFCs were open at the top with eight equally spaced metal grommets sewn into the fabric.

2. Simulated seawater was manufactured in the laboratory using Instant Ocean and following the manufacturer's instructions.
3. An acrylic column was used to submerge the GFCs in seawater during the experiment. Figure 5.2 illustrates the acrylic column.
4. A ring constructed from PVC was placed above the acrylic column as shown in Figure 5.3 GFCs were pulled through the ring to simulate deployment from the barge.
5. A Masterflex peristaltic pump (model 7529-10, Cole-Parmer Instrument Co., Vernon Hills IL) with a flow rate of 3.5 gpm (2.208×10^{-4} m^3/s) was used to mix the column and collect samples.
6. Scaffolding was erected around the column. An I-beam was secured to the top of the scaffolding, and V-winch and winch cables were mounted on the I-beam to raise and lower the GFCs.
7. A 500-lb (2.25 kN) load cell was attached to the winch cable to measure the force required to pull the GFCs through the ring.

5.3 Procedure

1. Fifty-five gallons (208.2 liter) of simulated seawater was mixed for testing.

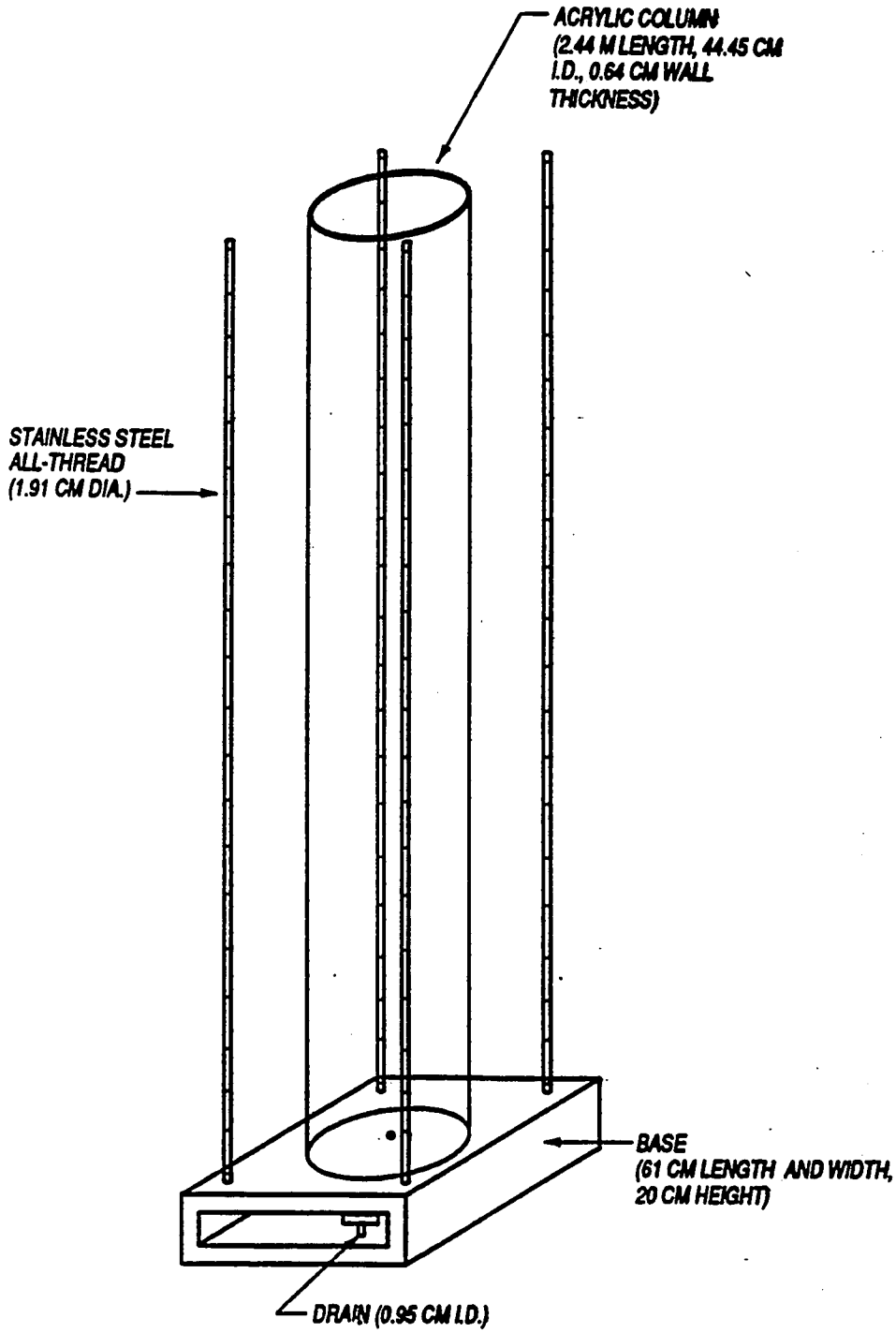

Figure 5.2 Acrylic Column Used in Barge Simulation Test.

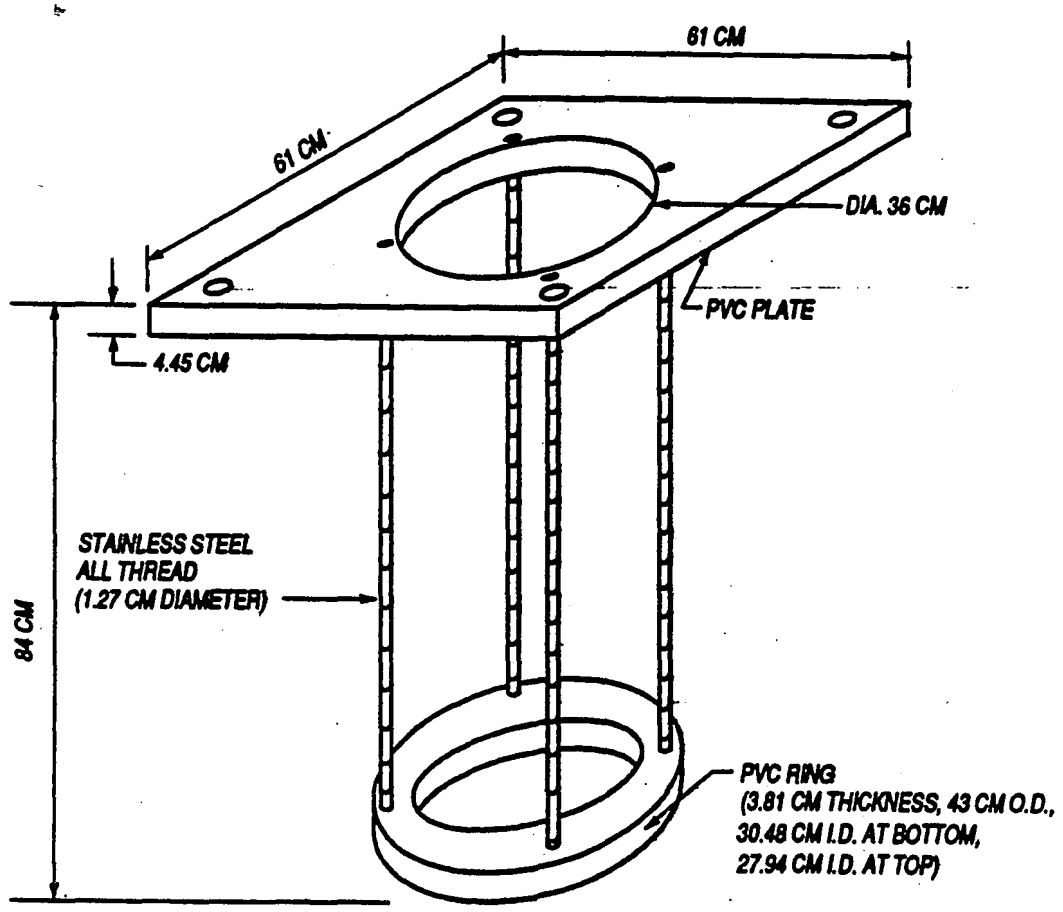

Figure 5.3 Ring Structure for Barge Simulation Test.

2. Fifty gallons (189.3 liters) of seawater were placed into the acrylic column. Samples (sample 1) were collected for analysis of PAH, PCB, dioxin, heavy metals, TOC, NH_3, and TSS.
3. The GFC was fastened to the winch cable and lowered into the column with the top of the GFC at water level, in order to wet the GFC it was then raised until the bottom of the GFC was at water level.
4. After thoroughly mixing the sediment, the GFC was filled with approximately 24 gallons (90.8 liters)of sediment. The sediment was loaded in 4-gallon (15.1 liters) intervals every 5 minutes. During the loading, the GFC was lowered 4 inches (10.2 centimeters) every 5 minutes into the water to simulate a barge displacing water during loading.
5. After loading the sediment, the GFC was allowed to sit undisturbed with one half of the GFC submerged in the seawater for 1 hour. This simulates self-weight consolidation in the barge.
6. After mixing the column with the pump for 30 minutes samples (Sample 2) were collected for contaminant analysis.
7. To simulate deployment from a barge, the sediment was completely submersed in the seawater. The ring was lowered into the column and bolted to the top of the column. The GFC was raised upward through the ring, simulating the squeezing effect of a GFC falling through a barge hull.
8. After pulling the GFC through the ring, the column was mixed again and samples (Sample 3) were collected for analysis

9. Samples were analyzed for the following parameters: total suspended solids, total organic carbons, ammonia, arsenic, cadmium, copper, iron, manganese, lead, mercury, zinc, nickel, silver, PAHs, PCBs, and polychloronated dioxins/furans.

5.4 Results

During the barge simulation test conducted on the A fabric, a change in the water clarity was noticed when the GFC was loaded and when it was pulled through the ring. After the GFC was loaded, and again when it was pulled through ring, black particles (seemingly insoluble) seeped through the fabric and settled to the bottom of the column. During the tests conducted on the A+B fabric configuration, a slight change in water clarity was noticed after the GFC was loaded and pulled through the ring. The A+D fabric configuration has no visible change in water clarity after it is loaded and pulled through the ring.

For each test, three sets of chemical samples were collected. Samples were collected after the sea water was placed into the column and thoroughly mixed (Sample #1), after the GFC was loaded with the sediment and was submerged in the sea water for one hour (Sample #2), and after the GFC was pulled through the ring (Sample #3).

Figure 5.4 plots TSS against the three samples collected for the three fabric configurations A, A+B and A+D. In the unlined configuration fabric A, there is an

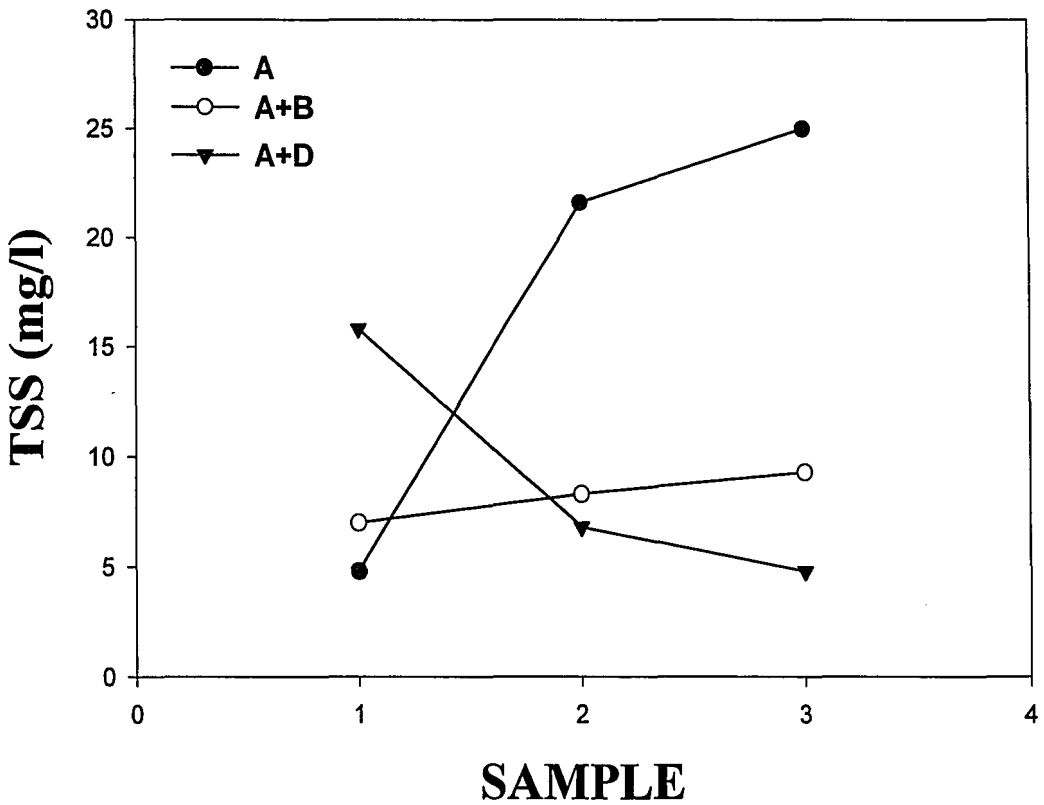

Figure 5.4 TSS Concentration for Barge Simulation Tests

increase in TSS from sample 1 (initial placement of the seawater into the column), to sample 2 (the GFC being loaded with sediment and submerged for one hour in the seawater). There is a further increase in TSS after the GFC is pulled through the ring (sample 3). This is consistent with earlier observations when there was a change in water clarity after the GFC was loaded and pulled through the ring. In the A+B configuration there is a progressive increase in the TSS concentration through sample1, sample 2, and sample 3 respectively. For this configuration the change in concentration is not as dramatic as in the unlined configuration. This is also consistent with the slight change in water clarity that was noticed. In the A+D configuration there is a progressive decrease in TSS from sample 1 to sample 3. This shows that this configuration is retaining more of the solids than the other two configurations. The fact that there is no visible change in water clarity suggests that there is more water than suspended solids being released from the GFC.

Figure 5.5 (plots) the loading rate required to pull the GFCs through the ring. The heavier fabric configuration (A+D) required the highest force to pull the fabric through the ring. The A fabric required slightly more force than the A+B fabric configuration when being pulled through the ring. The average maximum force required to pull the 12 inch (30.48 cm) diameter GFC through the 11 inch (27.94 cm) diameter ring was 250 lb. (1.112 kN).

Analysis for pH and NH_3-N were conducted, and in all three samples for all three configurations, the pH remained constant. NH_3-N concentrations increased as the GFC

was loaded and submerged for an hour, and a further increase was noticed as the GFC was pulled through the ring. This observation was consistent at all three configurations tested.

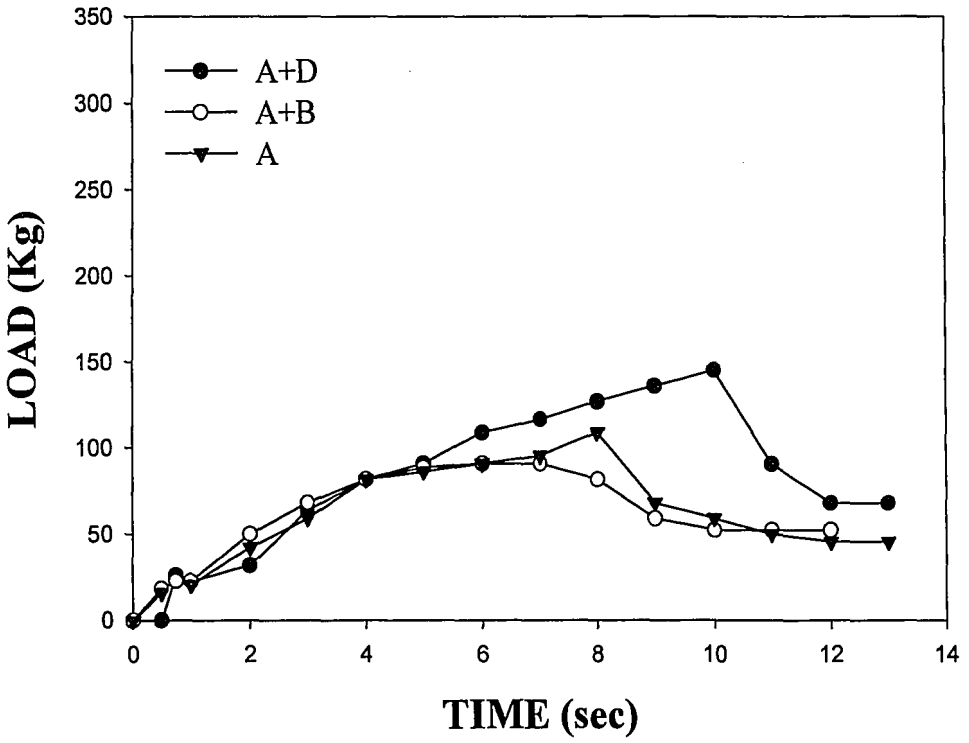

Figure 5.5 Loading Rates for Barge Simulation Tests

5.4.1 Metals

Table 5.1 summarizes the results of heavy metal analysis for the Barge simulation test. In the unlined configuration fabric A, with the exception of mercury and lead, there is no significant change in concentration at all three stages. The mercury concentration decreases by an order of magnitude when the GFC is loaded and submerged. There is no further change as the GFC is pulled through the ring. The lead concentration in the column increased by an order of magnitude as the GFC is loaded and submerged under the seawater. No further change is noticed as the GFC is pulled through the column.

In the A+B configuration the only change in heavy metal concentration is for iron and mercury. The iron concentration increases by an order of magnitude as the GFC is loaded and submerged into the column. No further change is noticed even after the GFC is pulled through the ring. The mercury concentration decreases by an order of magnitude as the GFC is loaded and submerged, but increases by two orders of magnitude as the GFC is pulled through the ring.

In the A+D configuration, the only noticeable change in heavy metal concentration occurs for mercury, which decreases by an order of magnitude as the GFC is loaded and submerged. No further change in concentration is observed when the GFC s pulled through the ring.

Table 5.1 Chemical Analysis for Barge Simulation Tests

	A			A+B			A+D		
	1	2	3	1	2	3	1	2	3
Chemical	mg/l	mg/l	mg/l	mg/l	mg/l	mg/l	mg/l	mg/l	mg/l
NH_3 –N	0.21	0.993	1.16	0.212	0.746	1.28	0.224	0.968	1.17
TOC	1.5	3.4	3.7	1.3	3.7	4.4	1.2	6.8	7.2
Chromium	0.00882	0.00950	0.0111	0.00745	0.00830	0.00716	0.0110	0.0081	0.00806
Copper	0.0239	0.0344	0.0369	0.0247	0.0244	0.0269	0.0266	0.0277	0.0293
Iron	0.398	0.602	0.612	0.050	0.395	0.349	0.0850	0.0747	0.080
Manganese	0.0267	0.0357	0.0369	0.0287	0.0285	0.0327	0.0286	0.0319	0.0331
Mercury	0.00001	0.000002	0.000002	0.00001	0.000002	0.00020	0.000029	0.000003	0.000002
Lead	0.0002	0.00718	0.00667	0.00108	0.00224	0.00265	0.00184	0.00733	0.00274
Arsenic	0.0020	0.0020	0.0027	0.0021	0.0020	0.0020	0.0033	0.0020	0.0022
Cadmium	0.00009	0.00008	0.00008	0.00009	0.00008	0.00008	0.00008	0.00008	0.00008
Zinc	0.0170	0.0280	0.0343	0.0226	0.0221	0.0211	0.0700	0.0705	0.0671
Nickel	0.0139	0.0149	0.0322	0.0150	0.0118	0.0130	0.0146	0.0143	0.0145
Silver	0.00022	0.00037	0.00037	0.00015	0.00021	0.00020	0.00016	0.00012	0.00013
PAH	<0.005	<0.005	<0.005	<0.005	<0.005	<0.005	<0.005	<0.005	<0.005
PCB	<0.003	<0.003	<0.003	<0.003	<0.003	<0.003	<0.003	<0.003	<0.003
Dioxins	$<2x10^{-7}$	$<2x10^{-7}$	$<2x10^{-7}$	$<2x10^{-7}$	$<2x10^{-7}$	$<2x10^{-7}$	$<2x10^{-7}$	$<2x10^{-7}$	$<2x10^{-7}$
Furans	$<2x10^{-7}$	$<2x10^{-7}$	$<2x10^{-7}$	$<2x10^{-7}$	$<2x10^{-7}$	$<2x10^{-7}$	$<2x10^{-7}$	$<2x10^{-7}$	$<2x10^{-7}$
TSS	4.8	21.6	25.0	7.0	8.3	9.3	15.8	6.8	4.8
pH	7.96	7.93	7.92	7.76	7.73	7.73	7.8	7.72	7.72

5.4.2 TOC

Table 5.1 also summarizes results for TOC determined during the Barge simulation test. After loading the sediment into the GFC in all three configurations and allowing it to be submerged for one hour, TOC concentrations increased. A slight increase was also noticed after the GFC was pulled through the ring.

5.4.3 PAHs

Table 5.1 summarizes the results of the PAH analysis of effluent from the A, A+B, and A+D respectively. A more detailed analysis is presented in appendix D.4-6. For the various fabric configurations, the PAH results indicate that there was no significant increase in the concentration of PAHs after submersion (Sample 2) and after pulling the GFCs through the ring (Sample 3). Individual PAH concentrations less than MDL (0.0003 mg/l) are not surprising when dilution from the barge simulation tank is considered.

An assumption was made that the volume of pore water exiting the GFCs during the barge simulation tests is equal to the volume of pore water leached during the hanging bag tests. The PAH concentrations in this pore water are also assumed to be equal to the PAH concentrations measured in the hanging bag filtrates. From these assumptions it was possible to calculate the PAH concentrations expected in the barge simulation tests. Using the highest observed concentration from the hanging bag tests (0.00208 mg/l) and the volume of water leached during that test (approximately 15 L) gives a mass of 0.0312

mg. The concentration in the barge simulation test, after dilution with 200 L of clean water is 0.0312 mg/200 L that gives 0.000156 mg/l approximately one half of the MDL of 0.0003 mg/l.

As discussed earlier, the GFCs were pulled through the ring during the barge simulation tests in order to account for the effects of changes in GFC geometry during GFC deployment. This "squeezing "effect should increase the amount of pore water exiting the GFCs, thereby increasing PAH concentrations in the barge simulation tank. Since all the observed PAH concentrations in the barge simulation tests were less than MDL, dilution effects were greater than the effects of squeezing the GFCs through the ring. These results indicate that PAH migration will not severely impact water quality when deploying a GFC containing New York Harbor sediment.

5.4.4 PCBs

Table 5.1 summarizes the results of the PCB analysis of effluent from the A, A+B, and A+D respectively. A more detailed analysis is presented in appendix D.1-3. Although in most of the analysis there is a very slight increase after submersion and after the GFC is pulled through the ring, the concentrations are on the order of <0.00003 ppm. Using a similar analysis as was done for PAH, we consider the highest observed concentration from the hanging bag test 0.00013mg/l. Again using the volume of water leached during this test (approximately 15 L) we obtain a mass of 0.00195 mg. When this is diluted with 200 liters of clean water the resulting concentration is 9.75×10^{-6} mg/l. This is

approximately 1/3 less than the instruments MDL of 0.00003 mg/l for the majority of the PCBs. Here also the squeezing effect of pulling the GFC through the ring is expected to increase the pore water exiting the GFC resulting in an increase in PCB concentration in the barge simulation tank. Since the observed PCB concentrations in the barge simulation tests were less than the MDL, the implication is that dilution effects were greater than the effects of squeezing the GFCs through the ring, as with the PAH data. Therefore this slight migration of PCBs will also not severely impact water quality during the deployment of a GFC containing New York Harbor sediment.

5.4.5 Dioxins and Furans

Table 5.1 summarizes the results of analysis for Dioxins and Furans. A more detailed analysis is presented in appendix D.7-9. It was found that most of the concentrations were undetectable. Few Dioxins and Furans were detected at low concentrations (picograms per liter).

Chapter 6

Fabric Apparent Open Size under Strain Test

6.1 Background

The purpose of this experiment was to determine the variation in the apparent opening size of the geotextile containers when exposed to different strains. During deployment of the containers at the disposal site, various stresses and strains will be experienced by the geotextiles as the containers are squeezed throughout the hull of the barge as shown in Figure 6.1. It is anticipated that the strain acting on the geotextile fabric will result in a variation in the AOS, ultimately impacting the quantity and rate of migration of fines through the container. The test is a modification of ASTM's designation D 4751 the major difference being that the geotextile being tested is under a predetermined strain.

1.2 Apparatus

The following apparatus was required to conduct the experiment:

1. A fabric-straining device is shown in Figure 6.2.
2. The GFCs supplied by the Nicolon Corporation were cut into rectangles of 24 by 20 cm along both the warp and weft directions.
3. Spherical glass beads were utilized with varying sizes

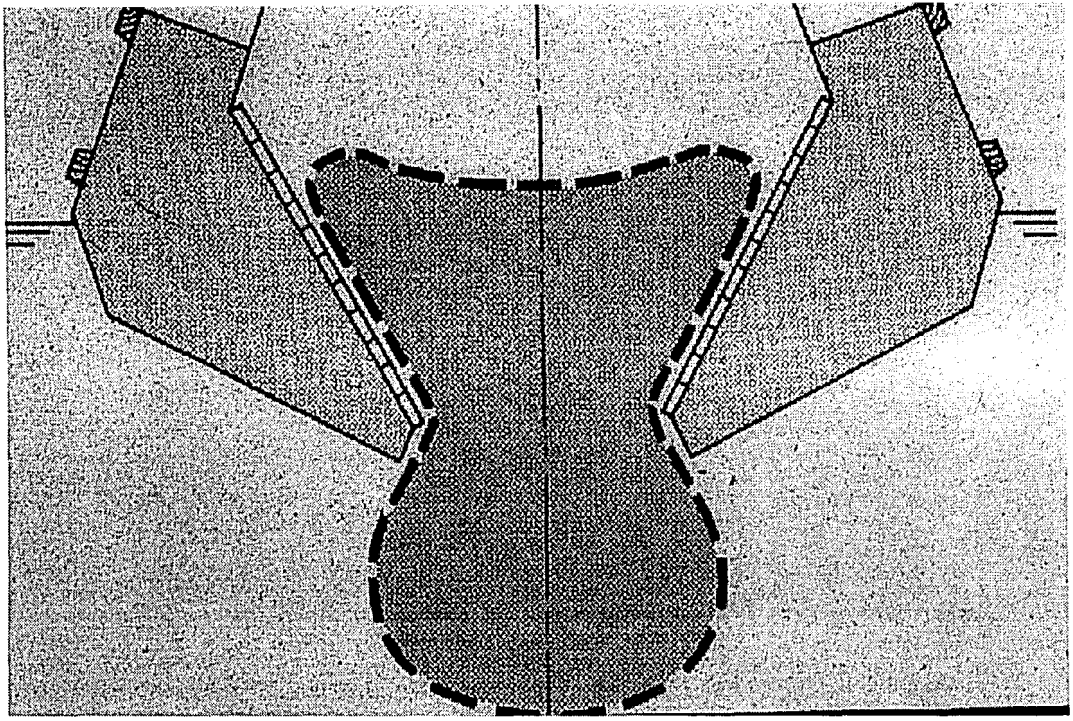

Figure 6.1 GFC Being Squeezed Through the Hull of a Barge.

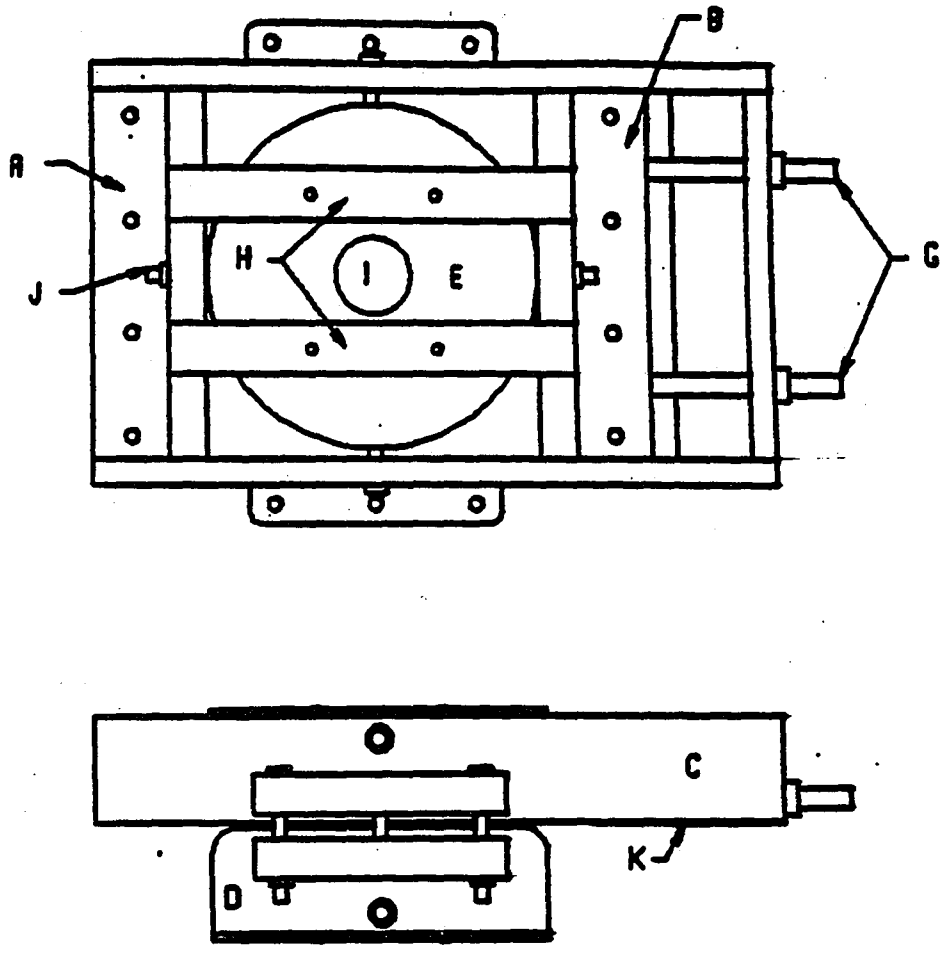

A: FIXED SAMPLE CLAMP
B: ADJUSTABLE SAMPLE CLAMP
C: UPPER JIG FIXTURE
D: LOWER JIG FIXTURE
E: UPPER SIEVE CUP
F: LOWER SIEVE CUP
G: ADJUSTING SCREWS FOR SAMPLE STRETCHING
H: SIEVE CUP RETAINING PLATES
I: SIEVE CUP LOADING PLUG
J: SIEVE CUP ALIGNMENT BOLTS TYP. 8 PLACES
K: ADJUSTABLE SAMPLE CLAMP RETAINING BOLTS

Figure 6.2 Fabric Straining Apparatus.

4. A Heavy duty Triple beam weighing balance with a capacity of 20 Kg was used to measure the weight of the fabric straining device
5. A Mettler balance with a capacity of 0-2500 g and accurate to 0.01 g was used to weigh the glass beads and geotextile samples.
6. A commercial spray Static Guard was used for static elimination
7. A Rototap mechanical Sieve Shaker was used to shake the fabric-straining device.
8. A 1.5 Hp (1.12 kilowatts) Sears Craftsman air compressor with an air delivery rate of 7.0 scfm at 40 psi (276 kPA), and 5.5 scfm at 90 psi (621 kPA) with a capacity of 12 gallons (45 liters) was utilized.
9. A Drying Oven.

6.3 Procedures

1. The specimens tested were prepared according to ASTM's D 4751 specimen preparation section.
2. Each of the geotextiles tested was initially coated uniformly with Static guard.
3. The geotextile being tested was then secured firmly on the straining device, such that at 0% strain the fabric was taut with no wrinkles or bulges. Initially there is no strain so this is at 0% strain.
4. Before mounting the bottom receiving cup onto the straining device, its weight was recorded

5. Before mounting the bottom cup onto, the weight of the straining device, including the geotextile was recorded
6. Fifty grams of the glass beads starting with the smallest diameter were then placed on top of the geotextile through the upper sieve cup-loading plug as shown in Figure 6.2. A set of 4 marbles was also placed on top of the geotextile. The upper sieve cup was then closed and secured.
7. The weight of the straining device, geotextile, and glass beads was then recorded.
8. The receiving cup was mounted onto the straining device.
9. The straining device, geotextile and bead configuration was secured onto a mechanical sieve shaker. A 2.54-cm block had to be placed between the straining device, and the hammer on the sieve shaker to ensure adequate contact. Marbles were used to aid in the bouncing of the glass beads so as to ensure that all the various orientations were presented to the sieving surface. This configuration was agitated for 15 minutes. Five specimens were tested from each of the five different geotextiles.
10. The bottom-receiving cup was then removed from the straining device, and its new weight recorded.
11. The weight of the straining device minus the bottom cup was also recorded.
12. The glass beads were then emptied out of both the receiving cup and the geotextile secured onto the straining device. To ensure that all the glass beads were removed, compressed air was blown through the geotextile, until the original weight was attained.

13. Steps 6 through 12 were repeated using the next larger bead size. This trial was repeated using successively larger bead sizes until the weight of the fraction that passed through was 5% or less.
14. The geotextile was then strained to the next marking, and steps 4 through 13 repeated. This trial by increasing strain was repeated until a maximum strain of 9% (The maximum strain that can be applied on the GFC before failure occurs).

6.4 Results

For each size of beads tested with each specimen, the percent of beads passing through the specimen is plotted against the bead size of each of the beads sizes used for each specimen on a semilog scale. The apparent opening size (AOS) is then determined as that size at which 5% or less of beads just pass through the geotextile. A summary of the AOS determined under the various strains is presented in Table 6.1. More detailed analysis are presented in appendix E Tables E.1-23. Appendix E also shows the plots for the percent of beads passing the geotextiles (Figures E.1-19). From these plots the AOS for the A fabric at 0,3,6 and 9% strain are 0.180, 0.212, 0.300, and 0.425 mm respectively. Fabric B at 0,3,6 and 9% strain has an AOS of 0.150, 0.150, 0.150, and 0.106 mm respectively. Fabrics C and D have an AOS of 0.106 mm at all strain values. The AOS for fabric E at 0,3,6 and 9% strain is 0.075 mm. A comparison of the obtained AOS with those specified by the manufacturers at 0% strain, reveal a much lower value for the AOS. This difference in values could be attributed to either laboratory or testing conditions.

An increase in the AOS with increase in strain was noticed for the woven fabric A. For the non-woven B fabric a slight decrease in the AOS is noticed at a 9% strain. For the other non-woven fabrics C, D, and E, there is no noticeable change in the AOS at all the strains in which they were tested.

Table 6.1 Results of Fabric Apparent Opening Size under Strain test

Strain (%)	Apparent Opening Size (AOS)				
	Fabric A (mm)	**Fabric B (mm)**	**Fabric C (mm)**	**Fabric D (mm)**	**Fabric E (mm)**
0	0.180	0.150	0.106	0.106	0.075
3	0.212	0.150	0.106	0.106	0.075
6	0.300	0.150	0.106	0.106	0.075
9	0.425	0.106	0.106	0.106	0.075

Chapter 7

Filtration Tests under Strain

7.1 Background

Bench top filtration tests were conducted to obtain information on the release of fines from the geosynthetic fabrics as these fabrics are exposed to various strains. The filtration procedure described in this method simulates the migration of fines through a GFC that is under strain. Cake formation results from the application of an applied load. As stated in chapter 3, cake formation due to self-weight consolidation occurs during the dredging operation, when the GFC is filled with the sediment. Cake formation also occurs after placement of the GFC in the disposal facility and is caused by consolidation under a hydrostatic pressure. Regardless of how the cake formation occurs and where the cake is formed the GFC may be distorted slightly resulting in strain being placed on its fabric. This strain may affect the amount and or rate of migration of fines from the GFC.

7.2 Apparatus

1. A Millipore Hazardous Waste Filtration System (Millipore Corporation, Bedford Ma) was used to conduct the pressure filtration tests as shown in Figure 3.1. This pressure filtration device is used for the Toxicity Characteristic Leaching Procedure (TCLP) in

hazardous waste testing (U.S. Environmental Protection Agency (EPA), 1982). The filtration device is made of stainless steel and is coated with Teflon to eliminate heavy metal contamination. A fabric straining device as shown in Figure 6.2. This device is marked with settings for 0,3,6 and 9% strains respectively.

2. A Customized filter holder that is able to hold the geotextiles under strain was utilized Figure 7.1. This filter holder was designed such that once the geotextile configuration being tested was secured onto it, the holder could be placed within the filtration device. The filtration area is approximately 41 cm^2, which is a reduction in filtration area from 97 cm^2 without the straining device.

7.3 Procedure

1. The geotextile being tested was secured firmly on the straining device, such that at 0% strain the fabric was taut with no wrinkles or bulges.
2. The customized filter holder was then secured onto the geotextile by sandwiching the geotextile between the two sides of the filter holder. The geotextile was then cut out of the straining device such that only the filter holder held the strained geotextile.
3. The lower portion of the filtration apparatus was assembled. The geosynthetic fabric and the customized filter holder were weighed.
4. The geosynthetic fabric was soaked in distilled water allowed to drip dry, and placed on the filter holder.

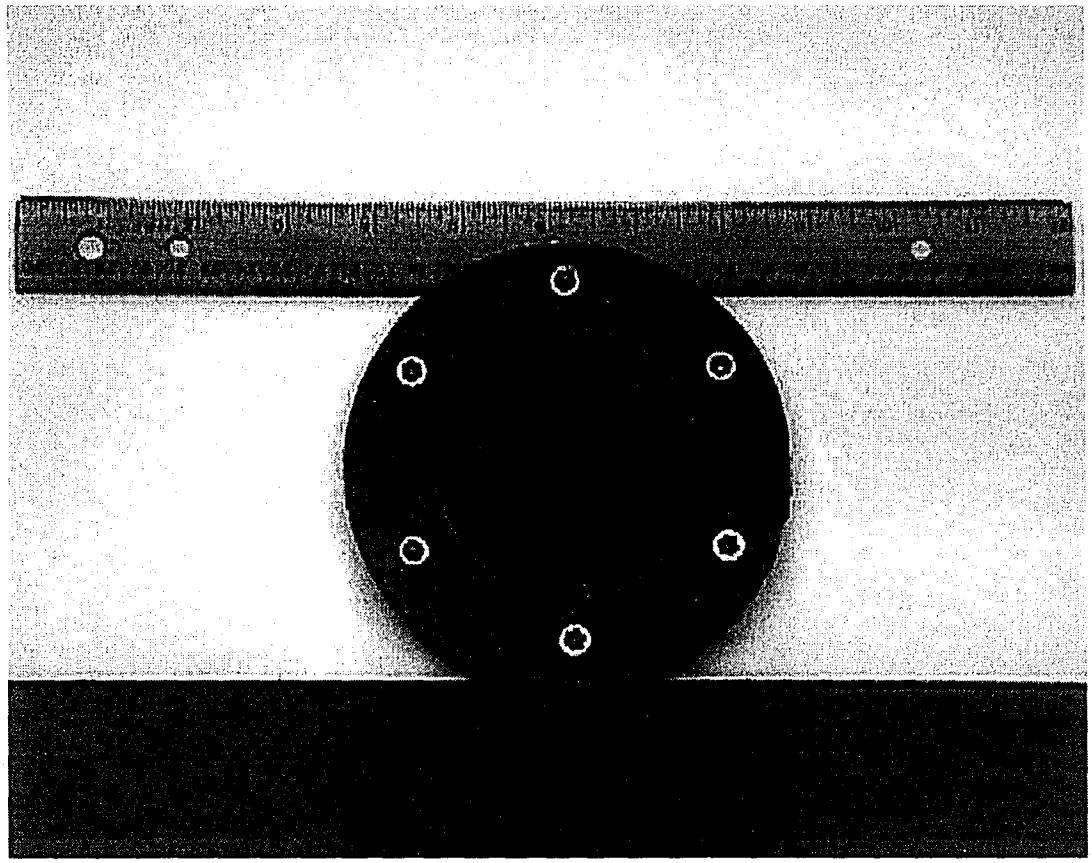

Figure 7.1 Strained Geotextile on Filter Holder.

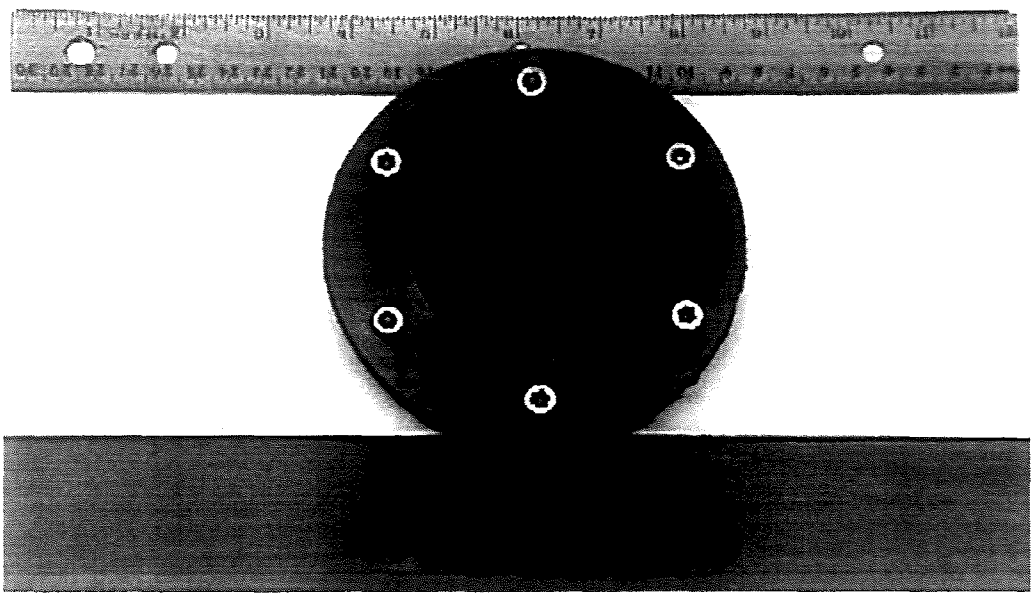

Figure 7.1 Strained Geotextile on Filter Holder.

The filter holder containing the geotextile configuration was then placed into the filtration apparatus, and approximately 200 grams of the sediment was weighed and placed into the filtration device. The slurry was allowed to settle before running the test.

5. The top plate was placed on top of the chamber and sealed. Silicone grease was used to reduce the loss of pressure between the chamber and the upper and lower plates.
6. Pressure from the nitrogen cylinder was gradually applied on top of the sample, until the desired pressure was achieved.
7. The volume of the filtrate was measured using a 100 ml graduated cylinder.
8. Tests were conducted until the pressure began to decrease, and no more filtrate passed through the filter. When consolidation of the sediment at the applied pressure was completed, the filter cake ruptured which caused a decrease in the applied pressure.
9. The filtration apparatus was disassembled, and the final water content of the filtered cake was obtained using ASTM procedure D-2216.
10. Total suspended solids (TSS) tests (Standard Methods for the Examination of Water and Wastewater method 2540D) were conducted on the collected filtrate.

7.4 Results

Attempts to carry out filtration tests at 5 psi (34.5 kPa) were not successful since this pressure was too low to give any filtrate. Thus, filtration tests of the contaminated sediment were conducted at pressures of 10 psi (69 kPa) and 20 psi (138 kPa). Three

samples for each configuration, and at the four different strains, resulting in a total of 120 filtration tests. A summary of the results showing the initial and final water contents, initial solids concentration, final TSS of the filtrate, and the filtering efficiency is presented in Tables 7.1 and 7.2. More detailed analysis is presented in appendix F Tables F.1-7.

The filtration efficiency is determined using equation 3.1. At all configurations and under all strains the filtering efficiency was at least 99.9%. It was noticed that the filtrate although pretty clear, contained more suspended solids for the unlined configuration with fabric A, as opposed to the lined configurations. The general trend was that filtrate TSS seemed to decrease with the utilization of a heavier weight liner in the configuration. Figures 7.2 and 7.3 plots the TSS and Fabric weight relationship at 69 and 138 kPA respectively. Both plots follow a second order linear regression with equations:

$$y = 213.79 - 0.74x + 7.61x^2 \quad (7.1)$$

$$y = 246.06 - 0.9x + 9.55x^2 \quad (7.2)$$

Equations 7.1 and 7.2 are for figures 7.2 and 7.3 respectively where:

'y' = TSS in mg/l and 'x' = fabric weight in g/m^2

Figures 7.4-7.7 plot the relationship between TSS and AOS at 0, 3, 6, and 9% strain. All the relationships are second order linear relationships and these relationships are determined by the following equations

Table 7.1 Filtration Results at 10 psi (69 kPA)

Fabric	Initial Water Content (%)	Final Water Content (%)	Initial TS (mg/l)	Filtrate TSS (mg/l)	Filtering Efficiency (%)
A					
0%	203.5	115.2	491390.9	192.5	99.9
3%	186.5	128.7	536193.	208.8	99.8
6%	196.4	118.8	509165.0	217.9	99.9
9%	210.2	131.7	47537.4	240.6	99.9
A+B					
0%	201.6	115.0	496031.7	117.9	99.9
3%	203.6	115.1	491159.1	120.4	99.9
6%	208.2	121.5	480307.4	129.4	99.9
9%	206.0	121.2	485436.9	132.1	99.9
A+C					
0%	202.2	117.5	494559.8	58.2	99.9
3%	196.8	121.2	508130.1	64.6	99.9
6%	203.6	120.8	491159.1	76.9	99.9
9%	187.6	128.9	533049.0	79.8	99.9
A+D					
0%	180.5	119.6	554016.6	33.2	99.9
3%	194.6	115.2	513874.6	42.3	99.9
6%	214.8	137.0	465549.3	53.8	99.9
9%	183.2	124.2	545851.5	36.2	99.9
A+E					
0%	182.3	123.6	548546.4	40.0	99.9
3%	201.4	118.6	496524.3	38.7	99.9
6%	210.5	117.7	475059.4	44.0	99.9
9%	198.6	120.6	503524.7	28.0	99.9

Table 7.2 Filtration Results at 20 psi (138 kPA)

Fabric	Initial Water Content (%)	Final Water Content (%)	Initial TS (mg/l)	Filtrate TSS (mg/l)	Filtering Efficiency (%)
A					
0%	198.6	111.0	503524.7	249.1	99.9
3%	211.3	118.7	473260.8	270.2	99.9
6%	186.7	105.5	535618.6	295.4	99.9
9%	198.2	112.7	504540.9	307.4	99.9
A+B					
0%	212.1	124.7	471475.7	133.7	99.9
3%	215.6	128.1	463821.9	134.4	99.9
6%	179.3	114.7	557724.5	137.6	99.9
9%	208.9	113.0	4786997.9	160	99.9
A+C					
0%	208.4	116.0	479846.4	76.4	99.9
3%	209.7	110.8	476871.7	82.8	99.9
6%	211.1	110.8	473709.1	77.7	99.9
9%	211.5	106.3	472813.2	81.6	99.9
A+D					
0%	206.5	113.2	484261.5	39.2	99.9
3%	199.6	120.4	501002.0	33.8	99.9
6%	206.3	120.7	484731.0	24.2	99.9
9%	214.6	114.9	465983.2	45.4	99.9
A+E					
0%	199.3	109.9	501756.1	37.4	99.9
3%	197.5	113.9	506329.1	31.7	99.9
6%	209.5	122.2	477327.0	16.9	99.9
9%	193.9	115.0	515729.8	70.8	99.9

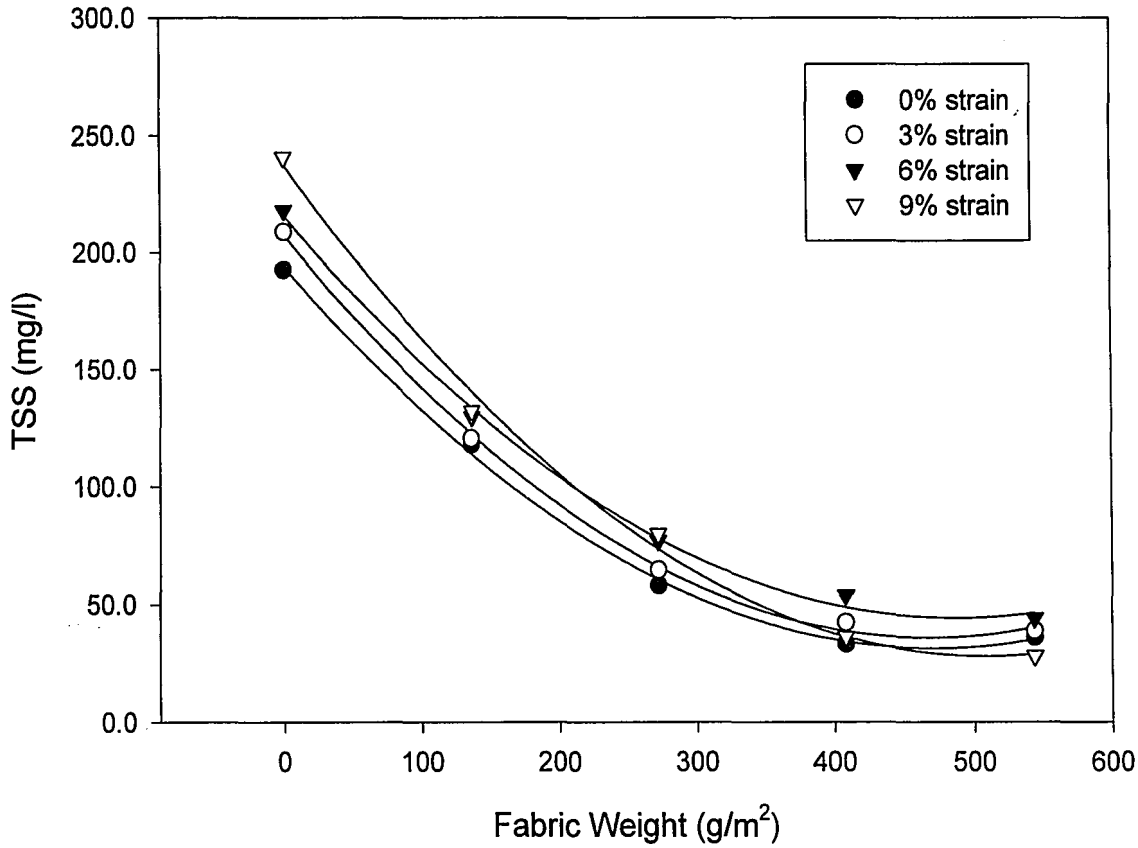

Figure 7.2 TSS vs. Fabric Weight at 69 kPA

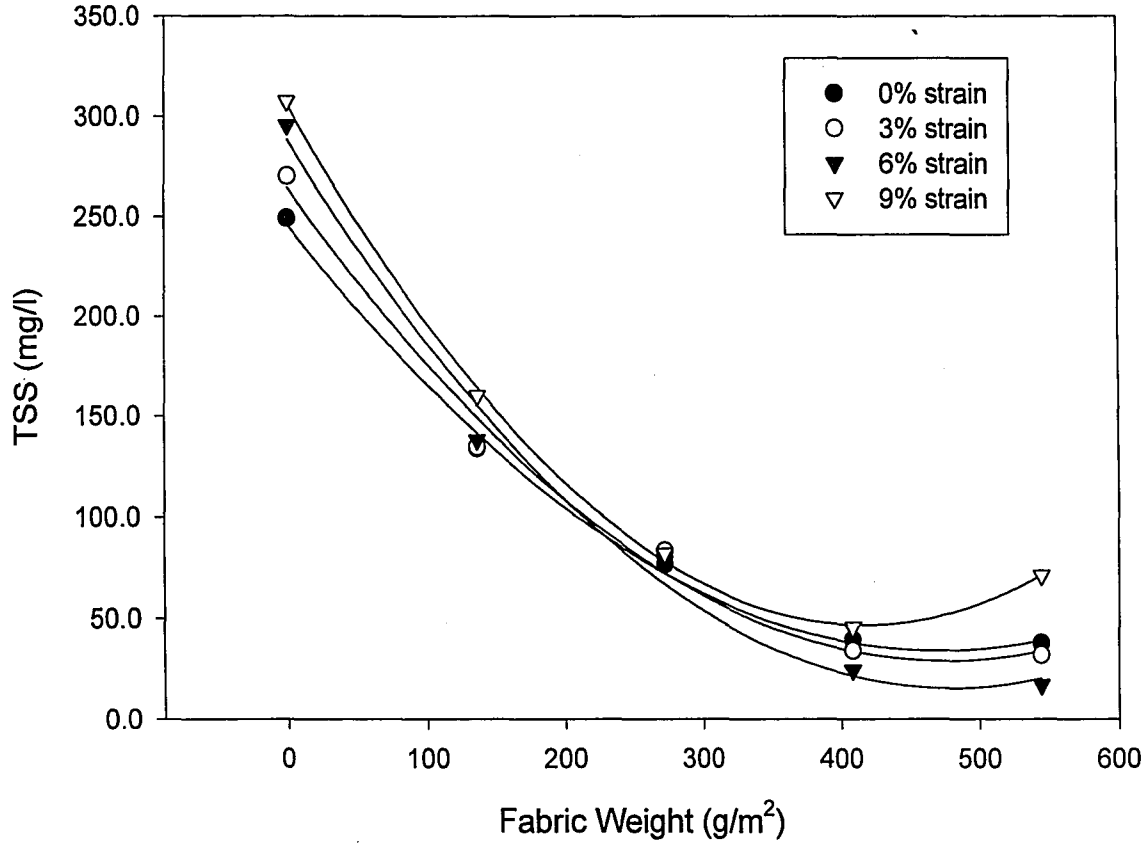

Figure 7.3 TSS vs. Fabric Weight at 138 kPA

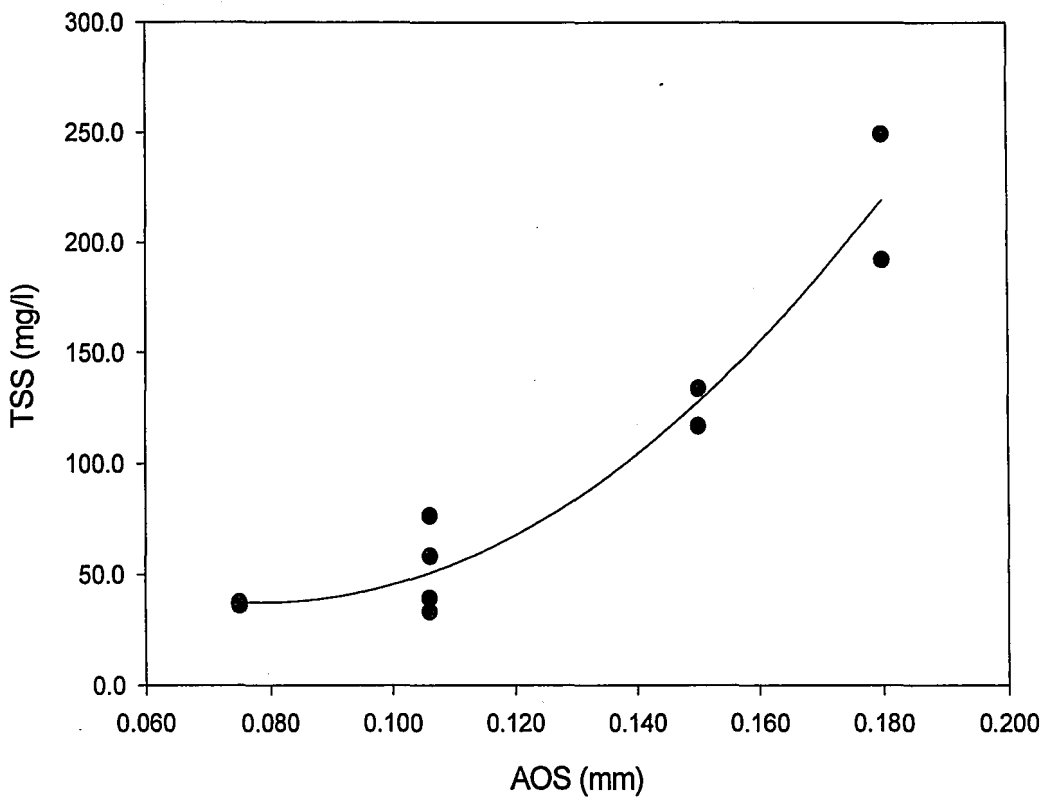

Figure 7.4 TSS vs. AOS at 0% strain

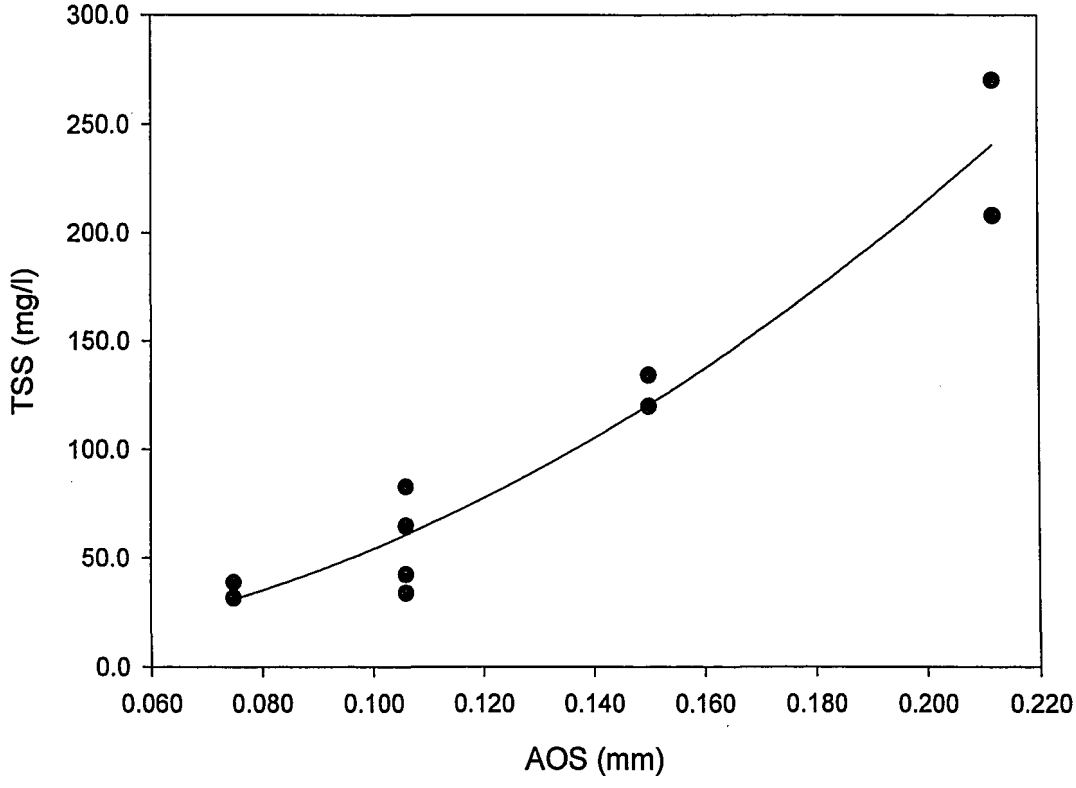

Figure 7.5 TSS vs. AOS at 3% strain

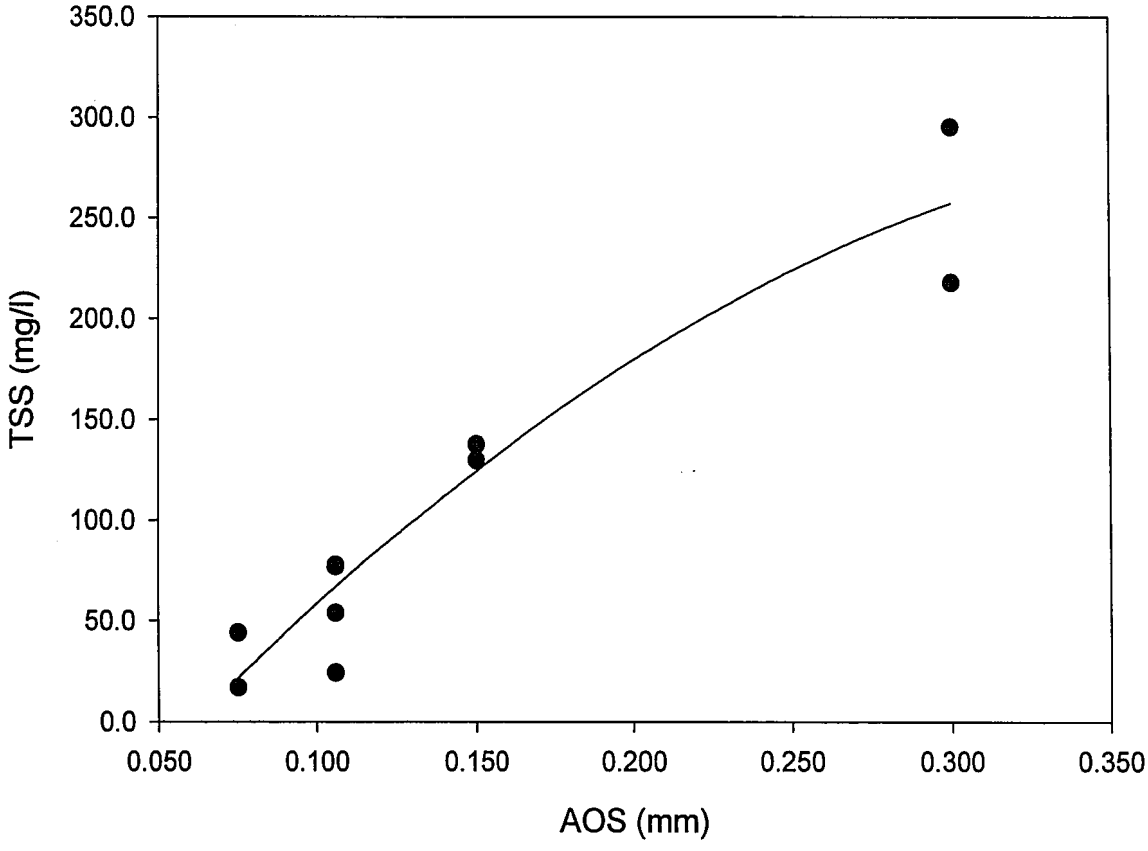

Figure 7.6 TSS vs. AOS at 6% strain

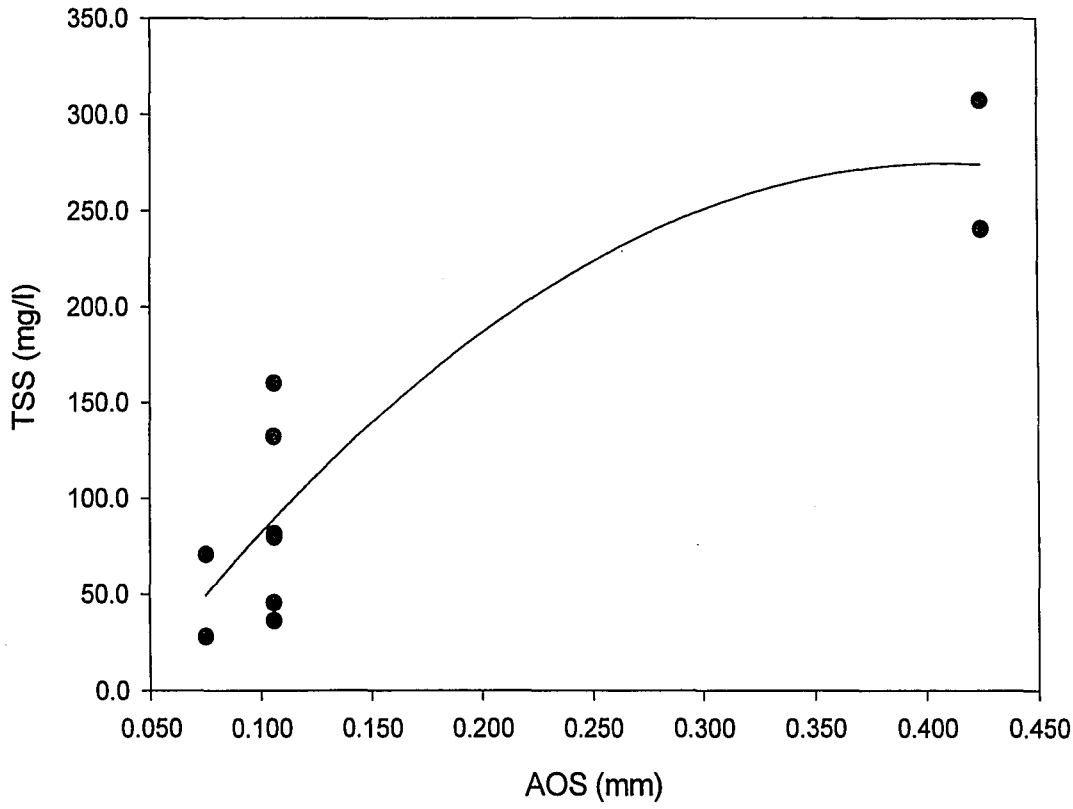

Figure 7.7 TSS vs. AOS at 9% strain

$$y = 124.55 - 2323.70x + 15028.62x^2 \quad (7.3)$$

$$y = 0.239 + 133.33x + 4038.60x^2 \quad (7.4)$$

$$y = -73.80 + 1619.73x - 215.49x^2 \quad (7.5)$$

$$y = -133.33 + 2422.97x - 3630x^2 \quad (7.6)$$

Equations 7.3-7.6 are for plots 7.4-7.7 respectively, where 'y' = TSS in mg/l and 'x' = AOS in mm. Figures 7.8 and 7.9 plot TSS vs. Strain for the five configurations at 69 and 138 kPA respectively. All the plots follow a first order linear relationship determined by the following equations:

$$y = 191 + 5.11x \quad (7.7)$$

$$y = 117.25 + 1.73x \quad (7.8)$$

$$y = 58.31 + 2.57x \quad (7.9)$$

$$y = 38.32 + 0.68x \quad (7.10)$$

$$y = 39.46 - 0.62x \quad (7.11)$$

$$y = 250.51 + 6.67x \quad (7.12)$$

$$y = 129.08 + 2.74x \quad (7.13)$$

$$y = 78.06 + 0.35x \quad (7.14)$$

$$y = 34.31 + 0.30x \quad (7.15)$$

$$y = 26.41 + 2.84x \quad (7.16)$$

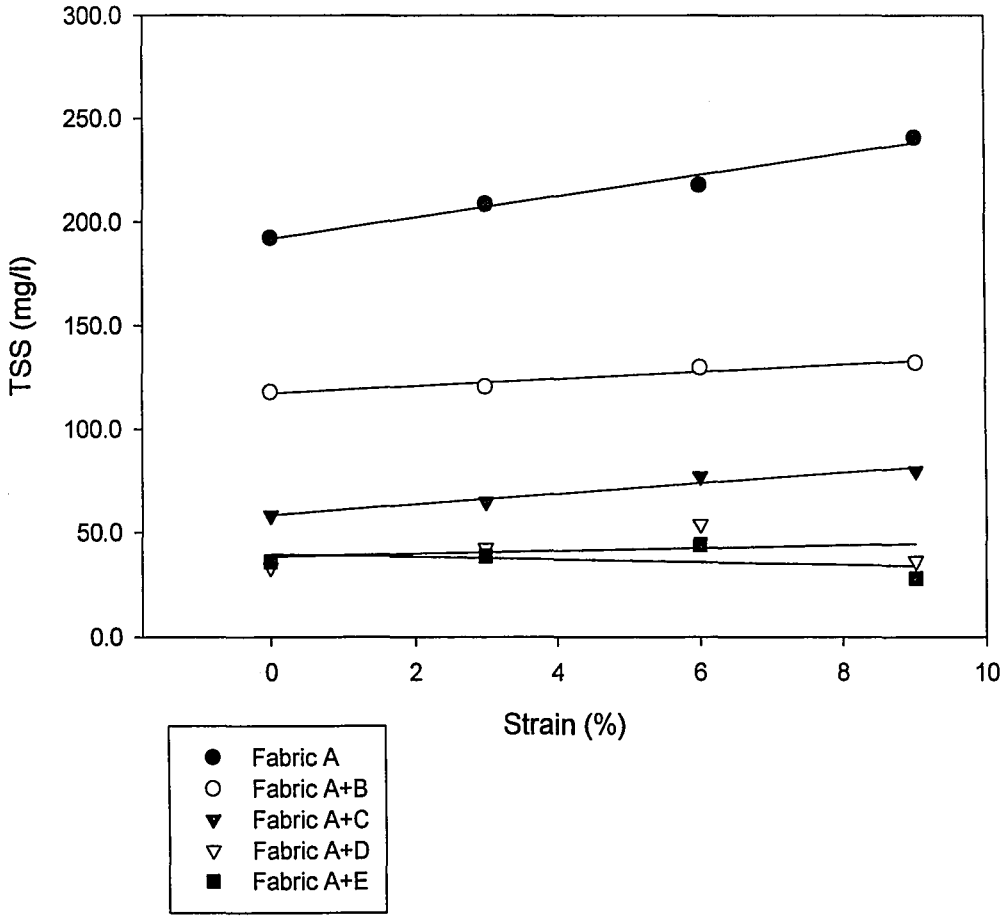

Figure 7.8 TSS vs. Strain at 69 kPA

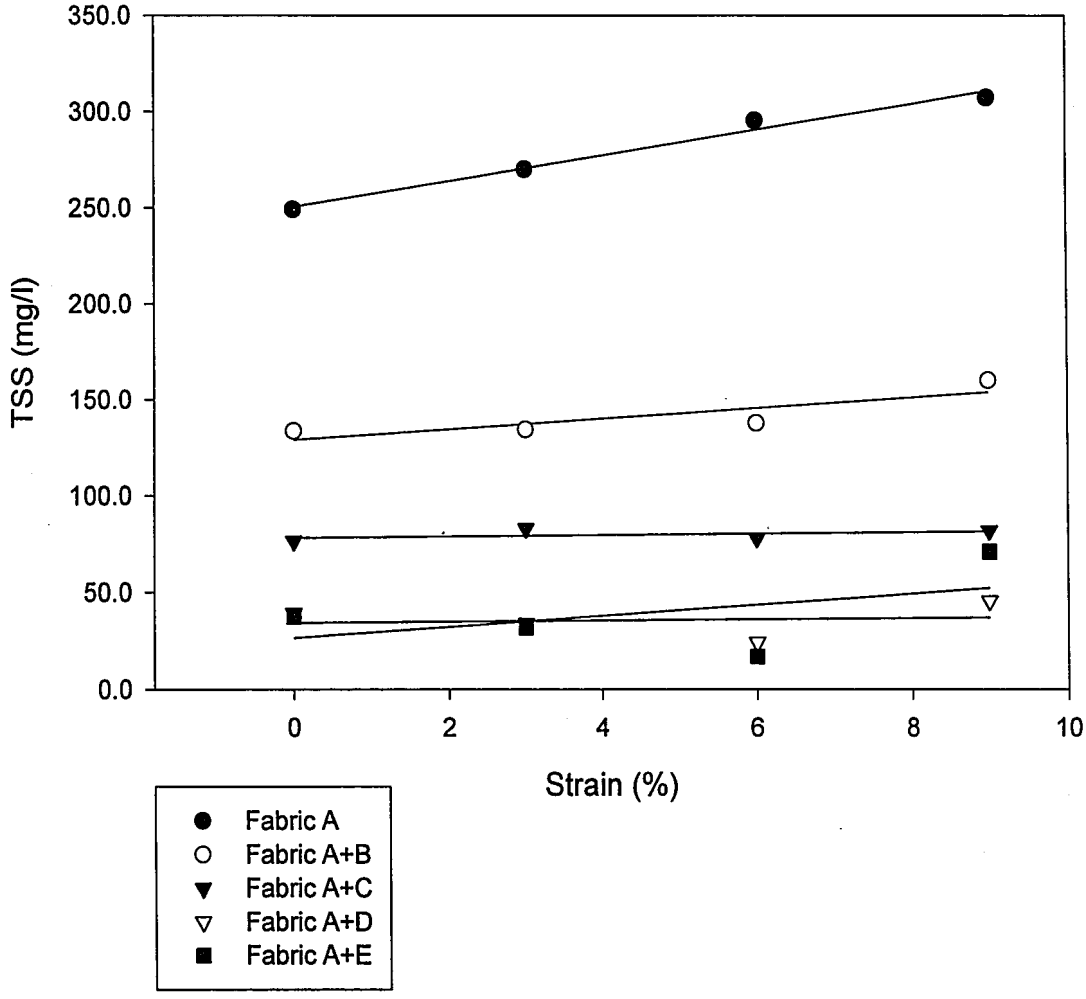

Figure 7.9 TSS vs. Strain at 138 kPA

Equations 7.7, 7.8, 7.9, 7.10, and 7.11 are the linear relationships of fabric configurations A, A+B, A+C, A+D, and A+E respectively at 69kPA. Equations 7.12, 7.13, 7.14, 7.15, and 7.16 are the linear relationships of fabric configurations A, A+B, A+C, A+D, and A+E respectively at 138 kPA, where 'y' is TSS in mg/l and 'x' is the strain in percent.

An increase in the pressure applied also showed a marked increase in the filtrate TSS. This indicates that although a certain configuration may be able to filter out various solids under lighter loads an increase in pressure forces these solids through the filter. This could be attributed to the openings or pore spaces being enlarged. Another explanation to this increase could be due to blocking; a filtration mechanism that involves the structural modification of fabric see Figure 7.1 (Mylnarek et al., 1990). A breakup of these blocked particles due to a pressure increase could also explain the increase in suspended solids that would otherwise be trapped by the filter.

The rate of filtrate collection was very erratic and initially there seemed to be some resistance to its passage. When the filtrate eventually passed through the filter, it did not come out smoothly as one would expect, but rather seemed to burst through the geotextile configuration in a very short period of time. Even though consolidation is taken into account, it only explains the time lag before any filtrate is observed. (Dierickx, 1996) noted that some geotextiles require substantially high water heads before flow can be initiated. This phenomenon is what we believe accounts for this sudden release of filtrate.

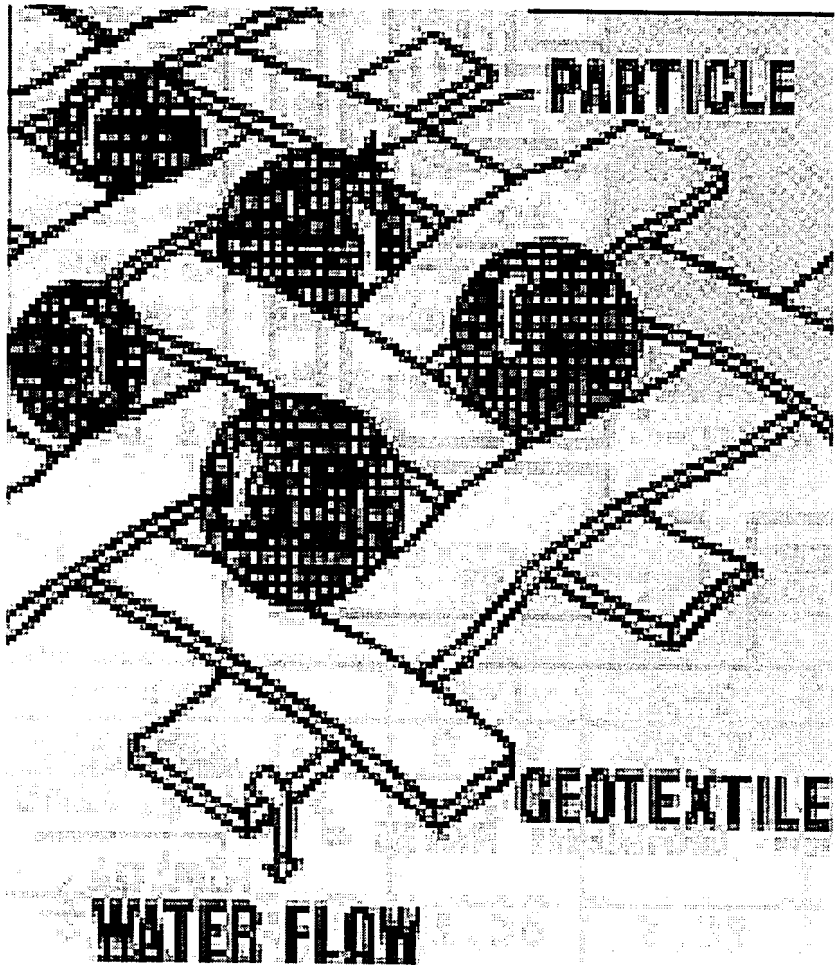

Figure 7.10 Schematic of Blocking Mechanism

Chapter 8

Conclusions

The feasibility of using GFCs to contain contaminated sediment from the New York Harbor was studied. Laboratory filtration tests were conducted to determine the flow rate of suspended solids through a GFC system. Hanging bag tests were conducted to determine the release of fines and contaminants through a GFC system. Laboratory barge simulation tests were conducted to estimate the release of contaminants through the GFC when the sediment is reworked. Fabric AOS strain tests were conducted to determine the variation in the apparent opening size with strain. Pressure filtration tests were conducted on the fabrics under strain to determine how the release of fines would be affected. From these tests, the following conclusions were drawn:

1. Filtration tests showed that GFC fabrics reduce the amount of TSS migrating to the water column in comparison to open water disposal. The D fabric has the lowest TSS concentration passing through the material.
2. Hanging bag tests revealed that the contaminant concentration (Heavy metals, PAH, PCB, Dioxins and Furans) passing through the GFC are much lower than the contaminant concentrations in the sediment. This suggests that there is a low

contaminant release rate. The A+D GFC configuration will contain the sediment and reduce water quality impacts.

3. Barge simulation tests showed that hydrophobic organic chemicals (PAH, PCB, Dioxins and Furans) released from GFCs would not significantly impact the water column. However, ammonia and TOC concentrations may increase in water immediately adjacent to a GFC during deployment from a barge. It is assumed that contaminant (PAH, PCB, Dioxins and Furans) concentrations in the pore water from the Hanging bag test filtrate are equal to the contaminant (PAH, PCB, Dioxins and Furans) concentrations from the pore water in the Barge simulation test. The squeezing effect as the GFC is pulled through the ring is expected to increase contaminant (PAH, PCB, Dioxins and Furans) concentration in the barge simulation tank. All the observed contaminant (PAH, PCB, Dioxins and Furans) concentrations were less than MDL showing that dilution effects were greater than the effects of squeezing the GFCs through the ring. It was shown that due to dilution effects Barge simulation results indicate that the A+D configuration will have the least impact on the water column.
4. Fabric AOS under strain tests show that with the exception of the outer strength layer, strain should not greatly affect particle retention performance of the GFC. Any Strain above 10% will rupture the outer strength layer and ultimately cause the GFC to fail. Therefore no testing was conducted beyond 9% strain.
5. Filtration tests with varying strain indicate that the geotextiles were more than adequate in filtering the solids, and the strain did not greatly affect their performance.

6. Field trials to determine the strains experienced by GFCs show that maximum stress occur when the GFCs are exiting the barge (Fowler et al 1994; Fowler and Toups, 1996). Analysis conducted on a 3058 cubic meter GFC filled with New York harbor sediment revealed a maximum strain of about 5% (Fowler and Toups, 1996). From the laboratory experiments conducted in this study, a GFC of 3058 cubic meter should perform adequately in containing the contaminated sediment. Important parameters that may govern the proper functioning of a GFC include seam strength, and the weight of dredged material supported by the fabric over the barge opening (Fowler and Toups, 1996). Seam strengths that are less than the maximum stresses experienced by the GFC will cause the GFC to fail. GFCs that are very large may fail if the maximum weight of the submerged sediments as the GFC is exiting the barge impart stresses greater than the maximum stresses the fabric can handle. There is a need for better designs to minimize the friction the GFCs experience as they exit the barge.

Chapter 9

Recommendation for Future Work

Current laboratory procedures provide no measurement of contaminant sorption and retention by GFCs. Hydrophobic organic contaminants, such as polychlorinated biphenyl's (PCBs) and polychlorinated dibenzo-p-dioxins/furans (PCDDs/PCDFs) are known to sorb to organic material. Since the GFCs are synthetic organics, sorption and retention by the liners and outer fabric may reduce the transmission of dissolved PCBs and PCDDs/PCDFs. This effect is over and above the particle retention properties of GFCs. Equilibrium and kinetic adsorption constants should be determined in the laboratory batch measurements involving small pieces of GFC in contact with the contaminated sediment.

During dredged material loading, the potential for rupture of GFCs is increased by the presence of sharp objects in the dredged materials. Damage from sharp objects can also occur during impact of the GFCs with the bottom. Survivability of a GFC is critical in all applications. Tensile strength tests, puncture tests (ASTM D-3787), impact tests, tear tests (ASTM D-1424), fatigue strength tests using cyclic loading, and burst strength tests (ASTM D-774) should be conducted to obtain a better understanding of the mechanical properties of GFCs.

References

Bogossian, T., Smith, R.T., Vertematti, J.C., and Yazbek, O. (1982). "Continuous Retaining Dikes by Means of Geotextiles," *Second International Conference on Geotextiles*, Las Vegas, NV, 211-216.

Bricka, R.M., Holmes, T.T., and Cullinane, M.J. (1992). "A comparative Evaluation of Two Extraction Procedures: The TCLP and the EP," Waterways Experiment Station, *Technical Report EL-92-33.* Vicksburg, MS.

Christopher, B.R. and Holtz, R.D. (1985). "Geotextile Engineering Manual," *FHWA-TS-86-203*. Washington, D.C. Federal Highways Administration.

Duarte, F., Fowler, J., Toups, D., and Gilbert, P. (1995). "Geotextile Contained DredgedMaterial, Red Eye Crossing, Baton Rouge, LA," Final Report. Nicolon Corp.

Dierickx, W. (1996) " Determination of Water Penetration Resistance of Geotextiles," *Recent Developments in Geotextile Filters and Prefabricated Drainage* Geocomposites, ASTM STP 1281, Shobha K. Bhatia and L. David Suits, Eds., American Society for Testing and Materials.

Eckenfelder, W.W. (1966). *Industrial Water Pollution Control.* McGraw-Hill: New York.

Fowler, J. and Sprague, C.J. (1993). "Dredged material-Filled Geotextile in Containers," in *Proceedings of Coastal Zone '93,* ASCE, New York, NY, p 2415-2428.

Fowler, J., Sprague, C.J., and Toups, D. (1994). "Dredged material-Filled Geotextile Containers," *Environmental Effects of Dredging Technical Notes*, U.S. Army Waterways Experiments Station, Vicksburg, MS.

Fowler, J., Sprague, C.J., and Toups, D. (1995). "Dredged material-Filled Geotextile Containers, *Environmental Effects of Dredging Technical Notes Note EEDP –05-01*, U.S. Army Waterways Experiments Station, Vicksburg, MS

Fowler, J. and Toups ,D (1996). A 4000 CY Geotextile Container Filled With Maintenance Dredged Material, Port Authority of New York and New Jersey. Final Report. Nicolon Corp.

Garbarino, S.D., Blama, R.N., Landin, M.C., Maynord, S.R., Patin, T.R. (1994). "Environmental Restoration and Enhancement Using Dredged Material in Chesapeake Bay, Maryland." *Second International Conference on Dredging and Dredged Material*, Lake Buena Vista, FL, Vol. 1, 384-393.

Henry, K.S. and Hunnewell, S.T. (1995). "Silt Fence Testing for Eagle River Flats Dredging," *Report 95-27.* Cold Regions Research and Engineering Laboratory. Hanover, NH.

Jagt, H.J. (1988). "Bed Protection, Old Meuse, By Means of Geocontainers, *Rijkswaterstaat*, Public Works Department of the Netherlands, April.

Koerner, R.M. (1998). *Designing with Geosynthetics.* Prentice Hall, Englewood Cliffs.

Landin, M.C., Fowler, J., Allen, H.H (1994). "New Applications and Practices for beneficial uses of dredged material." *Second International Conference on Dredging and Dredged Material*, Lake Buena Vista, FL, Vol. 1, 526-536.

Mesa, C. (1995). "Containerization of contaminated dredged sediment-the Marina del Rey Experience," *Proceedings of the 25th Texas A&M Annual Dredging Seminar,* TAMU Center for Dredging Studies, College Station, TX.

Mylarnek, J., Rollin, A. L., Lafleur, J. and Bolduc, G., (1990) "Microstructural Analysis of a Soil/Geotextile System," *Geosynthetics: Microstructure and Performance*, ASTM STP 1076, I. D. Peggs, Ed., American Society for Testing and Materials, Philadelphia, pp. 137 -46.

Pilarczyk, K.W. (1994). "Novel Systems in Coastal Engineering, Geotextile System and Other Methods, An Overview," *Rijkswaterstaat*, Road and Hydraulic Engineering Division, Delft, The Netherlands.

Perrier, H. (1986). "Use of Soil-Filled Synthetic Pillows for Erosion Protection," *Third International Conference on Geotextiles*, Vienna, Austria, pp. 1115-1119.

Risko, A.J. (1995). "Memorandum for the Record, FY 95 Marina Del Ray Detailed Project Summary," *U.S. Army Engineer District*, Los Angeles, Los Angeles, CA.

U.S. Environmental Protection Agency. (1982). "Test Methods for Evaluating Solid Waste," *SW-846*, 2nd ed., Office of Solid Waste and Emergency Response, Washington, D.C.

APPENDIX A. Chemical Analysis of Sediment for PAH, PCB, Dioxin and Furan

Table A.1 PAH Analysis of Sediment

Chemical	Replicates in mg/kg						Average
	1	2	3	4	5	6	
Naphthalene	2.81	2.35	2.09	2.2	2.3	2.5	2.38
Acenaphthene	1.74	1.63	1.60	1.4	1.5	1.5	1.56
Phenanthrene	11.1	10.2	9.97	7.9	8.8	8.2	9.36
Acenaphthylene	0.12	0.08	0.09	<0.15	<0.15	<0.15	<0.15
Fluorene	2.76	2.54	2.34	2	2.1	2.1	2.31
Anthracene	5.12	6.9	4.83	4.1	4.1	4.1	4.86
Fluoranthene	18.3	16.1	17.5	18.3	16.4	16.4	17.2
Chrysene	7.9	6.51	7.63	9.4	6.5	7	7.49
Benzo (b)Fluoranthene	4.78	4.2	4.94	5.5	4.2	4.5	4.69
Pyrene	14.5	13.2	14.9	18.5	16.5	16.8	15.73
Benzo (a) Anthracene	7.54	6.52	7.52	8.7	7.1	7.7	7.51
Benzo (k) Fluoranthene	4.78	4.20	4.94	4.5	3.6	4.5	4.15
Benzo (9a) Pyrene	5.64	4.88	5.72	5	4.4	4.9	5.09
Dibenzo (A,H) Anthracene	0.80	0.55	0.65	0.99	0.9	1	0.82
2-Methylnaphthalene	1.44	1.22	1.14				
(1, 2, 3-C, D) Pyrene	3.13	2.56	3.24	3.1	2.7	2.9	2.94
Benzo (G,H,I) Perylene	3.06	2.56	3.22	2.8	2.6	2.8	2.84

Table A.2 PCB Analysis of Sediment

Chemical	Replicates in mg/kg						Avg
	1	2	3	4	5	6	mg /kg
PCB 1016	<1.0	<1.0	<1.0	<1.0	<1.0	<1.0	<1.0
PCB 1221	<1.0	<1.0	<1.0	<1.0	<1.0	<1.0	<1.0
PCB 1232	<1.0	<1.0	<1.0	<1.0	<1.0	<1.0	<1.0
PCB 1242	<1.74	<1.32	<1.32	1.04	1.08	0.851	<1.0
PCB 1248	<1.0	<1.0	<1.0	<1.0	<1.0	<1.0	<1.0
PCB 1254	<1.0	<1.0	<1.0	<1.0	<1.0	<1.0	<1.0
PCB 1260	1.95	1.47	1.43	0.82	0.93	0.657	1.21
PCB 7 24-Dichlorobiphenyl	0.0034	0.011	0.011	0.0011	<1.0	<1.0	<1.0
PCB 8 24'-Dichlorobiphenyl	0.056	0.054	0.060	0.057	0.062	0.049	0.056
PCB 15 44'-Dichlorobiphenyl	0.086	0.077	0.082	0.046	0.052	0.041	0.064
PCB 18 22'5-Trichlorobiphenyl	0.165	0.114	0.140	0.027	0.0066	0.01	0.0771
PCB 28 244-Trichlorobiphenyl	0.186	0.119	0.114	0.104	0.117	0.089	0.1215
PCB 31 24'5-Trichlorobiphenyl	0.214	0.210	0.228	0.23	0.258	0.197	0.0223
PCB 40 22'33'-Tetrachlorobiphenyl	0.010	0.010	0.011	0.014	0.0077	0.0055	0.0097
PCB 44 22'35'-Tetrachlorobiphenyl	0.102	0.098	0.107	0.051	0.056	0.042	0.076
PCB 49 22'45'-Tetrachlorobiphenyl	0.059	0.051	0.056	0.0039	<0.010	0.0037	<0.010
PCB 50 22'46-Tetrachlorobiphenyl	<0.010	<0.010	<0.010	<1.0	<1.0	<1.0	<0.010
PCB 52 22'55'-Tetrachlorobiphenyl	0.051	0.050	0.040	0.0045	0.004	0.0043	0.0256
PCB 54 22'66'-Tetrachlorobiphenyl	0.048	0.025	0.022	0.015	0.023	0.017	0.025
PCB 60 2344'-Tetrachlorobiphenyl	0.055	0.055	0.060	<0.0.0	<0.010	<0.010	<0.010
PCB 70 23'4'5-Tetrachlorobiphenyl	0.010	0.010	0.011	0.039	0.044	0.033	0.0245
PCB 77 33'44'-Tetrachlorobiphenyl	0.079	0.151	0.179	0.18	0.203	0.152	0.1573
PCB 82 22'33'4-Pentachlorobiphenyl	<0.010	<0.010	<0.010	0.025	0.031	0.024	<0.010
PCB 86 22'345-Pentachlorobiphenyl	<0.010	<0.010	<0.010	0.02	0.032	00017	<0.010
PCB 87 22'345'-Pentachlorobiphenyl	0.0066	<0.010	<0.010	0.019	0.023	0.016	<0.010
PCB 97 22'3'45-Pentachlorobiphenyl	0.0031	0.0042	0.0049	0.018	0.02	0.015	0.0109
PCB 101 22'455'-Pentachlorobiphenyl	0.069	0.064	0.066	0.036	0.041	0.031	0.0512
PCB 103 22'45'6-Pentachlorobiphenyl	<0.010	<0.010	<0.010	<0.010	<0.010	<0.010	<0.010
PCB 105 233'44'-Pentachlorobiphenyl	<0.010	<0.010	<0.010	0.029	0.032	0.024	<0.010
PCB 114 2344'5-Pentachlorobiphenyl	<0.010	<0.010	<0.010	0.0017	<0.010	<0.010	<0.010
PCB 118 23'44'5-Pentachlorobiphenyl	0.109	0.090	0.092	0.078	0.087	0.066	0.087
PCB 121 23'45'6-Pentachlorobiphenyl	<0.010	<0.010	<0.010	0.0043	0.0048	0.0035	<0.010
PCB 128 22'33'44'-Hexachlorobiphenyl	0.056	0.040	0.038	0.048	0.056	0.039	<0.010
PCB 129 22'33'45-Hexachlorobiphenyl	<0.010	<0.010	<0.010	0.013	0.013	0.012	<0.010
PCB 136 22'33'66'-Hexachlorobiphenyl	<0.010	<0.010	<0.010	0.028	0.032	0.032	<0.010
PCB 137 22'344'5-Hexachlorobiphenyl	<0.010	<0.010	<0.010	0.014	0.013	0.013	<0.010

Table A.2 cont'd PCB Analysis of Sediment

	Replicates in mg/kg						Avg
	1	2	3	4	5	6	
PCB 138 22'344'5'-Hexachlorobiphenyl	0.128	0.097	0.096	<0.010	<0.010	<0.010	<0.010
PCB 141 22'3455'-Hexachlorobiphenyl	0.061	0.040	0.037	0.015	0.017	0.017	0.0312
PCB 143 22'3456'-Hexachlorobiphenyl	0.037	0.039	0.044	0.0021	0.0021	0.0021	0.0211
PCB 151 22'355'6-Hexachlorobiphenyl	<0.010	<0.010	<0.010	0.025	0.031	0.031	<0.010
PCB 153 22'44'55-Hexachlorobiphenyl	0.120	0.091	0.089	0.079	0.102	0.102	0.0972
PCB 154 22'44'56'-Hexachlorobiphenyl	0.010	0.041	0.041	0.021	0.021	0.024	0.0263
PCB 156 233'44'5-Hexachlorobiphenyl	<0.010	<0.010	0.0099	0.016	0.018	0.018	<0.010
PCB 159 233'455'-Hexachlorobiphenyl	0.0030	<0.010	<0.010	0.0016	0.0051	0.0051	<0.010
PCB 170 22'33'44'5-Heptachlorobiphenyl	<0.010	<0.010	<0.010	0.015	0.017	0.017	<0.010
PCB 171 22'33'44'6-Heptachlorobiphenyl	0.019	0.017	0.024	0.019	0.022	0.022	0.0205
PCB 173 22'33'456-Heptachlorobiphenyl	<0.010	<0.010	<0.010	<0.010	<0.010	<0.010	<0.010
PCB 180 22'344'55'-Heptachlorobiphenyl	0.091	0.067	0.066	0.071	0.081	0.055	0.0718
PCB 182 22'344'56'-Heptachlorobiphenyl	0.0040	0.0042	0.0045	0.012	0.014	0.0098	0.0081
PCB 183 22'344'5'6-Heptachlorobiphenyl	<0.010	<0.010	<0.010	0.015	0.018	0.007	<0.010
PCB 185 22'3455'6-Heptachlorobiphenyl	0.0038	0.0019	0.0016	<0.010	<0.010	<.010	<0.010
PCB 187 22'34'55'6-Heptachlorobiphenyl	0.047	0.033	0.031	0.033	0.039	0.027	0.035
PCB 189 233'44'55'-Heptachlorobiphenyl	<0.010	<0.010	<0.010	<0.010	<0.010	<0.010	<0.010
PCB 191 233'44'5'6-Heptachlorobiphenyl	<0.010	<0.010	<0.010	<0.010	<0.010	<0.010	<0.010
PCB 194 22'33'44'55'-Octachlorobiphenyl	0.0029	0.021	0.015	0.018	0.021	0.014	0.0153
PCB 195 22'33'44'56-Octachlorobiphenyl	0.013	0.0096	0.0083	0.007	0.0087	0.0059	0.0088
PCB 196 22'33'44'56'-Octachlorobiphenyl	0.024	0.019	0.015	0.028	0.033	0.023	0.0237
PCB 199 22'33'455'6'-Octachlorobiphenyl	<0.010	<0.010	<0.010	0.02	0.023	0.016	<0.010
PCB 201 22'33'45'66'-Octachlorobiphenyl	<0.010	<0.010	<0.010	0.0042	0.004	0.0026	<0.010
PCB 202 22'33'55'66'-Octachlorobiphenyl	<0.010	<0.010	0.0136	0.0018	0.0018	0.0016	<0.010
PCB 203 22'344'55'6'-Octachlorobiphenyl	0.019	0.015	0.012	0.026	0.029	0.02	0.0202
PCB 205 233'44'55'6-Octachlorobiphenyl	<0.010	<0.010	<0.010	<0.010	<0.010	<0.010	<0.010
PCB 206 22'33'44'55'6-Nonachlorobiphenyl	0.018	0.017	0.014	0.019	0.022	0.018	0.018
PCB 207 22'33'44'566'-Nonaachlorobiphenyl	<0.010	<0.010	<0.010	<0.010	<0.010	<0.010	<0.010
PCB 208 22'33'455'66'-Nonachlorobiphenyl	0.010	0.0089	0.0089	0.006	0.0067	0.0051	0.0076
PCB 66 23'44'-Tetrachlorobiphenyl	0.049	0.046	0.041	0.044	0.046	0.039	0.0442
PCB 155 22'44'66-Hexachlorobiphenyl	0.085	0.085	0.090	<0.010	<0.010	<0.010	<0.010
PCB 184 22'344'66'-Heptachlorobiphenyl	<0.010	<0.010	<0.010	0.0022	0.0025	0.0015	<0.010

Table A.3 Dioxin and Furan Analysis of Sediment

Isomer	Replicate in pg/g						Average
	1	2	3	4	5	6	
2,3,7,8-TCDF	214	205	150	105	104	118	149
2,3,7,8-TCDD	13.6	16.0	18.6	17.2	30.0	21.9	19.6
1,2,3,7,8-PeCDF	147	148	122	120	144	123	134
2,3,4,7,8-PeCDF	134.0	133.0	95.9	93.6	95.3	92.8	107.4
1,2,3,7,8-PeCDD	70.6	61.3	49.2	50.5	66.7	41.3	5606.0
1,2,3,4,7,8-HxCDF	483	516	440	538	646	589	535
1,2,3,6,7,8-HxCDF	208	225	176	208	234	209	210
2,3,4,6,7,8-HxCDF	149	112	126	167	158	170	147
1,2,3,7,8,9-HxCDF	7.95	9.85	6.07	9.11	13.3	7.93	9.04
1,2,3,4,7,8-HxCDD	99.6	84.8	64.8	64.6	90.7	69.6	77.35
1,2,3,6,7,8-HxCDD	182	175	134	123	136	132	147
1,2,3,7,8,9-HxCDD	219	214	186	198	217	198	205
1,2,3,4,6,7,8-HpCDF	2260	2540	2450	2380	2700	2490	2470
1,2,3,4,7,8,9-HpCDF	96.7	113.0	92.2	102.0	139.0	105.0	108.0
1,2,3,4,6,7,8-HpCDD	1910	1900	1740	1560	1720	2120	1825
OCDF	(2340)J	2080	1930	1910	2340	1980	2097
OCDD	(10600)J	10500	10600	10200	10600	18800	11883
TCDF	1550	1290	643	263	320	216	714
TCDD	445.0	451.0	78.1	31.0	38.8	57.8	183.6
PECDF	2190	2050	1590	1220	1570	1170	1632
PECDD	638	775	600	440	710	548	619
HXCDF	2090	2160	1870	2280	2450	2310	2193
HXCDD	2340	2310	1630	1540	1770	1800	1898
HPCDF	3120	3410	3220	3170	3810	3200	3321
HPCDD	4080	3990	3510	3050	3330	4130	3681

pg/g (picograms per gram)
J Corresponding labeled analog recovery outside criteria of 25 to 150%

APPENDIX B. Chemical Analysis of Hanging Bag Test for PAH, PCB, Dioxin and Furan

Table B.1 PAH Analysis in the Hanging Bag Test

Chemical	A mg/l	Fraction Retained	A + B mg/l	Fraction Retained	A + D mg/l	Fraction Retained
Naphthalene	0.00027	99.98	0.00011	99.99	0.00009	99.99
Acenaphthylene	<0.0003	99.98	<0.0003	99.99	<0.0003	99.99
Phenanthrene	0.00182	99.98	0.00174	99.99	0.00081	99.99
Acenaphthene	0.00067	99.30	0.00077	99.99	0.00038	99.99
Fluorene	0.00058	99.98	0.00062	99.99	0.00028	99.99
Anthracene	0.00071	99.88	0.00056	99.99	0.00022	99.99
Fluoranthene	0.00208	99.99	0.00154	99.99	0.00062	99.99
Pyrene	0.00148	99.98	0.00141	99.99	0.00057	99.99
Chrysene	0.00065	99.99	0.00043	99.99	0.00016	99.99
Benzo (a) Anthracene	0.00082	99.99	0.00056	99.99	0.00022	99.99
Benzo (b)Fluoranthene	0.00056	99.99	0.00081	99.99	0.00047	99.99
Benzo (k) Fluoranthene	0.00028	99.99	0.00022	99.99	0.00042	99.99
Benzo (a) Pyrene	0.00053	99.99	0.00032	99.99	0.00014	99.99
(1, 2, 3-C, D) Pyrene	0.00033	99.95	0.00012	99.99	0.00009	99.99
Dibenzo (A,H) Anthracene.	<0.0003	99.98	<0.0003	99.99	<0.0003	99.99
Benzo (G, H, I) Perylene	0.00029J	99.99	0.00016J	99.99	0.00007J	99.99
2-Methylnaphthalene	0.00041	99.98	0.0004	99.99	0.00022	99.99

Table B.2 PCB Analysis for Hanging Bag Test

Chemical	A mg/l	A+B mg/l	A+D mg/l
PCB 1016	<0.00020	<0.00020	<0.00020
PCB 1221	<0.00020	<0.00020	<0.00020
PCB 1232	<0.00020	<0.00020	<0.00020
PCB 1242	<0.00020	<0.00020	<0.00020
PCB 1248	<0.00020	<0.00020	<0.00020
PCB 1254	<0.00020	<0.00020	<0.00020
PCB 1260	<0.00020	<0.00020	<0.00020
PCB 7 24-Dichlorobiphenyl	<0.000030	<0.000030	<0.000030
PCB 8 24'-Dichlorobiphenyl	<0.000030	<0.000030	<0.000030
PCB 15 44'-Dichlorobiphenyl	<0.000012	<0.000014	<0.000010
PCB 18 22'5-Trichlorobiphenyl	<0.000030	<0.000030	<0.000030
PCB 28 244-Trichlorobiphenyl	0.000014	0.000010	0.000017
PCB 31 24'5-Trichlorobiphenyl	<0.000030	0.000011	<0.000030
PCB 40 22'33'-Tetrachlorobiphenyl	<0.000030	<0.000030	<0.000030
PCB 44 22'35'-Tetrachlorobiphenyl	0.000014	0.000013	0.000011
PCB 49 22'45'-Tetrachlorobiphenyl	0.000012	0.000013	<0.000030
PCB 50 22'46-Tetrachlorobiphenyl	0.000014	<.000030	0.000017
PCB 52 22'55'-Tetrachlorobiphenyl	0.000023	0.000025	<0.000030
PCB 54 22'66'-Tetrachlorobiphenyl	0.000050	<0.000030	0.000057
PCB 60 2344'-Tetrachlorobiphenyl	0.000019 J	<0.000030	<0.000030
PCB 70 23'4'5-Tetrachlorobiphenyl	<0.000030	<0.000030	<0.000030
PCB 77 33'44'-Tetrachlorobiphenyl	0.000028 BJ	0.000035	0.000022 BJ
PCB 82 22'33'4-Pentachlorobiphenyl	<0.000030	<0.000030	<0.000030
PCB 86 22'345-Pentachlorobiphenyl	<0.000030	<0.000030	<0.000030
PCB 87 22'345'-Pentachlorobiphenyl	<0.000030	<0.000030	<0.000030
PCB 97 22'3'45-Pentachlorobiphenyl	<0.000030	<0.000030	<0.000030
PCB 101 22'455'-Pentachlorobiphenyl	<0.000030	<0.000030	0.000013
PCB 103 22'45'6-Pentachlorobiphenyl	<0.000030	<0.000030	<0.000030
PCB 105 233'44'-Pentachlorobiphenyl	<0.000030	<0.000030	<0.000030
PCB 114 2344'5-Pentachlorobiphenyl	<0.000030	<0.000030	<0.000030
PCB 118 23'44'5-Pentachlorobiphenyl	<0.000030	<0.000030	<0.000030
PCB 121 23'45'6-Pentachlorobiphenyl	<0.000030	<0.000030	<0.000030
PCB 128 22'33'44'-Hexachlorobiphenyl	<0.000030	<0.000030	<0.000030
PCB 129 22'33'45-Hexachlorobiphenyl	<0.000030	<0.000030	<0.000030
PCB 136 22'33'66'-Hexachlorobiphenyl	<0.000030	<0.000030	<0.000030

Table B.2 cont'd PCB Analysis for Hanging Bag Test

Chemical	A mg/l	A+B mg/l	A+D mg/l
PCB 137 22'344'5-Hexachlorobiphenyl	<0.000030	<0.000030	<0.000030
PCB 138 22'344'5'-Hexachlorobiphenyl	0.000023	0.000023	0.000021
PCB 141 22'3455'-Hexachlorobiphenyl	<0.000030	<0.000030	<0.000030
PCB 143 22'3456'-Hexachlorobiphenyl	<0.000030	<0.000030	<0.000030
PCB 159 233'455'-Hexachlorobiphenyl	<0.000030	<0.000030	<0.000030
PCB 170 22'33'44'5-Heptachlorobiphenyl	<0.000030	<0.000030	<0.000030
PCB 171 22'33'44'6-Heptachlorobiphenyl	<0.000030	<0.000030	<0.000030
PCB 173 22'33'456-Heptachlorobiphenyl	<0.000030	<0.000030	<0.000030
PCB 180 22'344'55'-Heptachlorobiphenyl	<0.000030	<0.000030	<0.000030
PCB 182 22'344'56'-Heptachlorobiphenyl	<0.000030	<0.000030	0.000015
PCB 183 22'344'5'6-Heptachlorobiphenyl	<0.000030	<0.000030	<0.000030
PCB 185 22'3455'6-Heptachlorobiphenyl	<0.000030	<0.000030	<0.000030
PCB 187 22'34'55'6-Heptachlorobiphenyl	<0.000030	<0.000030	0.00013
PCB 189 233'44'55'-Heptachlorobiphenyl	<0.000030	<0.000030	<0.000030
PCB 191 233'44'5'6-Heptachlorobiphenyl	<0.000030	<0.000030	<0.000030
PCB 194 22'33'44'55'-Octachlorobiphenyl	<0.000030	<0.000030	<0.000030
PCB 195 22'33'44'56-Octachlorobiphenyl	<0.000030	<0.000030	<0.000030
PCB 196 22'33'44'56'-Octachlorobiphenyl	<0.000030	<0.000030	<0.000030
PCB 199 22'33'455'6'-Octachlorobiphenyl	<0.000030	<0.000030	<0.000030
PCB 201 22'33'45'66'-Octachlorobiphenyl	<0.000030	<0.000030	<0.000030
PCB 202 22'33'55'66'-Octachlorobiphenyl	<0.000030	<0.000030	<0.000030
PCB 203 22'344'55'6'-Octachlorobiphenyl	<0.000030	<0.000030	<0.000030
PCB 205 233'44'55'6-Octachlorobiphenyl	<0.000030	<0.000030	<0.000030
PCB 206 22'33'44'55'6-Nonachlorobiphenyl	<0.000030	<0.000030	<0.000030
PCB 207 22'33'44'566'-Nonachlorobiphenyl	<0.000030	<0.000030	<0.000030
PCB 208 22'33'455'66'-Nonachlorobiphenyl	<0.000030	<0.000030	<0.000030
PCB 66 23'44'-Tetrachlorobiphenyl	0.000024	0.000023	0.000048
PCB 155 22'44'66-Hexachlorobiphenyl	0.000024	<0.000030	0.000032
PCB 184 22'344'66'-Heptachlorobiphenyl	0.000012	0.000011	<0.000030

Table B.3 Dioxin and Furan Analysis for Hanging Bag Test

Isomer	A pg/l	A+B pg/l	A+D pg/l
2,3,7,8-TCDF	43.8	16.56	U(9.50)
2,3,7,8-TCDD	U(8.3)	U(7.72)	U(9.88)
1,2,3,7,8-PeCDF	U(16.0EMPC)	U(8.10EMPC)	U(8.51)
2,3,4,7,8-PeCDF	U(12.2EMPC)	U(7.10EMPC)	U(7.56)
1,2,3,7,8-PeCDD	U(15.0)	U(1.25)	U(1.78)
1,2,3,4,7,8-HxCDF	27.4	U(15.7EMPC)	U(2.78)
1,2,3,6,7,8-HxCDF	13.6	6.38	8.70
2,3,4,6,7,8-HxCDF	U(10.0EMPC)	U(0.256)	U(5.76EMPC)
1,2,3,7,8,9-HxCDF	U(0.194)	U(1.68EMPC)	U(2.98)
1,2,3,4,7,8-HxCDD	5.58	U(7.75)	U(1.58)
1,2,3,6,7,8-HxCDD	U(9.99EMPC)	U(4.78EMPC)	U(1.50)
1,2,3,7,8,9-HxCDD	10.3	U(3.12EMPC)	U(1.45)
1,2,3,4,6,7,8-HpCDF	114	53.4	71.1
1,2,3,4,7,8,9-HpCDF	U(8.64EMPC)	U(10.3)	U(11.6EMPC)
1,2,3,4,6,7,8-HpCDD	75.3	U(44.4EMPC)	304
OCDF	84.5	44.3	150
OCDD	426	235	1870
TCDF	79.4	7.45	U(9.50)
TCDD	U(11.4)	U(7.72)	U(9.88)
PECDF	81.0	29.3	16.1
PECDD	U(15.2)	U(13.8)	U(10.5)
HXCDF	76.4	34.9	32.8
HXCDD	34.6	U(7.40)	16.1
HPCDF	149	68.2	168
HPCDD	148	42.1	512

APPENDIX C. Ratios of Estimated Particulate to observed for PAH, PCB, Heavy metal, Dioxin and Furan concentrations

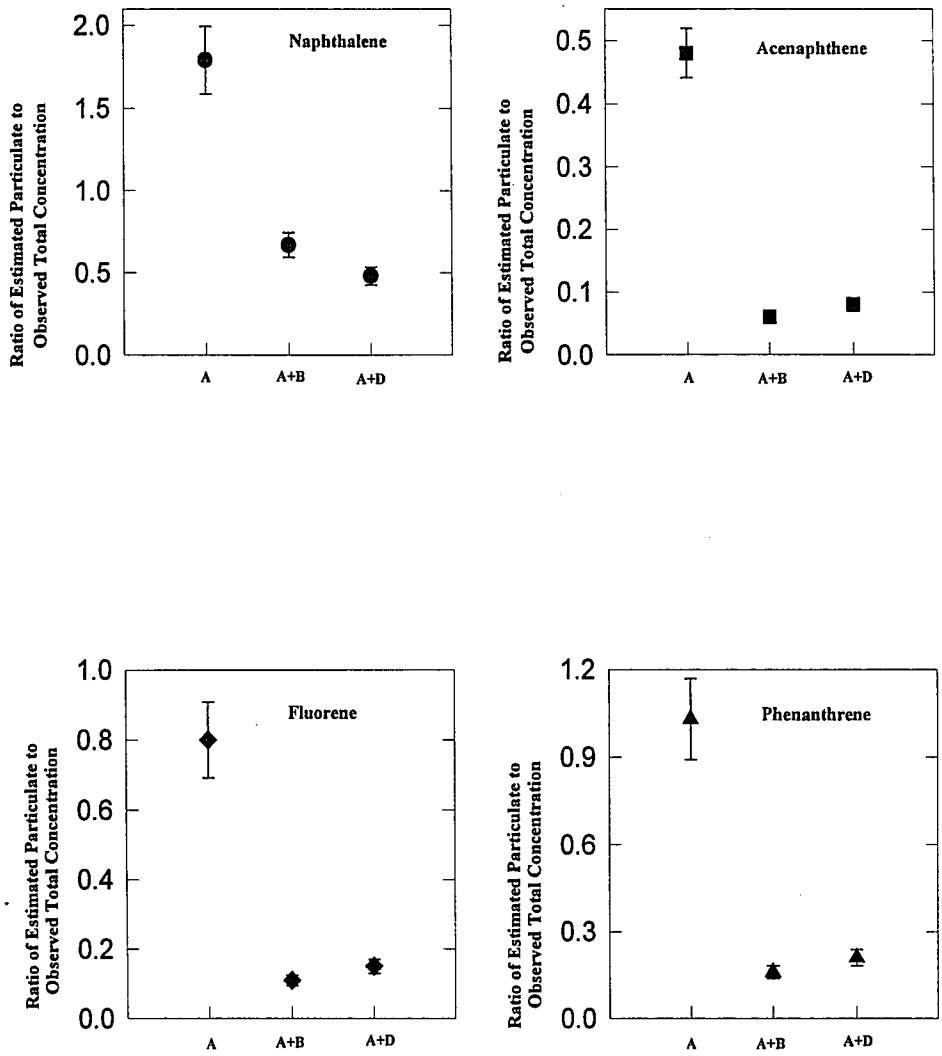

Figure C.1 Ratios of Estimated Particulate to Observed PAH (Naphthalene, Acenaphthene, Fluorene and Phenanthrene) Concentrations

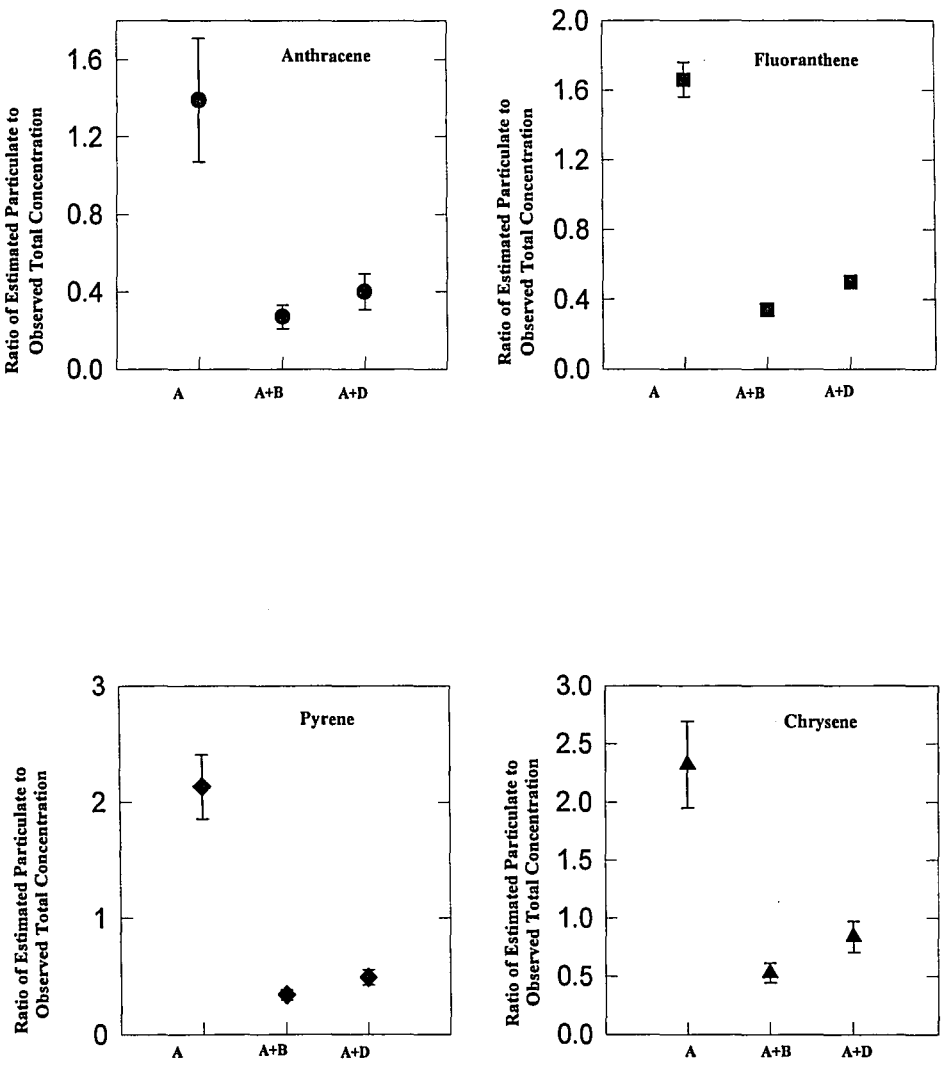

Figure C.2 Ratios of Estimated Particulate to Observed PAH (Anthracene, Fluoranthene, Pyrene and Chrysene) Concentrations

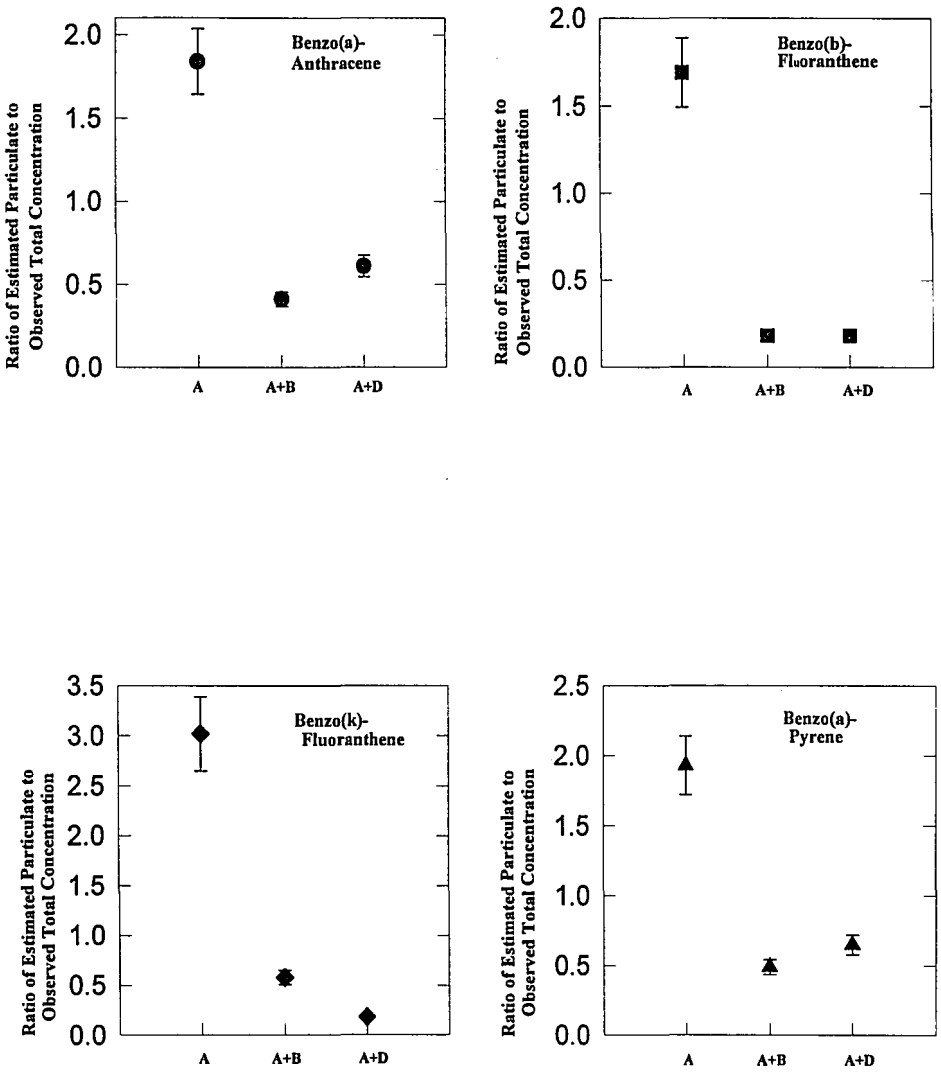

Figure C.3 Ratios of Estimated Particulate to Observed PAH (Benzo(a)-Anthracene, Benzo(b)-Fluoranthene, Benzo(k)-Fluoranthene and Benzo(a)-Pyrene) Concentrations

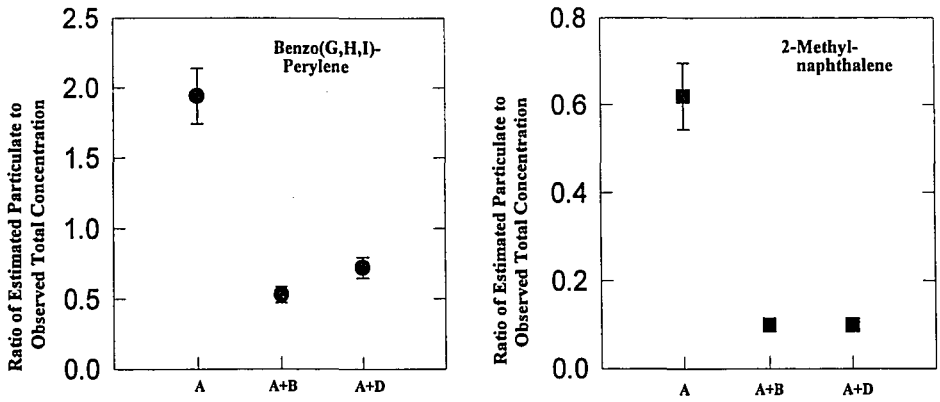

Figure C.4 Ratios of Estimated Particulate to Observed PAH (Benzo(GHI)-Perylene and 2-Methyl-naphthalene) Concentrations

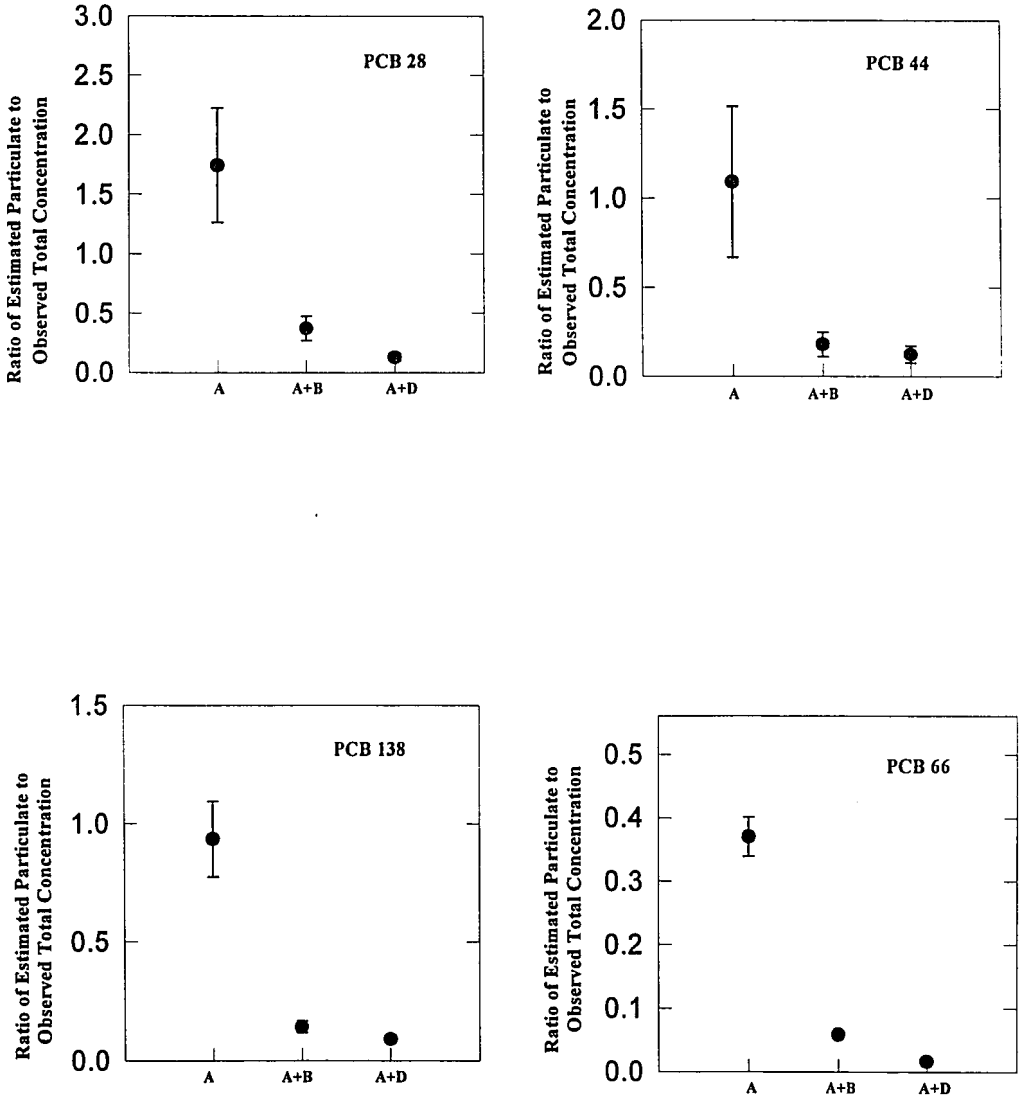

Figure C.5 Ratios of Estimated Particulate to Observed PCB (PCB 28, PCB 44, PCB 138, and PCB 66) Concentrations

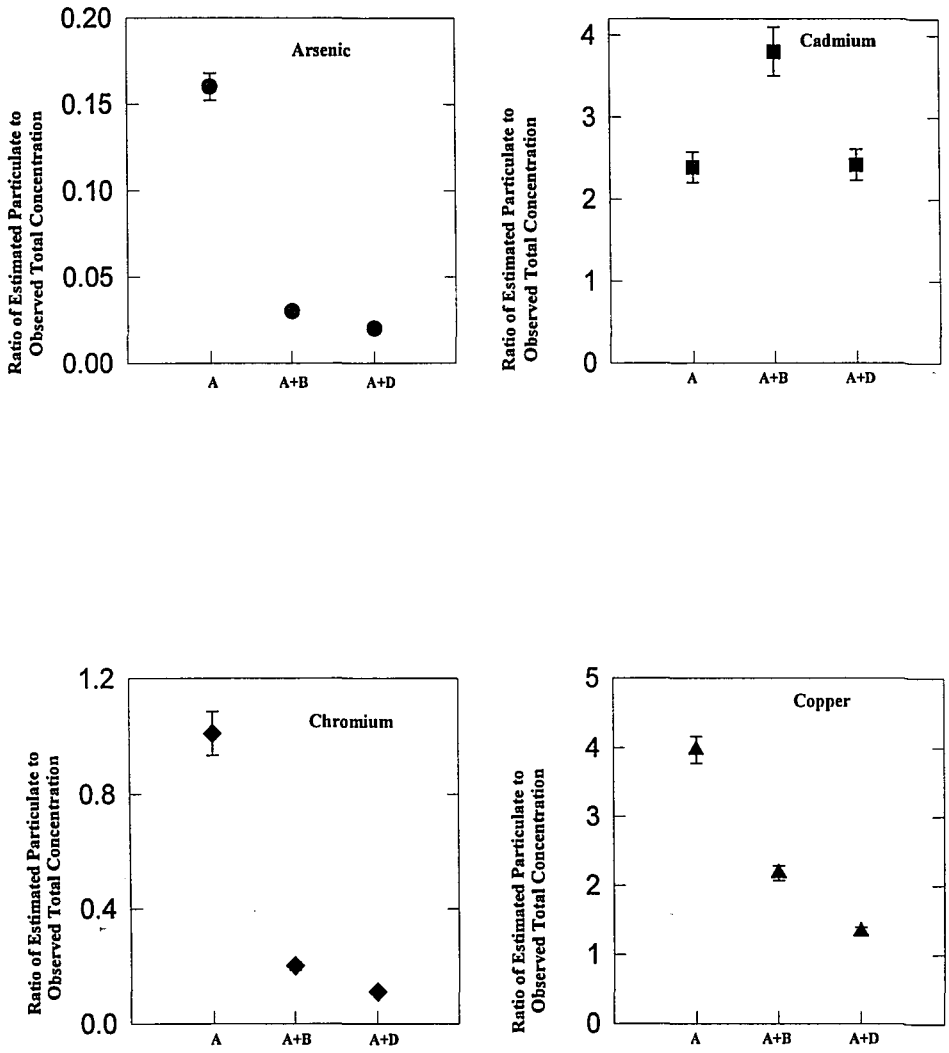

Figure C.6 Ratios of Estimated Particulate to Observed Metal (Arsenic, Cadmium, Chromium, and Copper) Concentrations

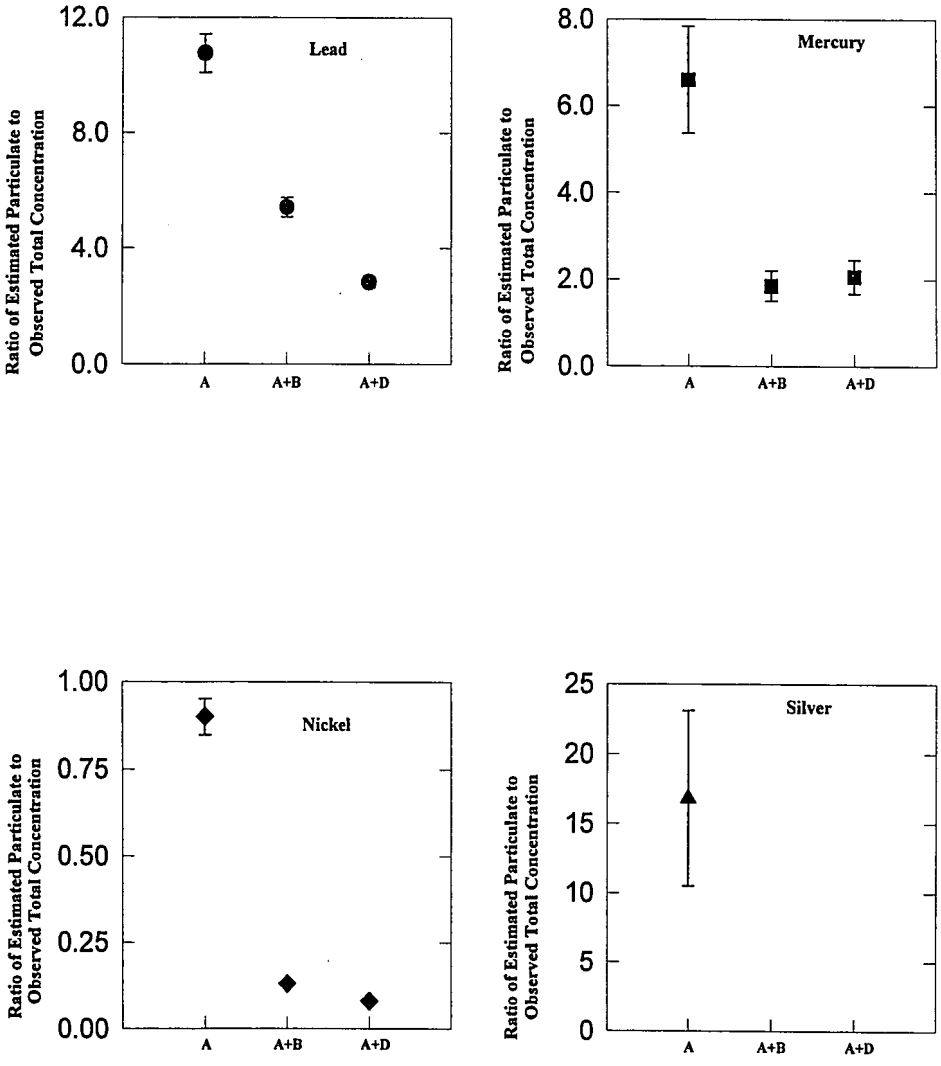

Figure C.7 Ratios of Estimated Particulate to Observed Metal (Lead, Mercury, Nickel, and Silver) Concentrations

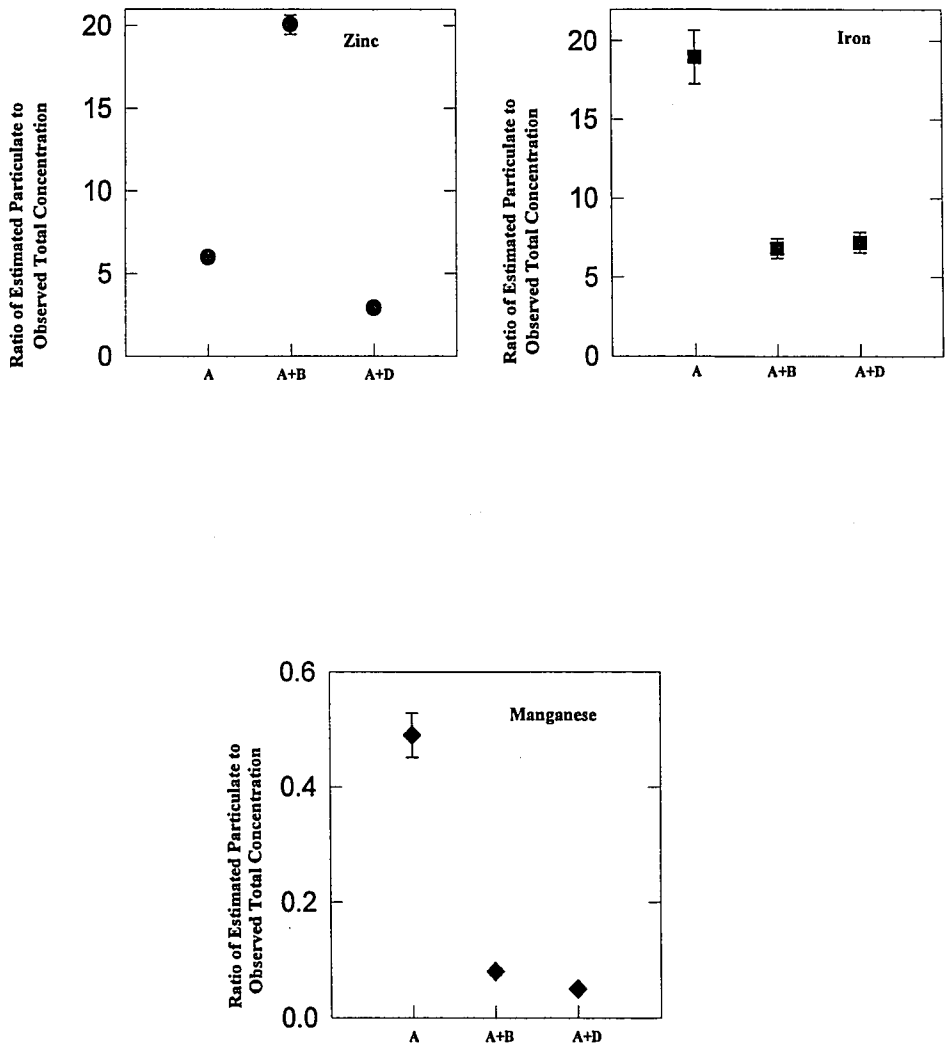

Figure C.8 Ratios of Estimated Particulate to Observed Metal (Zinc, Iron, and Manganese) concentrations

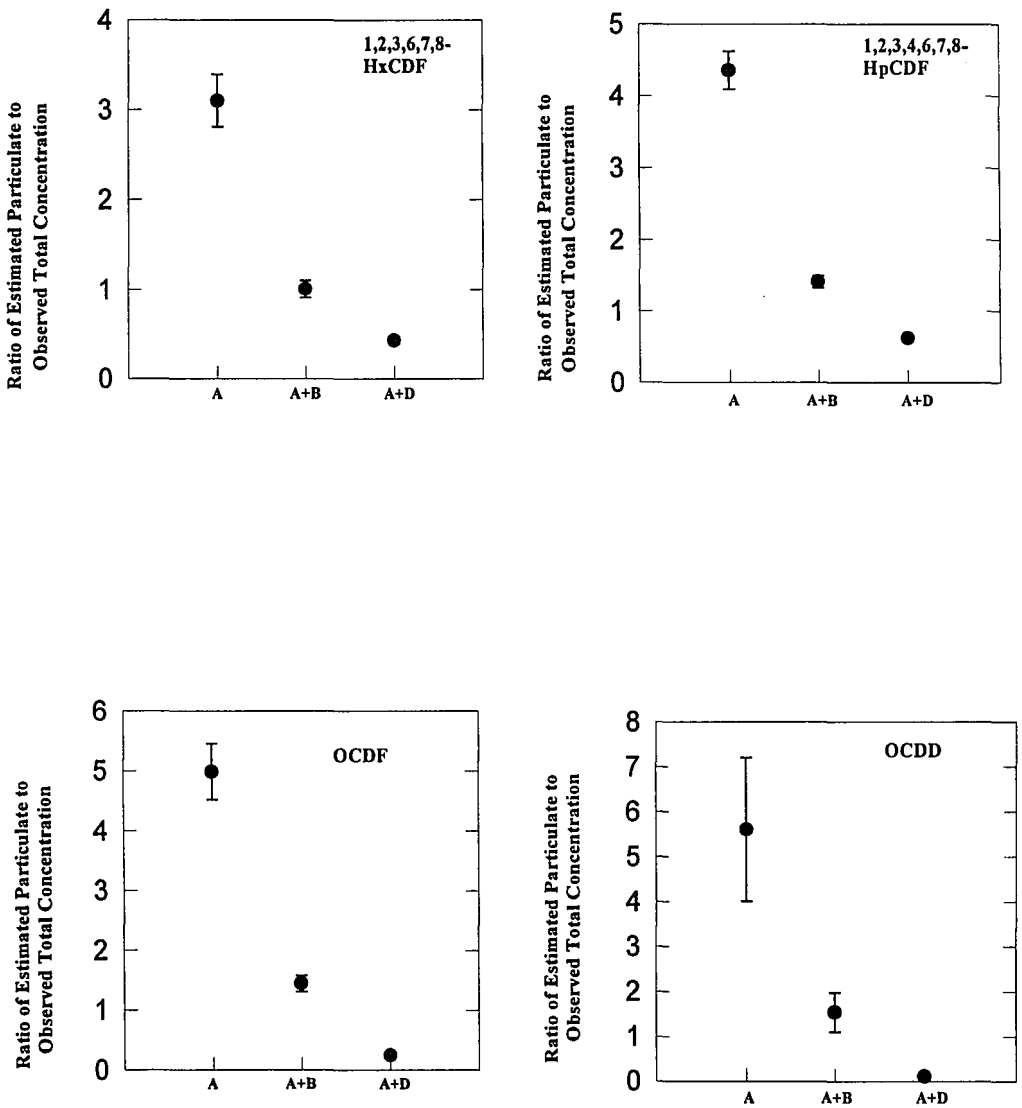

Figure C.9 Ratios of Estimated Particulate to Observed Dioxin and Furan (1,2,3,6,7,8-HxCDF, 1,2,3,4,6,7,8-HpCDF, OCDF and OCDD) Concentrations.

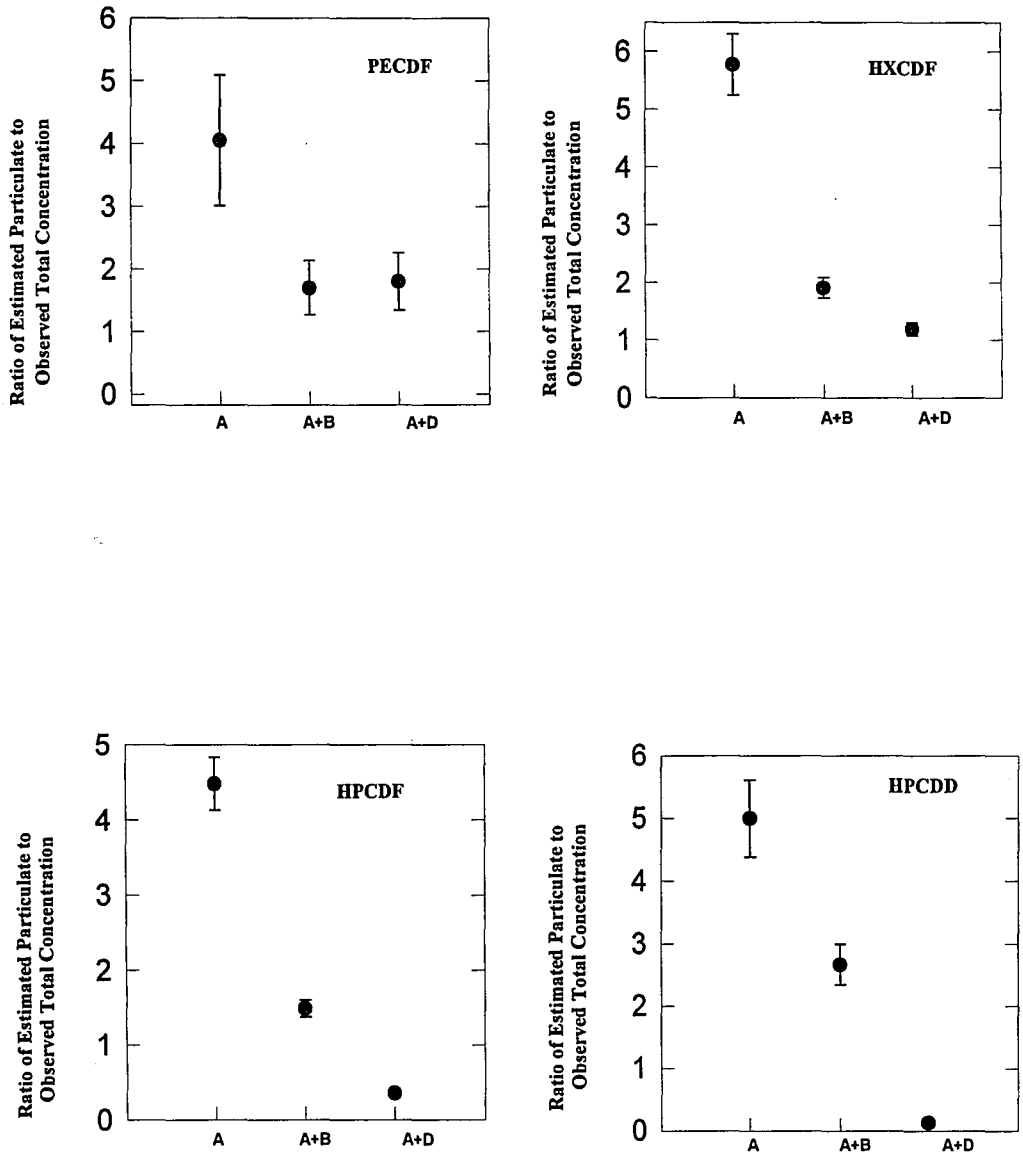

Figure C.10 Ratios of Estimated Particulate to Observed Dioxin and Furan (PECDF, HXCDF, HPCDF, and HPCDD) Concentrations

APPENDIX D. Chemical Analysis of Barge Simulation Test for PCB, PAH, Dioxin and Furan

Table D.1 PCB Analysis for Fabric A Barge Simulation Test

	Sample 1	Sample 2	Sample 3
Chemical			
	mg/l	mg/l	mg/l
PCB 1016	<0.00020	<0.00020	<0.00020
PCB 1221	<0.00020	<0.00020	<0.00020
PCB 1232	<0.00020	<0.00020	<0.00020
PCB 1242	<0.00020	<0.00020	<0.00020
PCB 1248	<0.00020	<0.00020	<0.00020
PCB 1254	<0.00020	<0.00020	<0.00020
PCB 1260	<0.00020	<0.00020	<0.00020
PCB 7 24-Dichlorobiphenyl	<0.000030	0.000044	0.000034
PCB 8 24'-Dichlorobiphenyl	0.000012	<.000030	0.000016
PCB 15 44'-Dichlorobiphenyl	<0.000030	<0.000030	0.000021 J
PCB 18 22'5-Trichlorobiphenyl	<0.000030	<0.000030	<0.000030
PCB 28 244-Trichlorobiphenyl	<0.000030	<0.000030	<0.000030
PCB 31 24'5-Trichlorobiphenyl	<0.000030	<0.000030	<0.000030
PCB 40 22'33'-Tetrachlorobiphenyl	<0.000030	<0.000030	<0.000030
PCB 44 22'35'-Tetrachlorobiphenyl	0.000041	0.000012 J	0.000010 J
PCB 49 22'45'-Tetrachlorobiphenyl	<0.000030	<0.000030	<0.000030
PCB 50 22'46-Tetrachlorobiphenyl	<0.000030	<0.000030	<0.000030
PCB 52 22'55'-Tetrachlorobiphenyl	<0.000030	<0.000030	<0.000030
PCB 54 22'66'-Tetrachlorobiphenyl	<0.000030	<0.000030	<0.000030
PCB 60 2344'-Tetrachlorobiphenyl	<0.000030	<0.000030	<0.000030
PCB 70 23'4'5-Tetrachlorobiphenyl	<0.000030	<0.000030	0.000042
PCB 77 33'44'-Tetrachlorobiphenyl	<0.000030	<0.000030	<0.000030
PCB 82 22'33'4-Pentachlorobiphenyl	<0.000030	<0.000030	<0.000030
PCB 86 22'345-Pentachlorobiphenyl	<0.000030	<0.000030	<0.000030
PCB 87 22'345'-Pentachlorobiphenyl	<0.000030	<0.000030	<0.000030
PCB 97 22'3'45-Pentachlorobiphenyl	<0.000030	<0.000030	<0.000030
PCB 101 22'455'-Pentachlorobiphenyl	<0.000030	<0.000030	<0.000030
PCB 103 22'45'6-Pentachlorobiphenyl	<0.000030	<0.000030	<0.000030
PCB 105 233'44'-Pentachlorobiphenyl	<0.000030	0.000085	0.000045
PCB 114 2344'5-Pentachlorobiphenyl	<0.000030	<0.000030	<0.000030
PCB 118 23'44'5-Pentachlorobiphenyl	<0.000030	<0.000030	<0.000030
PCB 121 23'45'6-Pentachlorobiphenyl	<0.000030	<0.000030	<0.000030
PCB 128 22'33'44'-Hexachlorobiphenyl	<0.000030	0.000058	0.000044
PCB 129 22'33'45-Hexachlorobiphenyl	<0.000030	<0.000030	<0.000030
PCB 136 22'33'66'-Hexachlorobiphenyl	<0.000030	<0.000030	<0.000030
PCB 137 22'344'5-Hexachlorobiphenyl	<0.000030	0.000063	0.000032
PCB 138 22'344'5'-Hexachlorobiphenyl	<0.000030	0.000066	0.000068

Table D.1 Cont'd PCB Analysis for Fabric A Barge Simulation Test

PCB 141	22'3455'-Hexachlorobiphenyl	<0.000030	0.000057	0.000038
PCB 143	22'3456'-Hexachlorobiphenyl	<0.000030	<0.000030	<0.000030
PCB 151	22'355'6-Hexachlorobiphenyl	<0.000030	<0.000030	<0.000030
PCB 153	22'44'55'-Hexachlorobiphenyl	<0.000030	0.000094	0.000072
PCB 154	22'44'56'-Hexachlorobiphenyl	<0.000030	<0.000030	<0.000030
PCB 156	233'44'5-Hexachlorobiphenyl	<0.000030	<0.000030	0.000035
PCB 159	233'455'-Hexachlorobiphenyl	<0.000030	<0.000030	<0.000030
PCB 170	22'33'44'5-Heptachlorobiphenyl	<0.000030	<0.000030	<0.000030
PCB 171	22'33'44'6-Heptachlorobiphenyl	<0.000030	<0.000030	<0.000030
PCB 173	22'33'456-Heptachlorobiphenyl	<0.000030	<0.000030	0.000025 J
PCB 180	22'344'55'-Heptachlorobiphenyl	0.000027 J	0.000039	<0.000030
PCB 182	22'344'56'-Heptachlorobiphenyl	<0.000030	<0.000030	0.00012
PCB 183	22'344'5'6-Heptachlorobiphenyl	<0.000030	<0.000030	0.000034
PCB 185	22'3455'6-Heptachlorobiphenyl	<0.000030	<0.000030	0.000028
PCB 187	22'34'55'6-Heptachlorobiphenyl	<0.000030	<0.000030	<0.000030
PCB 189	233'44'55'-Heptachlorobiphenyl	<0.000030	<0.000030	<0.000030
PCB 191	233'44'5'6-Heptachlorobiphenyl	<0.000030	0.000022	0.000027
PCB 194	22'33'44'55'-Octachlorobiphenyl	<0.000030	<0.000030	<0.000030
PCB 195	22'33'44'56-Octachlorobiphenyl	<0.000030	<0.000030	<0.000030
PCB 196	22'33'44'56'-Octachlorobiphenyl	<0.000030	<0.000030	<0.000030
PCB 199	22'33'455'6'-Octachlorobiphenyl	<0.000030	<0.000030	<0.000030
PCB 201	22'33'45'66'-Octachlorobiphenyl	<0.000030	0.000021 J	0.000032
PCB 202	22'33'55'66'-Octachlorobiphenyl	<0.000030	<0.000030	<0.000030
PCB 203	22'344'55'6'-Octachlorobiphenyl	<0.000030	<0.000030	<0.000030
PCB 205	233'44'55'6-Octachlorobiphenyl	<0.000030	<0.000030	0.000021 J
PCB 206	22'33'44'55'6-Nonachlorobiphenyl	<0.000030	<0.000030	<0.000030
PCB 207	22'33'44'566'-Nonaachlorobiphenyl	<0.000030	<0.000030	<0.000030
PCB 208	22'33'455'66'-Nonachlorobiphenyl	<0.000030	<0.000030	<0.000030
PCB 66	23'44'-Tetrachlorobiphenyl	<0.000030	<0.000030	<0.000030
PCB 155	22'44'66-Hexachlorobiphenyl	<0.000030	<0.000030	<0.000030
PCB 184	22'344'66'-Heptachlorobiphenyl	<0.000030	0.000065	0.000071

Table D.2 PCB Analysis for Fabric A+B Barge Simulation Test

	Sample 1	Sample 2	Sample 3
Chemical			
	mg/l	mg/l	mg/l
PCB 1016	<0.00020	<0.00020	<0.00020
PCB 1221	<0.00020	<0.00020	<0.00020
PCB 1232	<0.00020	<0.00020	<0.00020
PCB 1242	<0.00020	<0.00020	<0.00020
PCB 1248	<0.00020	<0.00020	<0.00020
PCB 1254	<0.00020	<0.00020	<0.00020
PCB 1260	<0.00020	<0.00020	<0.00020
PCB 7 24-Dichlorobiphenyl	<0.000030	<0.000030	<0.000030
PCB 8 24'-Dichlorobiphenyl	0.000019	0.000055	0.000018 J
PCB 15 44'-Dichlorobiphenyl	<0.000030	0.000030 J	<0.000030
PCB 18 22'5-Trichlorobiphenyl	<0.000030	0.000016 J	<0.000030
PCB 28 244-Trichlorobiphenyl	<0.000030	<0.000030	<0.000030
PCB 31 24'5-Trichlorobiphenyl	<0.000030	<0.000030	<0.000030
PCB 40 22'33'-Tetrachlorobiphenyl	<0.000030	<0.000030	<0.000030
PCB 44 22'35'-Tetrachlorobiphenyl	0.000018 J	0.000023 J	0.000023 J
PCB 49 22'45'-Tetrachlorobiphenyl	<0.000030	<0.000030	<0.000030
PCB 50 22'46-Tetrachlorobiphenyl	<0.000030	<0.000030	<0.000030
PCB 52 22'55'-Tetrachlorobiphenyl	<0.000030	<0.000030	<0.000030
PCB 54 22'66'-Tetrachlorobiphenyl	<0.000030	<0.000030	<0.000030
PCB 60 2344'-Tetrachlorobiphenyl	<0.000030	0.000019	0.000030
PCB 70 23'4'5-Tetrachlorobiphenyl	<0.000030	0.000032	<0.000030
PCB 77 33'44'-Tetrachlorobiphenyl	<0.000030	0.000057	0.000067
PCB 82 22'33'4-Pentachlorobiphenyl	<0.000030	<0.000030	<0.000030
PCB 86 22'345-Pentachlorobiphenyl	<0.000030	<0.000030	0.000031
PCB 87 22'345'-Pentachlorobiphenyl	<0.000030	0.000024 J	0.000050 J
PCB 97 22'3'45-Pentachlorobiphenyl	<0.000030	0.000016	0.000028 J
PCB 101 22'455'-Pentachlorobiphenyl	<0.000030	0.000029 J	0.000037
PCB 103 22'45'6-Pentachlorobiphenyl	<0.000030	<0.000030	<0.000030
PCB 105 233'44'-Pentachlorobiphenyl	<0.000030	0.000072	0.000095
PCB 114 2344'5-Pentachlorobiphenyl	<0.000030	<0.000030	0.000036
PCB 118 23'44'5-Pentachlorobiphenyl	<0.000030	<0.000030	<0.000030
PCB 121 23'45'6-Pentachlorobiphenyl	<0.000030	<0.000030	<0.000030
PCB 128 22'33'44'-Hexachlorobiphenyl	0.000046	0.00019	0.00016
PCB 129 22'33'45-Hexachlorobiphenyl	<0.000030	0.000040	0.000030
PCB 136 22'33'66'-Hexachlorobiphenyl	<0.000030	0.000032	0.000035
PCB 137 22'344'5-Hexachlorobiphenyl	<0.000030	0.00010	0.00010
PCB 138 22'344'5'-Hexachlorobiphenyl	<0.000030	0.000095	0.000091

Table D.2 Cont'd PCB Analysis for Fabric A+B Barge Simulation Test

PCB 141	22'3455'-Hexachlorobiphenyl	<0.000030	0.000083	0.000056
PCB 143	22'3456'-Hexachlorobiphenyl	<0.000030	<0.000030	<0.000030
PCB 151	22'355'6-Hexachlorobiphenyl	<0.000030	0.000025 J	0.000037
PCB 153	22'44'55'-Hexachlorobiphenyl	<0.000030	<0.000030	0.000041
PCB 154	22'44'56'-Hexachlorobiphenyl	<0.000030	0.000016 J	0.000032
PCB 156	233'44'5-Hexachlorobiphenyl	<0.000030	0.000049	0.000052
PCB 159	233'455'-Hexachlorobiphenyl	<0.000030	<0.000030	<0.000030
PCB 170	22'33'44'5-Heptachlorobiphenyl	<0.000030	<0.000030	<0.000030
PCB 171	22'33'44'6-Heptachlorobiphenyl	<0.000030	0.000034	0.000035
PCB 173	22'33'456-Heptachlorobiphenyl	<0.000030	0.000059	0.000076
PCB 180	22'344'55'-Heptachlorobiphenyl	0.000013 J	0.000040	0.000098
PCB 182	22'344'56'-Heptachlorobiphenyl	<0.000030	0.000041	0.000098
PCB 183	22'344'5'6-Heptachlorobiphenyl	<0.000030	0.000058	0.000064
PCB 185	22'3455'6-Heptachlorobiphenyl	<0.000030	0.000075	0.000081
PCB 187	22'34'55'6-Heptachlorobiphenyl	<0.000030	<0.000030	<0.000030
PCB 189	233'44'55'-Heptachlorobiphenyl	<0.000030	<0.000030	<0.000030
PCB 191	233'44'5'6-Heptachlorobiphenyl	<0.000030	0.000062	0.000042
PCB 194	22'33'44'55'-Octachlorobiphenyl	<0.000030	<0.000030	<0.000030
PCB 195	22'33'44'56-Octachlorobiphenyl	<0.000030	<0.000030	<0.000030
PCB 196	22'33'44'56'-Octachlorobiphenyl	<0.000030	<0.000030	<0.000030
PCB 199	22'33'455'6'-Octachlorobiphenyl	<0.000030	<0.000030	<0.000030
PCB 201	22'33'45'66'-Octachlorobiphenyl	<0.000030	0.000072	0.000093
PCB 202	22'33'55'66'-Octachlorobiphenyl	<0.000030	0.000034	0.000032
PCB 203	22'344'55'6'-Octachlorobiphenyl	<0.000030	<0.000030	<0.000030
PCB 205	233'44'55'6-Octachlorobiphenyl	<0.000030	<0.000030	<0.000030
PCB 206	22'33'44'55'6-Nonachlorobiphenyl	0.000066	<0.000030	<0.000030
PCB 207	22'33'44'566'-Nonaachlorobiphenyl	<0.000030	<0.000030	<0.000030
PCB 208	22'33'455'66'-Nonachlorobiphenyl	<0.000030	0.000018 J	0.000015 J
PCB 66	23'44'-Tetrachlorobiphenyl	<0.000030	0.000022 J	0.000025 J
PCB 155	22'44'66-Hexachlorobiphenyl	<0.000030	0.000023 J	0.000026 J
PCB 184	22'344'66'-Heptachlorobiphenyl	<0.000030	<0.000030	0.000077

Table D.3 PCB Analysis for Fabric A+D Barge Simulation Test

Chemical	Sample 1 mg/l	Sample 2 mg/l	Sample 3 mg/l
PCB 1016	<0.00020	<0.00020	<0.00020
PCB 1221	<0.00020	<0.00020	<0.00020
PCB 1232	<0.00020	<0.00020	<0.00020
PCB 1242	<0.00020	<0.00020	<0.00020
PCB 1248	<0.00020	<0.00020	<0.00020
PCB 1254	<0.00020	<0.00020	<0.00020
PCB 1260	<0.00020	<0.00020	<0.00020
PCB 7 24-Dichlorobiphenyl	<0.000030	0.000018	0.000026
PCB 8 24'-Dichlorobiphenyl	0.000010	<0.000030	0.000012
PCB 15 44'-Dichlorobiphenyl	0.000028	0.000049	0.000036
PCB 18 22'5-Trichlorobiphenyl	<0.000030	<0.000030	<0.000030
PCB 28 244-Trichlorobiphenyl	<0.000030	<0.000030	<0.000030
PCB 31 24'5-Trichlorobiphenyl	<0.000030	<0.000030	<0.000030
PCB 40 22'33'-Tetrachlorobiphenyl	<0.000030	<0.000030	<0.000030
PCB 44 22'35'-Tetrachlorobiphenyl	0.000016 J	0.000024 J	0.000018 J
PCB 49 22'45'-Tetrachlorobiphenyl	<0.000030	0.000033	0.000022
PCB 50 22'46-Tetrachlorobiphenyl	<0.000030	<0.000030	<0.000030
PCB 52 22'55'-Tetrachlorobiphenyl	<0.000030	0.000038	0.000024 J
PCB 54 22'66'-Tetrachlorobiphenyl	<0.000030	0.000083	0.000044
PCB 60 2344'-Tetrachlorobiphenyl	<0.000030	<0.000030	<0.000030
PCB 70 23'4'5-Tetrachlorobiphenyl	<0.000030	<0.000030	<0.000030
PCB 77 33'44'-Tetrachlorobiphenyl	<0.000030	0.000065	<0.000030
PCB 82 22'33'4-Pentachlorobiphenyl	<0.000030	0.000047	<0.000030
PCB 86 22'345-Pentachlorobiphenyl	<0.000030	0.000041	<0.000030
PCB 87 22'345'-Pentachlorobiphenyl	<0.000030	0.000033	0.000028
PCB 97 22'3'45-Pentachlorobiphenyl	<0.000030	0.000039	<0.000030
PCB 101 22'455'-Pentachlorobiphenyl	<0.000030	<0.000030	<0.000030
PCB 103 22'45'6-Pentachlorobiphenyl	<0.000030	<0.000030	<0.000030
PCB 105 233'44'-Pentachlorobiphenyl	<0.000030	0.000064	0.000068
PCB 114 2344'5-Pentachlorobiphenyl	<0.000030	<0.000092	0.000037
PCB 118 23'44'5-Pentachlorobiphenyl	<0.000030	<0.000030	0.000078
PCB 121 23'45'6-Pentachlorobiphenyl	<0.000030	<0.000030	<0.000030
PCB 128 22'33'44'-Hexachlorobiphenyl	<0.000030	0.000072	0.00014
PCB 129 22'33'45-Hexachlorobiphenyl	<0.000030	0.000032	0.000029
PCB 136 22'33'66'-Hexachlorobiphenyl	<0.000030	0.000037	0.000031
PCB 137 22'344'5-Hexachlorobiphenyl	<0.000030	0.000044	0.000034
PCB 138 22'344'5'-Hexachlorobiphenyl	<0.000030	<0.000088	0.000082

Table D.3 Cont'd PCB Analysis for Fabric A+D Barge Simulation Test

PCB 141	22'3455'-Hexachlorobiphenyl	<0.000030	0.000090	0.00012
PCB 143	22'3456'-Hexachlorobiphenyl	<0.000030	0.000081	<0.000030
PCB 151	22'355'6-Hexachlorobiphenyl	<0.000030	0.000037	0.000011 J
PCB 153	22'44'55'-Hexachlorobiphenyl	<0.000030	0.00010	0.000074
PCB 154	22'44'56'-Hexachlorobiphenyl	<0.000030	0.000034	<0.000030
PCB 156	233'44'5-Hexachlorobiphenyl	<0.000030	0.000038	0.000036
PCB 159	233'455'-Hexachlorobiphenyl	<0.000030	0.000081	0.000053
PCB 170	22'33'44'5-Heptachlorobiphenyl	<0.000030	<0.000030	<0.000030
PCB 171	22'33'44'6-Heptachlorobiphenyl	<0.000030	0.000039	0.000020 J
PCB 173	22'33'456-Heptachlorobiphenyl	<0.000030	0.000044	0.000046
PCB 180	22'344'55'-Heptachlorobiphenyl	<0.000030	0.000031	0.000040
PCB 182	22'344'56'-Heptachlorobiphenyl	<0.000030	0.000059	0.000040
PCB 183	22'344'5'6-Heptachlorobiphenyl	<0.000030	0.000048	0.000041
PCB 185	22'3455'6-Heptachlorobiphenyl	<0.000030	0.000042	0.000038
PCB 187	22'34'55'6-Heptachlorobiphenyl	<0.000030	<0.000030	<0.000030
PCB 189	233'44'55'-Heptachlorobiphenyl	<0.000030	0.000023 J	0.000031
PCB 191	233'44'5'6-Heptachlorobiphenyl	<0.000030	0.000016 J	0.000019 J
PCB 194	22'33'44'55'-Octachlorobiphenyl	<0.000030	<0.000030	<0.000030
PCB 195	22'33'44'56-Octachlorobiphenyl	<0.000030	<0.000030	<0.000030
PCB 196	22'33'44'56'-Octachlorobiphenyl	<0.000030	<0.000030	<0.000030
PCB 199	22'33'455'6'-Octachlorobiphenyl	<0.000030	<0.000030	<0.000030
PCB 201	22'33'45'66'-Octachlorobiphenyl	<0.000030	0.000096	0.000099
PCB 202	22'33'55'66'-Octachlorobiphenyl	<0.000030	<0.000030	0.000026 J
PCB 203	22'344'55'6'-Octachlorobiphenyl	<0.000030	<0.000030	<0.000030
PCB 205	233'44'55'6-Octachlorobiphenyl	<0.000030	<0.000030	<0.000030
PCB 206	22'33'44'55'6-Nonachlorobiphenyl	<0.000030	<0.000030	<0.000030
PCB 207	22'33'44'566'-Nonaachlorobiphenyl	<0.000030	<0.000030	<0.000030
PCB 208	22'33'455'66'-Nonachlorobiphenyl	<0.000030	0.000011 J	0.000019 J
PCB 66	23'44'-Tetrachlorobiphenyl	<0.000030	<0.000030	<0.000030
PCB 155	22'44'66-Hexachlorobiphenyl	<0.000030	<0.000030	<0.000030
PCB 184	22'344'66'-Heptachlorobiphenyl	<0.000030	0.000071	0.000015 J

Table D.4 PAH Analysis for Fabric A Barge Simulation Test

	Sample	Sample	Sample	Sample	Sample	Sample
Chemical	**T-1**	**D-1**	**T-2**	**D-2**	**T-3**	**D-3**
	mg/l	mg/l	mg/l	mg/l	mg/l	mg/l
Naphthalene	<0.0003	<0.0003	<0.0003	0.00006	<0.0003	0.00007
Adenaphthylene	<0.0003	<0.0003	<0.0003	<0.0003	<0.0003	<0.0003
Acenaphthene	<0.0003	<0.0003	<0.0003	<0.0003	<0.0003	<0.0003
Fluorene	<0.0003	<0.0003	<0.0003	0.00006	0.00007	0.00006
Phenanthrene	<0.0003	<0.0003	0.0016	0.0001	0.00016	0.0001
Anthracene	<0.0003	<0.0003	0.00006	<0.0003	0.00006	0.0003
Fluoranthene	<0.0003	<0.0003	0.00024	0.00011	0.00022	0.0001
Pyrene	<0.0003	<0.0003	.0002	0.00009	0.00019	0.00009
Chrysene	<0.0003	<0.0003	0.00009	<0.0003	0.00007	<0.0003
Benzo (a) Anthracene	<0.0003	<0.0003	0.00009	<0.0003	0.00009	<0.0003
Benzo (b)Fluoranthene	<0.0003	<0.0003	0.00006	<0.0003	0.00006	<0.0003
Benzo (k) Fluoranthene	<0.0003	<0.0003	0.00005	<0.0003	<0.0003	<0.0003
Benzo (9a) Pyrene	<0.0003	<0.0003	<0.0003	<0.0003	<0.0003	<0.0003
(1, 2, 3-C, D) Pyrene	<0.0003	<0.0003	<0.0003	<0.0003	<0.0003	<0.0003
Dibenzo (A,H) Anthracene.	<0.0003	<0.0003	<0.0003	<0.0003	<0.0003	<0.0003
Benzo (G, H, I) Perylene	<0.0003	<0.0003	<0.0003	<0.0003	<0.0003	<0.0003
Methylnaphthalene	<0.0003	<0.0003	<0.0003	<0.0003	<0.0003	<0.0003

Table D.5 PAH Analysis for Fabric A + B Barge Simulation Test

	Sample	Sample	Sample	Sample	Sample	Sample
Chemical	**T-1**	**D-1**	**T-2**	**D-2**	**T-3**	**D-3**
	mg/l	mg/l	mg/l	mg/l	mg/l	mg/l
Naphthalene	<0.0003	<0.0003	<0.0003	<0.0003	<0.0003	0.00007
Adenaphthylene	<0.0003	<0.0003	<0.0003	<0.0003	<0.0003	<0.0003
Acenaphthene	<0.0003	<0.0003	<0.0003	<0.0003	<0.0003	<0.0003
Fluorene	<0.0003	<0.0003	<0.0003	<0.0003	<0.0003	<0.0003
Phenanthrene	<0.0003	<0.0003	<0.0003	<0.0003	0.00008	0.00006
Anthracene	<0.0003	<0.0003	<0.0003	<0.0003	0.00006	<0.0003
Fluoranthene	<0.0003	<0.0003	<0.0003	<0.0003	0.00008	<0.0003
Pyrene	<0.0003	<0.0003	<0.0003	<0.0003	0.00007	<0.0003
Chrysene	<0.0003	<0.0003	<0.0003	<0.0003	<0.0003	<0.0003
Benzo (a) Anthracene	<0.0003	<0.0003	<0.0003	<0.0003	<0.0003	<0.0003
Benzo (b)Fluoranthene	<0.0003	<0.0003	<0.0003	<0.0003	<0.0003	<0.0003
Benzo (k) Fluoranthene	<0.0003	<0.0003	<0.0003	<0.0003	<0.0003	<0.0003
Benzo (9a) Pyrene	<0.0003	<0.0003	<0.0003	<0.0003	<0.0003	<0.0003
(1, 2, 3-C, D) Pyrene	<0.0003	<0.0003	<0.0003	<0.0003	<0.0003	<0.0003
Dibenzo (A,H) Anthracene.	<0.0003	<0.0003	<0.0003	<0.0003	<0.0003	<0.0003
Benzo (G, H, I) Perylene	<0.0003	<0.0003	<0.0003	<0.0003	<0.0003	<0.0003
Methylnaphthalene	<0.0003	<0.0003	<0.0003	<0.0003	<0.0003	<0.0003

Table D.6 PAH Analysis for Fabric A +D Barge Simulation Test

	Sample	Sample	Sample	Sample	Sample	Sample
Chemical	**T-1**	**D-1**	**T-2**	**D-2**	**T-3**	**D-3**
	mg/l	mg/l	mg/l	Mg/l	mg/l	mg/l
Naphthalene	<0.0003	<0.0003	<0.0003	<0.0003	<0.0003	0.00007
Adenaphthylene	<0.0003	<0.0003	<0.0003	<0.0003	<0.0003	<0.0003
Acenaphthene	<0.0003	<0.0003	<0.0003	<0.0003	<0.0003	<0.0003
Fluorene	<0.0003	<0.0003	<0.0003	<0.0003	<0.0003	<0.0003
Phenanthrene	<0.0003	<0.0003	<0.0003	<0.0003	<0.0003	<0.0003
Anthracene	<0.0003	<0.0003	<0.0003	<0.0003	<0.0003	<0.0003
Fluoranthene	<0.0003	<0.0003	<0.0003	<0.0003	<0.0003	<0.0003
Pyrene	<0.0003	<0.0003	<0.0003	<0.0003	<0.0003	<0.0003
Chrysene	<0.0003	<0.0003	<0.0003	<0.0003	<0.0003	<0.0003
Benzo (a) Anthracene	<0.0003	<0.0003	<0.0003	<0.0003	<0.0003	<0.0003
Benzo (b)Fluoranthene	<0.0003	<0.0003	<0.0003	<0.0003	<0.0003	<0.0003
Benzo (k) Fluoranthene	<0.0003	<0.0003	<0.0003	<0.0003	<0.0003	<0.0003
Benzo (9a) Pyrene	<0.0003	<0.0003	<0.0003	<0.0003	<0.0003	<0.0003
(1, 2, 3-C, D) Pyrene	<0.0003	<0.0003	<0.0003	<0.0003	<0.0003	<0.0003
Dibenzo (A,H) Anthracene.	<0.0003	<0.0003	<0.0003	<0.0003	<0.0003	<0.0003
Benzo (G, H, I) Perylene	<0.0003	<0.0003	<0.0003	<0.0003	<0.0003	<0.0003
Methylnaphthalene	<0.0003	<0.0003	<0.0003	<0.0003	<0.0003	<0.0003

Table D.7 Dioxin and Furan Analysis for Fabric A Barge Simulation Test

	Sample 1	Sample 2	Sample 3
Isomer			
	pg/l	pg/l	pg/l
2,3,7,8-TCDF	undetected	undetected	undetected
2,3,7,8-TCDD	undetected	undetected	undetected
1,2,3,7,8-PeCDF	undetected	1.81	undetected
2,3,4,7,8-PeCDF	undetected	undetected	undetected
1,2,3,7,8-PeCDD	undetected	undetected	undetected
1,2,3,4,7,8-HxCDF	undetected	3.21	undetected
1,2,3,6,7,8-HxCDF	undetected	undetected	undetected
2,3,4,6,7,8-HxCDF	1.59	2.13	2.07
1,2,3,7,8,9-HxCDF	undetected	undetected	undetected
1,2,3,4,7,8-HxCDD	undetected	undetected	undetected
1,2,3,6,7,8-HxCDD	undetected	undetected	undetected
1,2,3,7,8,9-HxCDD	undetected	undetected	undetected
1,2,3,4,6,7,8-HpCDF	3.39	9.17	6.65
1,2,3,4,7,8,9-HpCDF	undetected	undetected	undetected
1,2,3,4,6,7,8-HpCDD	7.99	10.5	12.3
OCDF	5.33	7.80	8.53
OCDD	91.9	68.2	106
TCDF	undetected	undetected	undetected
TCDD	undetected	undetected	undetected
PECDF	undetected	8.22	undetected
PECDD	undetected	1.06	undetected
HXCDF	undetected	5.35	2.07
HXCDD	undetected	1.79	undetected
HPCDF	6.65	9.17	5.38
HPCDD	12.3	19.9	7.99

Table D.8 Dioxin and Furan Analysis for Fabric A+B Barge Simulation Test

	Sample 1	Sample 2	Sample 3
Isomer			
	pg/l	pg/l	pg/l
2,3,7,8-TCDF	Undetected	undetected	undetected
2,3,7,8-TCDD	Undetected	undetected	undetected
1,2,3,7,8-PeCDF	Undetected	undetected	undetected
2,3,4,7,8-PeCDF	Undetected	undetected	undetected
1,2,3,7,8-PeCDD	Undetected	undetected	undetected
1,2,3,4,7,8-HxCDF	Undetected	undetected	0.562
1,2,3,6,7,8-HxCDF	Undetected	undetected	0.425
2,3,4,6,7,8-HxCDF	1.77	undetected	1.58
1,2,3,7,8,9-HxCDF	Undetected	undetected	undetected
1,2,3,4,7,8-HxCDD	Undetected	undetected	undetected
1,2,3,6,7,8-HxCDD	Undetected	undetected	2.05
1,2,3,7,8,9-HxCDD	Undetected	undetected	undetected
1,2,3,4,6,7,8-HpCDF	Undetected	20.4	9.53
1,2,3,4,7,8,9-HpCDF	Undetected	undetected	undetected
1,2,3,4,6,7,8-HpCDD	4.14	46.7	24.0
OCDF	Undetected	126	7.38
OCDD	27.3	163	80.5
TCDF	Undetected	58.1	undetected
TCDD	Undetected	undetected	undetected
PECDF	Undetected	31.9	undetected
PECDD	Undetected	undetected	undetected
HXCDF	1.77	undetected	7.30
HXCDD	Undetected	undetected	2.05
HPCDF	Undetected	20.4	22.2
HPCDD	7.84	119	39.9

Table D.9 Dioxin and Furan Analysis for Fabric A+D Barge Simulation Test

	Sample 1	Sample 2	Sample 3
Isomer			
	pg/l	pg/l	pg/l
2,3,7,8-TCDF	undetected	Undetected	undetected
2,3,7,8-TCDD	undetected	Undetected	undetected
1,2,3,7,8-PeCDF	undetected	Undetected	undetected
2,3,4,7,8-PeCDF	undetected	Undetected	undetected
1,2,3,7,8-PeCDD	2.68	Undetected	undetected
1,2,3,4,7,8-HxCDF	undetected	Undetected	undetected
1,2,3,6,7,8-HxCDF	undetected	Undetected	undetected
2,3,4,6,7,8-HxCDF	3.84	Undetected	3.34
1,2,3,7,8,9-HxCDF	3.27	Undetected	undetected
1,2,3,4,7,8-HxCDD	undetected	Undetected	undetected
1,2,3,6,7,8-HxCDD	undetected	undetected	undetected
1,2,3,7,8,9-HxCDD	4.64	undetected	undetected
1,2,3,4,6,7,8-HpCDF	7.16	undetected	2.21
1,2,3,4,7,8,9-HpCDF	undetected	undetected	undetected
1,2,3,4,6,7,8-HpCDD	12.6	3.12	7.26
OCDF	undetected	undetected	1.99
OCDD	215	20.3	92.5
TCDF	undetected	undetected	undetected
TCDD	undetected	undetected	undetected
PECDF	undetected	undetected	undetected
PECDD	2.68	undetected	undetected
HXCDF	7.50	undetected	3.43
HXCDD	4.64	undetected	undetected
HPCDF	9.94	undetected	2.21
HPCDD	12.6	3.12	7.26

APPENDIX E. Determination of Apparent Opening of Geotextile under Strain.

Table E.1 Determination of Apparent Opening Size of Geotextile A (Specimen 1)

Strain	U.S Sieve	Minimum Diameter	Wt F+G	Wt Beads input	Wt F+G w/Beads	Wt Pan Empty	Wt Pan w/Beads	% Passing
(%)	(mm)	(mm)	(g)	(g)	(g)	(g)	(g)	
0	100-140	0.106	9012	50	9062	3079	3096	34
0	80-100	0.150	9012	50	9062	3079	3084	10
0	70-80	0.180	9012	50	9062	3079	3081	4
0	60-70	0.212	9012	50	9062	3079	3080	2
3	80-100	0.150	9012	50	9062	3079	3089	20
3	70-80	0.180	9012	50	9062	3079	3085	12
3	60-70	0.212	9012	50	9062	3079	3082	6
3	45-60	0.250	9012	50	9062	3079	3080	2
6	80-100	0.150	9012	50	9062	3079	3099	40
6	70-80	0.180	9012	50	9062	3079	3092	26
6	45-60	0.250	9012	50	9062	3079	3082	6
6	40-50	0.300	9012	50	9062	3079	3081	4
9	70-80	0.180	9012	50	9062	3079	3098	38
9	45-60	0.250	9012	50	9062	3079	3090	22
9	40-50	0.300	9012	50	9062	3079	3083	8
9	30-40	0.425	9012	50	9062	3079	3080	2

F+G = Frame of Straining device with geotextile attached

Table E.2 Determination of Apparent Opening Size of Geotextile A (Specimen 2)

Strain	U.S Sieve	Minimum Diameter	Wt F+G	Wt Beads input	Wt F+G w/Beads	Wt Pan empty	Wt Pan w/Beads	% Passing
(%)	(mm)	(mm)	(g)	(g)	(g)	(g)	(g)	
0	100-140	0.106	9008	50	9058	3079	3089	20
0	80-100	0.150	9008	50	9058	3079	3085	12
0	70-80	0.180	9008	50	9058	3079	3080.5	3
0	60-70	0.212	9008	50	9058	3079	3079	0
3	80-100	0.150	9008	50	9058	3079	3091.5	25
3	70-80	0.180	9008	50	9058	3079	3087	16
3	60-70	0.212	9008	50	9058	3079	3081.5	5
3	45-60	0.250	9008	50	9058	3079	3080.5	3
6	80-100	0.150	9008	50	9058	3079	3095	32
6	70-80	0.180	9008	50	9058	3079	3089	20
6	45-60	0.250	9008	50	9058	3079	3083	8
6	40-50	0.300	9008	50	9058	3079	3080	2
9	70-80	0.180	9008	50	9058	3079	3100	42
9	45-60	0.250	9008	50	9058	3079	3091.5	25
9	40-50	0.300	9008	50	9058	3079	3084	10
9	30-40	0.425	9008	50	9058	3079	3081	4

F+G = Frame of Straining device with geotextile attached

Table E.3 Determination of Apparent Opening Size of Geotextile A (Specimen 3)

Strain	U.S Sieve	Minimum Diameter	Wt F+G	Wt Beads Input	Wt F+G w/Beads	Wt Pan empty	Wt Pan w/Beads	% Passing
(%)	(mm)	(mm)	(g)	(g)	(g)	(g)	(g)	
0	100-140	0.106	9014	50	9064	3079	3084	10
0	80-100	0.150	9014	50	9064	3079	3083	8
0	70-80	0.180	9014	50	9064	3079	3081	4
0	60-70	0.212	9014	50	9064	3079	3079.5	1
3	80-100	0.150	9014	50	9064	3079	3088	18
3	70-80	0.180	9014	50	9064	3079	3087	16
3	60-70	0.212	9014	50	9064	3079	3082	6
3	45-60	0.250	9014	50	9064	3079	3079	0
6	80-100	0.150	9014	50	9064	3079	3095	32
6	70-80	0.180	9014	50	9064	3079	3090.5	23
6	45-60	0.250	9014	50	9064	3079	3083.5	9
6	40-50	0.300	9014	50	9064	3079	3081.5	5
9	70-80	0.180	9014	50	9064	3079	3096	34
9	45-60	0.250	9014	50	9064	3079	3088	18
9	40-50	0.300	9014	50	9064	3079	3084	10
9	30-40	0.425	9014	50	9064	3079	3079.5	1

F+G = Frame of Straining device with geotextile attached

Table E.4 Determination of Apparent Opening Size of Geotextile A (Specimen 4)

Strain	U.S Sieve	Minimum Diameter	Wt F+G	Wt Beads Input	Wt F+G w/Beads	Wt Pan empty	Wt Pan w/Beads	% Passing
(%)	(mm)	(mm)	(g)	(g)	(g)	(g)	(g)	
0	100-140	0.106	9015	50	9065	3079	3101.5	45
0	80-100	0.150	9015	50	9065	3079	3095.5	33
0	70-80	0.180	9015	50	9065	3079	3080.5	3
0	60-70	0.212	9015	50	9065	3079	3079	0
3	80-100	0.150	9015	50	9065	3079	3103	48
3	70-80	0.180	9015	50	9065	3079	3097	36
3	60-70	0.212	9015	50	9065	3079	3081	4
3	45-60	0.250	9015	50	9065	3079	3079.5	1
6	80-100	0.150	9015	50	9065	3079	3103	48
6	70-80	0.180	9015	50	9065	3079	3096.5	35
6	45-60	0.250	9015	50	9065	3079	3085	12
6	40-50	0.300	9015	50	9065	3079	3081	4
9	70-80	0.180	9015	50	9065	3079	3104.5	51
9	45-60	0.250	9015	50	9065	3079	3100	42
9	40-50	0.300	9015	50	9065	3079	3088	18
9	30-40	0.425	9015	50	9065	3079	3082	6

F+G = Frame of Straining device with geotextile attached

Table E.5 Determination of Apparent Opening Size of Geotextile A (Specimen 5)

Strain	U.S Sieve	Minimum Diameter	Wt F+G	Wt Beads Input	Wt F+G w/Beads	Wt Pan empty	Wt Pan w/Beads	% Passing
(%)	(mm)	(mm)	(g)	(g)	(g)	(g)	(g)	
0	100-140	0.106	9014	50	9064	3079	3087	16
0	80-100	0.150	9014	50	9064	3079	3083	8
0	70-80	0.180	9014	50	9064	3079	3080	2
0	60-70	0.212	9014	50	9064	3079	3079	0
3	80-100	0.150	9014	50	9064	3079	3088.5	19
3	70-80	0.180	9014	50	9064	3079	3084.5	11
3	60-70	0.212	9014	50	9064	3079	3080.5	3
3	45-60	0.250	9014	50	9064	3079	3079.5	1
6	80-100	0.150	9014	50	9064	3079	3095.5	33
6	70-80	0.180	9014	50	9064	3079	3090	22
6	45-60	0.250	9014	50	9064	3079	3082	6
6	40-50	0.300	9014	50	9064	3079	3080.5	3
9	70-80	0.180	9014	50	9064	3079	3099.5	41
9	45-60	0.250	9014	50	9064	3079	3091.5	25
9	40-50	0.300	9014	50	9064	3079	3084	10
9	30-40	0.425	9014	50	9064	3079	3080.5	3

F+G = Frame of Straining device with geotextile attached

Table E.6 Determination of Apparent Opening Size of Geotextile B (Specimen 1)

Strain	U.S Sieve	Minimum Diameter	Wt F+G	Wt Beads Input	Wt F+G w/Beads	Wt Pan empty	Wt Pan w/Beads	% Passing
(%)	(mm)	(mm)	(g)	(g)	(g)	(g)	(g)	
0	140-200	0.075	8980	50	9030	3079	3106.5	55
0	100-140	0.106	8980	50	9030	3079	3095	32
0	80-100	0.150	8980	50	9030	3079	3082.5	7
0	70-80	0.180	8980	50	9030	3079	3079.5	1
3	140-200	0.075	8980	50	9030	3079	3108	58
3	100-140	0.106	8980	50	9030	3079	3102	46
3	80-100	0.150	8980	50	9030	3079	3081.5	5
3	70-80	0.180	8980	50	9030	3079	3080	2
6	140-200	0.075	8980	50	9030	3079	3105	52
6	100-140	0.106	8980	50	9030	3079	3095.5	33
6	80-100	0.150	8980	50	9030	3079	3082	6
6	70-80	0.180	8980	50	9030	3079	3080.5	3
9	140-200	0.075	8980	50	9030	3079	3100	42
9	100-140	0.106	8980	50	9030	3079	3086.5	15
9	80-100	0.150	8980	50	9030	3079	3080.5	3
9	70-80	0.180	8980	50	9030	3079	3079	0

F+G = Frame of Straining device with geotextile attached

Table E.7 Determination of Apparent Opening Size of Geotextile B (Specimen 2)

Strain	U.S Sieve	Minimum Diameter	Wt F+G	Wt Beads input	Wt F+G w/Beads	Wt Pan empty	Wt Pan w/Beads	% Passing
(%)	(mm)	(mm)	(g)	(g)	(g)	(g)	(g)	
0	140-200	0.075	8981	50	9031	3079	3104	50
0	100-140	0.106	898	50	9031	3079	3091	24
0	80-100	0.150	8981	50	9031	3079	3081	4
0	70-80	0.180	8981	50	9031	3079	3079.5	1
3	140-200	0.075	8981	50	9031	3079	3013.5	49
3	100-140	0.106	8981	50	9031	3079	3090.5	23
3	80-100	0.150	8981	50	9031	3079	3081.5	5
3	70-80	0.180	8981	50	9031	3079	3079.5	1
6	140-200	0.075	8981	50	9031	3079	3095.1	33
6	100-140	0.106	8981	50	9031	3079	3086.5	15
6	80-100	0.150	8981	50	9031	3079	3080.5	3
6	70-80	0.180	8981	50	9031	3079	3079	0
9	140-200	0.075	8981	50	9031	3079	3092	26
9	100-140	0.106	8981	50	9031	3079	3081	4
9	80-100	0.150	8981	50	9031	3079	3079.5	1
9	70-80	0.180	8981	50	9031	3079	3079	0

F+G = Frame of Straining device with geotextile attached

Table E.8 Determination of Apparent Opening Size of Geotextile B (Specimen 3)

Strain	U.S Sieve	Minimum Diameter	Wt F+G	Wt Beads Input	Wt F+G w/Beads	Wt Pan empty	Wt Pan w/Beads	% Passing
(%)	(mm)	(mm)	(g)	(g)	(g)	(g)	(g)	
0	140-200	0.075	8983	50	9033	3079	3102	46
0	100-140	0.106	8983	50	9033	3079	3086	14
0	80-100	0.150	8983	50	9033	3079	3080.5	3
0	70-80	0.180	8983	50	9033	3079	3079	0
3	140-200	0.075	8983	50	9033	3079	3099.5	41
3	100-140	0.106	8983	50	9033	3079	3088	18
3	80-100	0.150	8983	50	9033	3079	3080	2
3	70-80	0.180	8983	50	9033	3079	3079.5	1
6	140-200	0.075	8983	50	9033	3079	3097	36
6	100-140	0.106	8983	50	9033	3079	3085	12
6	80-100	0.150	8983	50	9033	3079	3081	4
6	70-80	0.180	8983	50	9033	3079	3079.5	1
9	140-200	0.075	8983	50	9033	3079	3096	34
9	100-140	0.106	8983	50	9033	3079	3080.5	3
9	80-100	0.150	8983	50	9033	3079	3079	0
9	70-80	0.180	8983	50	9033	3079	3079	0

F+G = Frame of Straining device with geotextile attached

Table E.9 Determination of Apparent Opening Size of Geotextile B (Specimen 4)

Strain	U.S Sieve	Minimum Diameter	Wt F+G	Wt Beads Input	Wt F+G w/Beads	Wt Pan empty	Wt Pan w/Beads	% Passing
(%)	(mm)	(mm)	(g)	(g)	(g)	(g)	(g)	
0	140-200	0.075	8980	50	9030	3079	3098	38
0	100-140	0.106	8980	50	9030	3079	3091.5	25
0	80-100	0.150	8980	50	9030	3079	3080	2
0	70-80	0.180	8980	50	9030	3079	3079	0
3	140-200	0.075	8980	50	9030	3079	3101.5	45
3	100-140	0.106	8980	50	9030	3079	3086.5	15
3	80-100	0.150	8980	50	9030	3079	3080.5	3
3	70-80	0.180	8980	50	9030	3079	3079	0
6	140-200	0.075	8980	50	9030	3079	3103	48
6	100-140	0.106	8980	50	9030	3079	3088	18
6	80-100	0.150	8980	50	9030	3079	3081.5	5
6	70-80	0.180	8980	50	9030	3079	3079.5	1
9	140-200	0.075	8980	50	9030	3079	3092	26
9	100-140	0.106	8980	50	9030	3079	3080	2
9	80-100	0.150	8980	50	9030	3079	3079	0
9	70-80	0.180	8980	50	9030	3079	3079	0

F+G = Frame of Straining device with geotextile attached

Table E.10 Determination of Apparent Opening Size of Geotextile B (Specimen 5)

Strain	U.S Sieve	Minimum Diameter	Wt F+G	Wt Beads Input	Wt F+G w/Beads	Wt Pan empty	Wt Pan w/Beads	% Passing
(%)	(mm)	(mm)	(g)	(g)	(g)	(g)	(g)	
0	140-200	0.075	8981	50	9031	3079	3100.5	43
0	100-140	0.106	8981	50	9031	3079	3087	16
0	80-100	0.150	8981	50	9031	3079	3080.5	3
0	70-80	0.180	8981	50	9031	3079	3079.5	1
3	140-200	0.075	8981	50	9031	3079	3100.5	43
3	100-140	0.106	8981	50	9031	3079	3088.5	19
3	80-100	0.150	8981	50	9031	3079	3079.5	1
3	70-80	0.180	8981	50	9031	3079	3079.5	1
6	140-200	0.075	8981	50	9031	3079	3093.5	29
6	100-140	0.106	8981	50	9031	3079	3085	12
6	80-100	0.150	8981	50	9031	3079	3080	2
6	70-80	0.180	8981	50	9031	3079	3079	0
9	140-200	0.075	8981	50	9031	3079	3086	14
9	100-140	0.106	8981	50	9031	3079	3082	6
9	80-100	0.150	8981	50	9031	3079	3080.5	3
9	70-80	0.180	8981	50	9031	3079	3079	0

F+G = Frame of Straining device with geotextile attached

Table E.11 Determination of Apparent Opening Size of Geotextile C (Specimen 1)

Strain	U.S Sieve	Minimum Diameter	Wt F+G	Wt Beads input	Wt F+G w/Beads	Wt Pan empty	Wt Pan w/Beads	% Passing
(%)	(mm)	(mm)	(g)	(g)	(g)	(g)	(g)	
0	140-200	0.075	8986	50	9036	3079	3101	44
0	100-140	0.106	8986	50	9036	3079	3084	10
0	80-100	0.150	8986	50	9036	3079	3081	4
3	140-200	0.075	8986	50	9036	3079	3097.5	37
3	100-140	0.106	8986	50	9036	3079	3083	8
3	80-100	0.150	8986	50	9036	3079	3081	4
6	140-200	0.075	8986	50	9036	3079	3102	46
6	100-140	0.106	8986	50	9036	3079	3081	4
6	80-100	0.150	8986	50	9036	3079	3079	0
9	140-200	0.075	8986	50	9036	3079	3100	42
9	100-140	0.106	8986	50	9036	3079	3082	6
9	80-100	0.150	8986	50	9036	3079	3079.5	1

F+G = Frame of Straining device with geotextile attached

Table E.12 Determination of Apparent Opening Size of Geotextile C (Specimen 2)

Strain	U.S Sieve	Minimum Diameter	Wt F+G	Wt Beads Input	Wt F+G w/Beads	Wt Pan empty	Wt Pan w/Beads	% Passing
(%)	(mm)	(mm)	(g)	(g)	(g)	(g)	(g)	
0	140-200	0.075	8986	50	9036	3079	3098	38
0	100-140	0.106	8986	50	9036	3079	3082	6
0	80-100	0.150	8986	50	9036	3079	3080	2
3	140-200	0.075	8986	50	9036	3079	3098	38
3	100-140	0.106	8986	50	9036	3079	3081.5	5
3	80-100	0.150	8986	50	9036	3079	3079.5	1
6	140-200	0.075	8986	50	9036	3079	3100	42
6	100-140	0.106	8986	50	9036	3079	3082	6
6	80-100	0.150	8986	50	9036	3079	3079.5	1
9	140-200	0.075	8986	50	9036	3079		34
9	100-140	0.106	8986	50	9036	3079		4
9	80-100	0.150	8986	50	9036	3079		3

F+G = Frame of Straining device with geotextile attached

Table E.13 Determination of Apparent Opening Size of Geotextile C (Specimen 3)

Strain	U.S Sieve	Minimum Diameter	Wt F+G	Wt Beads Input	Wt F+G w/Beads	Wt Pan empty	Wt Pan w/Beads	% Passing
(%)	(mm)	(mm)	(g)	(g)	(g)	(g)	(g)	
0	140-200	0.075	8986	50	9036	3079	3099	40
0	100-140	0.106	8986	50	9036	3079	3080.5	3
0	80-100	0.150	8986	50	9036	3079	3079.5	1
3	140-200	0.075	8986	50	9036	3079	3099.5	41
3	100-140	0.106	8986	50	9036	3079	3080	2
3	80-100	0.150	8986	50	9036	3079	3080.5	3
6	140-200	0.075	8986	50	9036	3079	3096	34
6	100-140	0.106	8986	50	9036	3079	3080.5	3
6	80-100	0.150	8986	50	9036	3079	3079.5	1
9	140-200	0.075	8986	50	9036	3079	3095	32
9	100-140	0.106	8986	50	9036	3079	3080.5	3
9	80-100	0.150	8986	50	9036	3079	3079.5	1

F+G = Frame of Straining device with geotextile attached

Table E.14 Determination of Apparent Opening Size of Geotextile C (Specimen 4)

Strain	U.S Sieve	Minimum Diameter	Wt F+G	Wt Beads input	Wt F+G w/Beads	Wt Pan empty	Wt Pan w/Beads	% Passing
(%)	(mm)	(mm)	(g)	(g)	(g)	(g)	(g)	
0	140-200	0.075	8984	50	9034	3079	3097	36
0	100-140	0.106	8984	50	9034	3079	3080.5	3
0	80-100	0.150	8984	50	9034	3079	3079	0
3	140-200	0.075	8984	50	9034	3079	3095	32
3	100-140	0.106	8984	50	9034	3079	3080.5	3
3	80-100	0.150	8984	50	9034	3079	3079.5	1
6	140-200	0.075	8984	50	9034	3079	3093.5	29
6	100-140	0.106	8984	50	9034	3079	3080	2
6	80-100	0.150	8984	50	9034	3079	3080.5	3
9	140-200	0.075	8984	50	9034	3079	3097	36
9	100-140	0.106	8984	50	9034	3079	3081.5	5
9	80-100	0.150	8984	50	9034	3079	3080.5	3

F+G = Frame of Straining device with geotextile attached

Table E.15 Determination of Apparent Opening Size of Geotextile C (Specimen 5)

Strain	U.S Sieve	Minimum Diameter	Wt F+G	Wt Beads Input	Wt F+G w/Beads	Wt Pan empty	Wt Pan w/Beads	% Passing
(%)	(mm)	(mm)	(g)	(g)	(g)	(g)	(g)	
0	140-200	0.075	8984	50	9034	3079	3091	24
0	100-140	0.106	8984	50	9034	3079	3080.5	3
0	80-100	0.150	8984	50	9034	3079	3079.5	1
3	140-200	0.075	8984	50	9034	3079	3097.5	37
3	100-140	0.106	8984	50	9034	3079	3079	0
3	80-100	0.150	8984	50	9034	3079	3079	0
6	140-200	0.075	8984	50	9034	3079	3092.5	27
6	100-140	0.106	8984	50	9034	3079	3079	0
6	80-100	0.150	8984	50	9034	3079	3079	0
9	140-200	0.075	8984	50	9034	3079	3093	28
9	100-140	0.106	8984	50	9034	3079	3079	0
9	80-100	0.150	8984	50	9034	3079	3079.5	1

F+G = Frame of Straining device with geotextile attached

Table E.16 Determination of Apparent Opening Size of Geotextile D (Specimen 1)

Strain	U.S Sieve	Minimum Diameter	Wt F+G	Wt Beads Input	Wt F+G w/Beads	Wt Pan empty	Wt Pan w/Beads	% Passing
(%)	(mm)	(mm)	(g)	(g)	(g)	(g)	(g)	
0	140-200	0.075	8992	50	9042	3079	3098	38
0	100-140	0.106	8992	50	9042	3079	3082	6
0	80-100	0.150	8992	50	9042	3079	3080	2
3	140-200	0.075	8992	50	9042	3079	3098	38
3	100-140	0.106	8992	50	9042	3079	3082	6
3	80-100	0.150	8992	50	9042	3079	3079.5	1
6	140-200	0.075	8992	50	9042	3079	3097	36
6	100-140	0.106	8992	50	9042	3079	3081	4
6	80-100	0.150	8992	50	9042	3079	3079	0
9	140-200	0.075	8992	50	9042	3079	3092	26
9	100-140	0.106	8992	50	9042	3079	3081	4
9	80-100	0.150	8992	50	9042	3079	3080	2

F+G = Frame of Straining device with geotextile attached

Table E.17 Determination of Apparent Opening Size of Geotextile D (Specimen 2)

Strain	U.S Sieve	Minimum Diameter	Wt F+G	Wt Beads Input	Wt F+G w/Beads	Wt Pan empty	Wt Pan w/Beads	% Passing
(%)	(mm)	(mm)	(g)	(g)	(g)	(g)	(g)	
0	140-200	0.075	8990	50	9040	3079	3097	36
0	100-140	0.106	8990	50	9040	3079	3081	4
0	80-100	0.150	8990	50	9040	3079	3079.5	1
3	140-200	0.075	8990	50	9040	3079	3093.5	29
3	100-140	0.106	8990	50	9040	3079	3081.5	5
3	80-100	0.150	8990	50	9040	3079	3079	0
6	140-200	0.075	8990	50	9040	3079	3092	26
6	100-140	0.106	8990	50	9040	3079	3080.5	3
6	80-100	0.150	8990	50	9040	3079	3081	4
9	140-200	0.075	8990	50	9040	3079	3087.5	17
9	100-140	0.106	8990	50	9040	3079	3080	2
9	80-100	0.150	8990	50	9040	3079	3079	0

F+G = Frame of Straining device with geotextile attached

Table E.18 Determination of Apparent Opening Size of Geotextile D (Specimen 3)

Strain	U.S Sieve	Minimum Diameter	Wt F+G	Wt Beads Input	Wt F+G w/Beads	Wt Pan empty	Wt Pan w/Beads	% Passing
(%)	(mm)	(mm)	(g)	(g)	(g)	(g)	(g)	
0	140-200	0.075	8991	50	9041	3079	3100	42
0	100-140	0.106	8991	50	9041	3079	3080.5	3
0	80-100	0.150	8991	50	9041	3079	3079	0
3	140-200	0.075	8991	50	9041	3079	3097.5	37
3	100-140	0.106	8991	50	9041	3079	3079.5	1
3	80-100	0.150	8991	50	9041	3079	3079	0
6	140-200	0.075	8991	50	9041	3079	3096	34
6	100-140	0.106	8991	50	9041	3079	3080	2
6	80-100	0.150	8991	50	9041	3079	3081.5	5
9	140-200	0.075	8991	50	9041	3079	3085.5	13
9	100-140	0.106	8991	50	9041	3079	3079.5	1
9	80-100	0.150	8991	50	9041	3079	3079	0

F+G = Frame of Straining device with geotextile attached

Table E.19 Determination of Apparent Opening Size of Geotextile D (Specimen 4)

Strain	U.S Sieve	Minimum Diameter	Wt F+G	Wt Beads input	Wt F+G w/Beads	Wt Pan Empty	Wt Pan w/Beads	% Passing
(%)	(mm)	(mm)	(g)	(g)	(g)	(g)	(g)	
0	140-200	0.075	8993	50	9043	3079	3096.5	35
0	100-140	0.106	8993	50	9043	3079	3081	4
0	80-100	0.150	8993	50	9043	3079	3079	0
3	140-200	0.075	8993	50	9043	3079	3097	36
3	100-140	0.106	8993	50	9043	3079	3082	6
3	80-100	0.150	8993	50	9043	3079	3080	2
6	140-200	0.075	8993	50	9043	3079	3092.5	27
6	100-140	0.106	8993	50	9043	3079	3082	6
6	80-100	0.150	8993	50	9043	3079	3079	0
9	140-200	0.075	8993	50	9043	3079	3093.5	29
9	100-140	0.106	8993	50	9043	3079	3082.5	7
9	80-100	0.150	8993	50	9043	3079	3080.5	3

F+G = Frame of Straining device with geotextile attached

Table E.20 Determination of Apparent Opening Size of Geotextile D (Specimen 5)

Strain	U.S Sieve	Minimum Diameter	Wt F+G	Wt Beads input	Wt F+G w/Beads	Wt Pan Empty	Wt Pan w/Beads	% Passing
(%)	(mm)	(mm)	(g)	(g)	(g)	(g)	(g)	
0	140-200	0.075	8992	50	9042	3079	3088	18
0	100-140	0.106	8992	50	9042	3079	3080	2
0	80-100	0.150	8992	50	9042	3079	3079	0
3	140-200	0.075	8992	50	9042	3079	3090	22
3	100-140	0.106	8992	50	9042	3079	3080.5	3
3	80-100	0.150	8992	50	9042	3079	3079.5	1
6	140-200	0.075	8992	50	9042	3079	3088	18
6	100-140	0.106	8992	50	9042	3079	3079.5	1
6	80-100	0.150	8992	50	9042	3079	3079.5	1
9	140-200	0.075	8992	50	9042	3079	3087	16
9	100-140	0.106	8992	50	9042	3079	3079	0
9	80-100	0.150	8992	50	9042	3079	3079	0

F+G = Frame of Straining device with geotextile attached

Table E.21 Determination of Apparent Opening Size of Geotextile E (Specimen 1)

Strain	U.S Sieve	Minimum Diameter	Wt F+G	Wt Beads input	Wt F+G w/Beads	Wt Pan Empty	Wt Pan w/Beads	% Passing
(%)	(mm)	(mm)	(g)	(g)	(g)	(g)	(g)	
	200-finer	-	8999	50	9049	3079	3111	64
	140-200	0.075	8999	50	9049	3079	3083	8
	100-140	0.106	8999	50	9049	3079	3079.5	1
3	200-finer	-	8999	50	9049	3079	3108.5	59
3	140-200	0.075	8999	50	9049	3079	3081	4
3	100-140	0.106	8999	50	9049	3079	3079	0
6	200-finer	-	8999	50	9049	3079	3110.5	63
6	140-200	0.075	8999	50	9049	3079	3081.5	5
6	100-140	0.106	8999	50	9049	3079	3080	2
9	200-finer	-	8999	50	9049	3079	3108.5	59
9	140-200	0.075	8999	50	9049	3079	3082	6
9	100-140	0.106	8999	50	9049	3079	3079.5	1

F+G = Frame of Straining device with geotextile attached

Table E.22 Determination of Apparent Opening Size of Geotextile E (Specimen 2)

Strain	U.S Sieve	Minimum Diameter	Wt F+G	Wt Beads Input	Wt F+G w/Beads	Wt Pan empty	Wt Pan w/Beads	% Passing
(%)	(mm)	(mm)	(g)	(g)	(g)	(g)	(g)	
0	200-finer	-	8998	50	9048	3079	3114.5	71
0	140-200	0.075	8998	50	9048	3079	3081	4
0	100-140	0.106	8998	50	9048	3079	3079	0
3	200-finer	-	8998	50	9048	3079	3107.5	57
3	140-200	0.075	8998	50	9048	3079	3080.5	3
3	100-140	0.106	8998	50	9048	3079	3079.5	1
6	200-finer	-	8998	50	9048	3079	3106.5	55
6	140-200	0.075	8998	50	9048	3079	3080	2
6	100-140	0.106	8998	50	9048	3079	3079	0
9	200-finer	-	8998	50	9048	3079	3110	62
9	140-200	0.075	8998	50	9048	3079	3082.5	7
9	100-140	0.106	8998	50	9048	3079	3079	0

F+G = Frame of Straining device with geotextile attached

Table E.23 Determination of Apparent Opening Size of Geotextile E (Specimen 3)

Strain	U.S Sieve	Minimum Diameter	Wt F+G	Wt Beads Input	Wt F+G w/Beads	Wt Pan empty	Wt Pan w/Beads	% Passing
(%)	(mm)	(mm)	(g)	(g)	(g)	(g)	(g)	
0	200-finer	-	8995	50	9045	3079	3098	38
0	140-200	0.075	8995	50	9045	3079	3080.5	3
0	100-140	0.106	8995	50	9045	3079	3080	2
3	200-finer	-	8995	50	9045	3079	3099.5	41
3	140-200	0.075	8995	50	9045	3079	3079.5	1
3	100-140	0.106	8995	50	9045	3079	3080.5	3
6	200-finer	-	8995	50	9045	3079	3094.5	31
6	140-200	0.075	8995	50	9045	3079	3079	0
6	100-140	0.106	8995	50	9045	3079	3079	0
9	200-finer	-	8995	50	9045	3079	3100	42
9	140-200	0.075	8995	50	9045	3079	3081	4
9	100-140	0.106	8995	50	9045	3079	3079	0

F+G = Frame of Straining device with geotextile attached

Table E.24 Determination of Apparent Opening Size of Geotextile E (Specimen 4)

Strain	U.S Sieve	Minimum Diameter	Wt F+G	Wt Beads Input	Wt F+G w/Beads	Wt Pan empty	Wt Pan w/Beads	% Passing
(%)	(mm)	(mm)	(g)	(g)	(g)	(g)	(g)	
0	200-finer	-	8996	50	9046	3079	3093.5	29
0	140-200	0.075	8996	50	9046	3079	3079.5	1
0	100-140	0.106	8996	50	9046	3079	3079.5	1
3	200-finer	-	8996	50	9046	3079	3095.5	33
3	140-200	0.075	8996	50	9046	3079	3080	2
3	100-140	0.106	8996	50	9046	3079	3080	2
6	200-finer	-	8996	50	9046	3079	3092.5	27
6	140-200	0.075	8996	50	9046	3079	3079	0
6	100-140	0.106	8996	50	9046	3079	3079	0
9	200-finer	-	8996	50	9046	3079	3093	28
9	140-200	0.075	8996	50	9046	3079	3080.5	3
9	100-140	0.106	8996	50	9046	3079	3079	0

F+G = Frame of Straining device with geotextile attached

Table E.25 Determination of Apparent Opening Size of Geotextile E (Specimen 5)

Strain	U.S Sieve	Minimum Diameter	Wt F+G	Wt Beads Input	Wt F+G w/Beads	Wt Pan empty	Wt Pan w/Beads	% Passing
(%)	(mm)	(mm)	(g)	(g)	(g)	(g)	(g)	
0	200.finer	-	8995	50	9045	3079	3088	18
0	140-200	0.075	8995	50	9045	3079	3079	0
0	100-140	0.106	8995	50	9045	3079	3079	0
3	200-finer	-	8995	50	9045	3079	3092.5	27
3	140-200	0.075	8995	50	9045	3079	3079.5	1
3	100-140	0.106	8995	50	9045	3079	3079.5	1
6	200-finer	-	8995	50	9045	3079	3095	32
6	140-200	0.075	8995	50	9045	3079	3080.5	3
6	100-140	0.106	8995	50	9045	3079	3079.5	1
9	200-finer	-	8995	50	9045	3079	3100	42
9	140-200	0.075	8995	50	9045	3079	3079.5	1
9	100-140	0.106	8995	50	9045	3079	3079	0

F+G = Frame of Straining device with geotextile attached

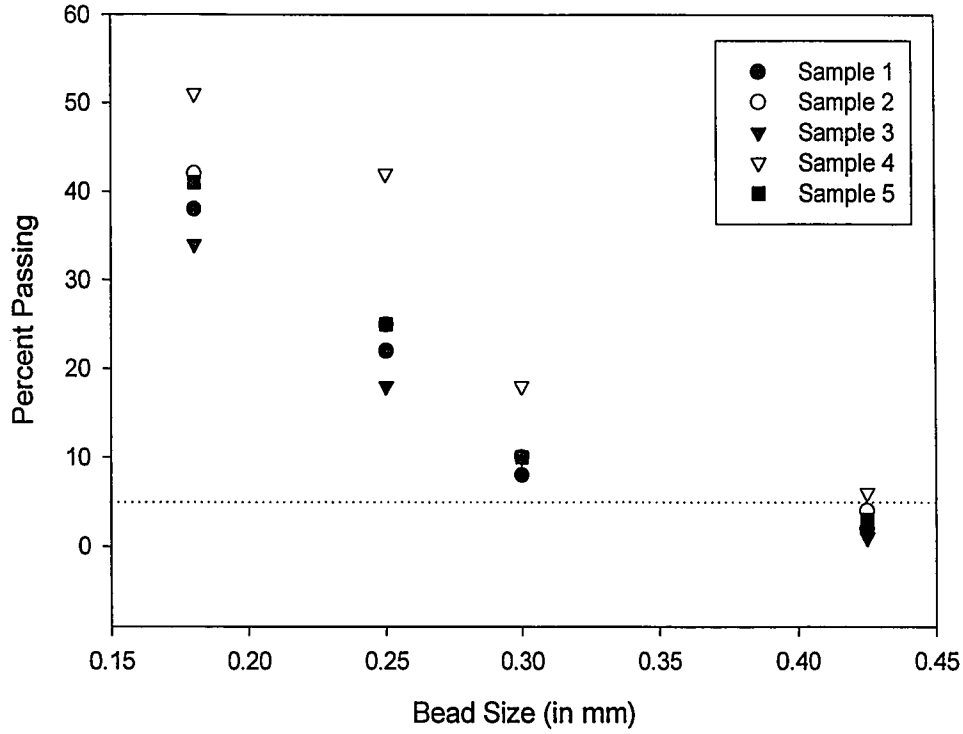

Figure E.1 Apparent Opening Size Plot for A at 0% Strain

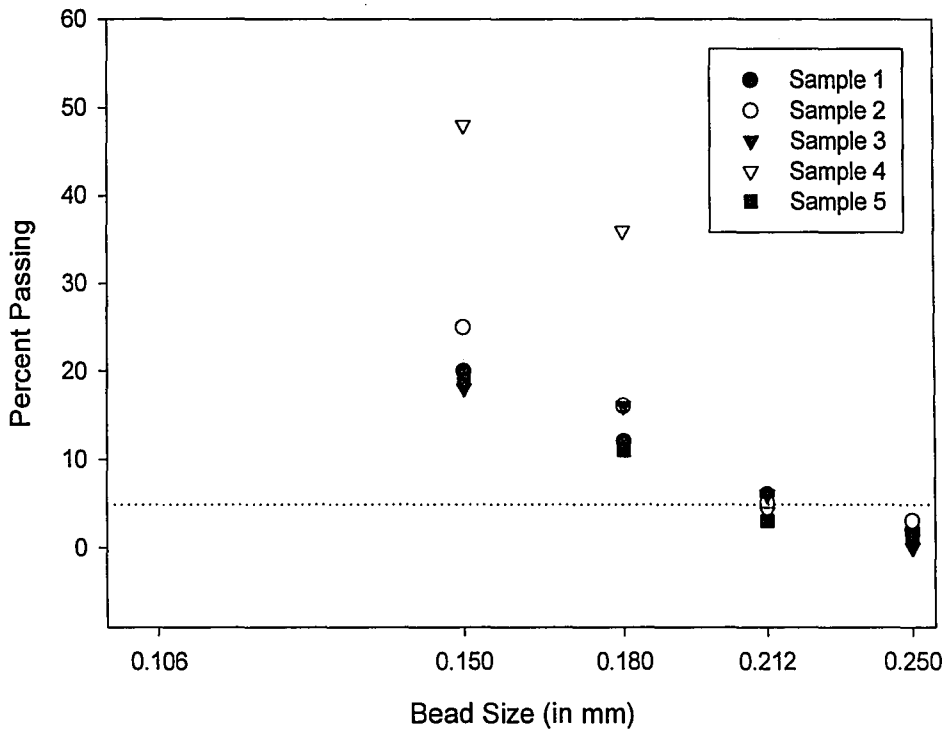

Figure E.2 Apparent Opening Size Plot for A at 3% Strain

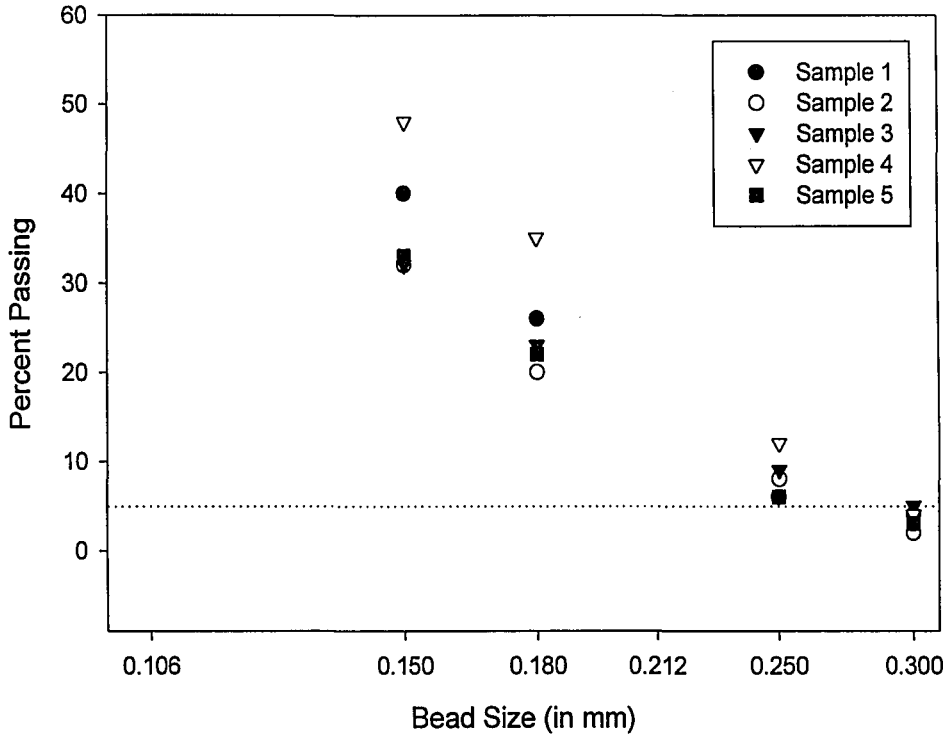

Figure E.3 Apparent Opening Size Plot for A at 6% Strain

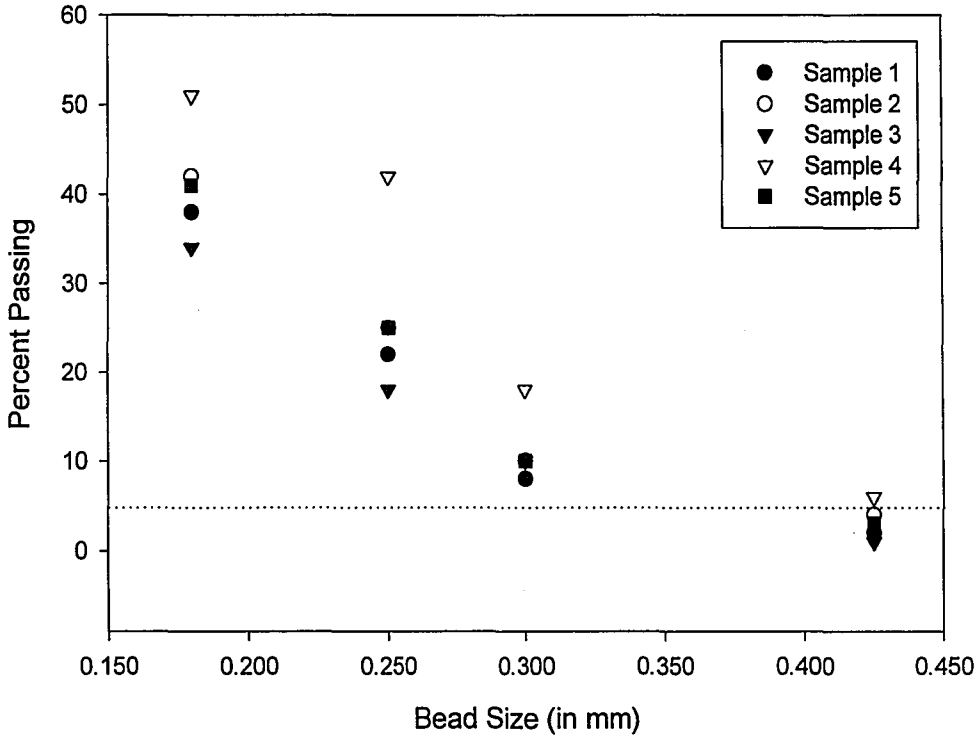

Figure E.4 Apparent Opening Size Plot for A at 9% Strain

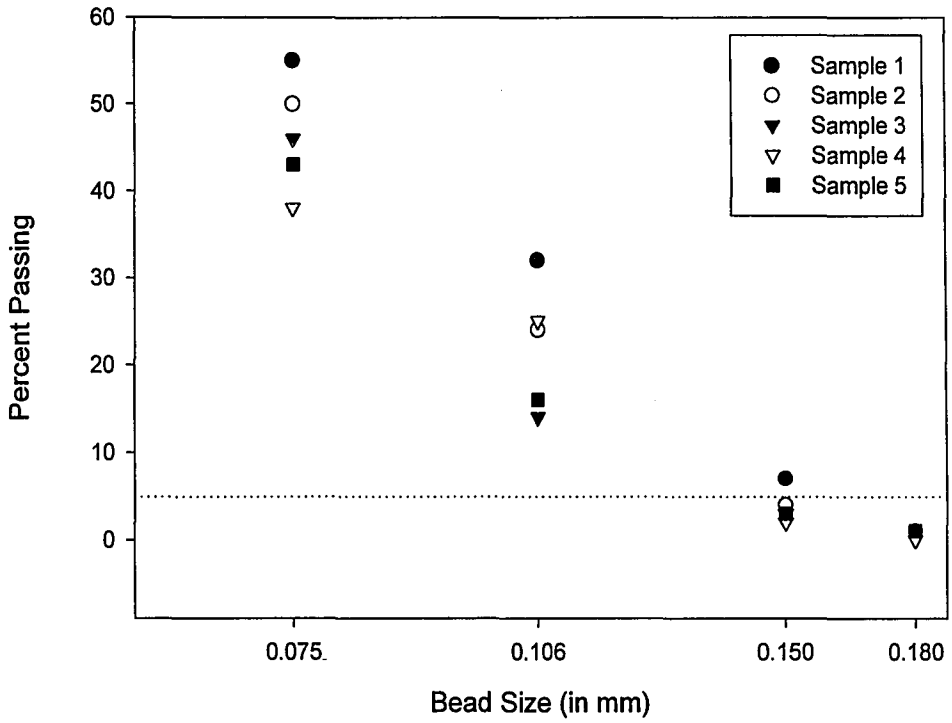

Figure E.5 Apparent Opening Size Plot for B at 0% Strain

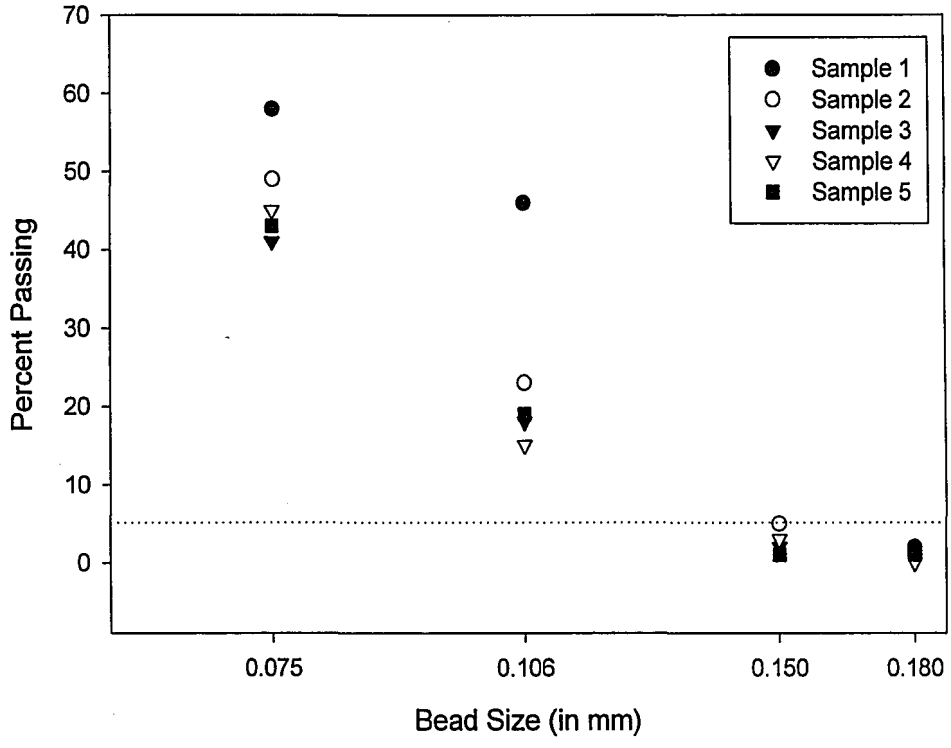

Figure E.6 Apparent Opening Size Plot for B at 3% Strain

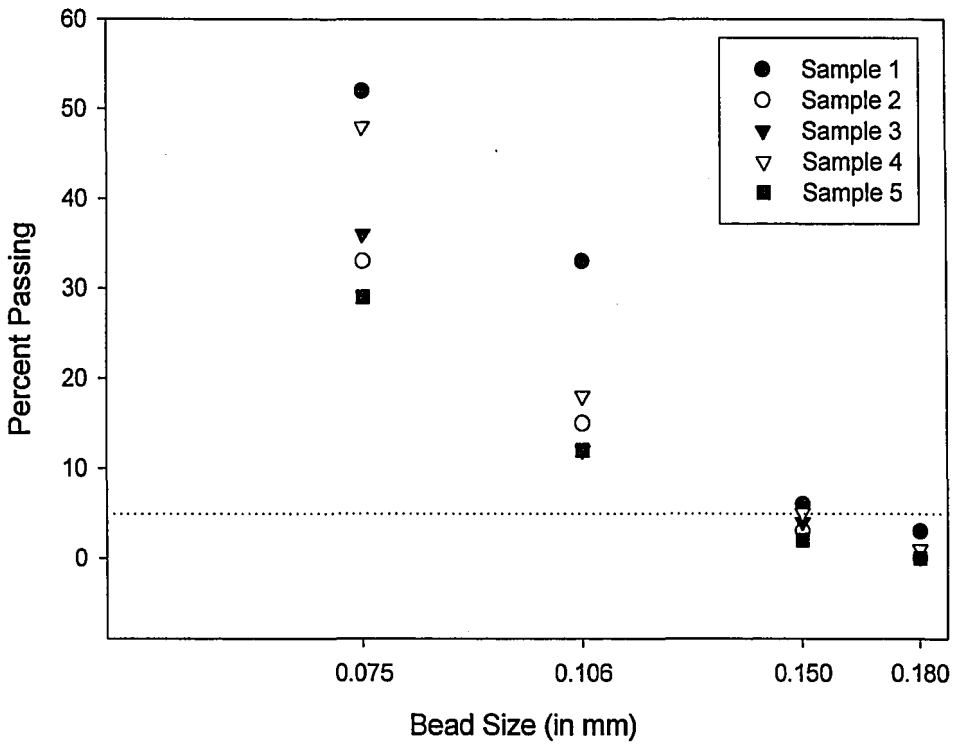

Figure E.7 Apparent Opening Size Plot for B at 6% Strain

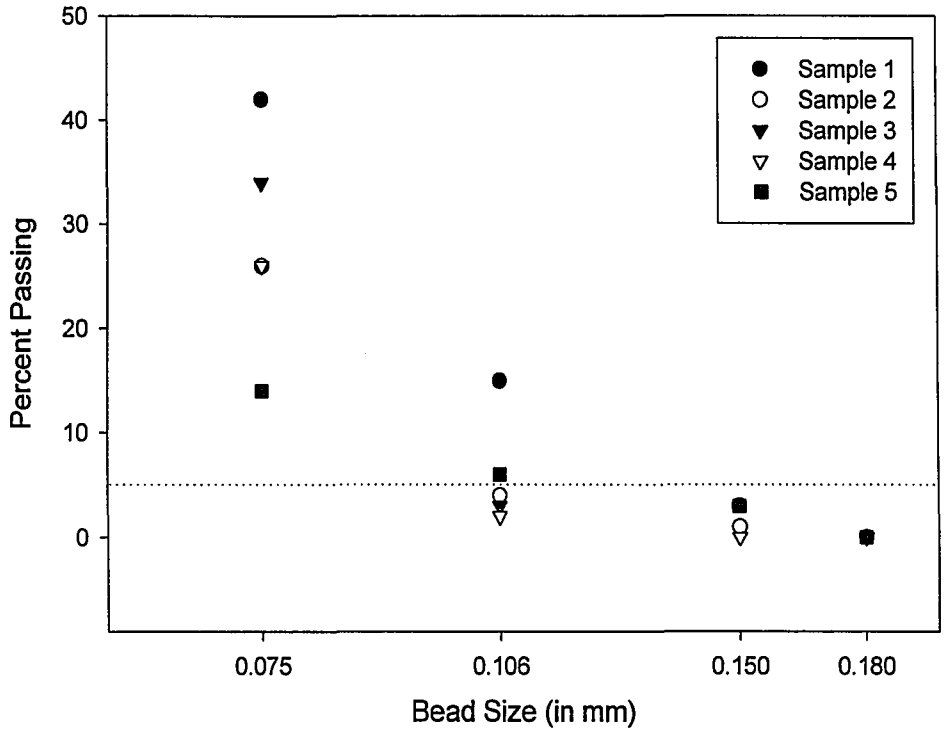

Figure E.8 Apparent Opening Size Plot for B at 9% Strain

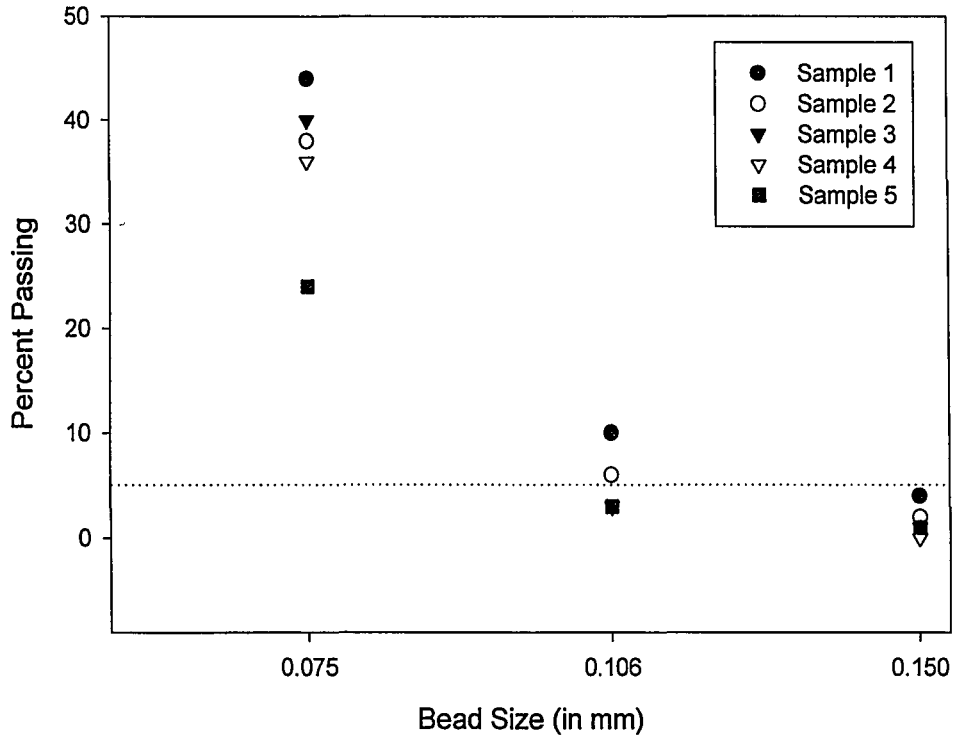

Figure E.9 Apparent Opening Size Plot for C at 0% Strain

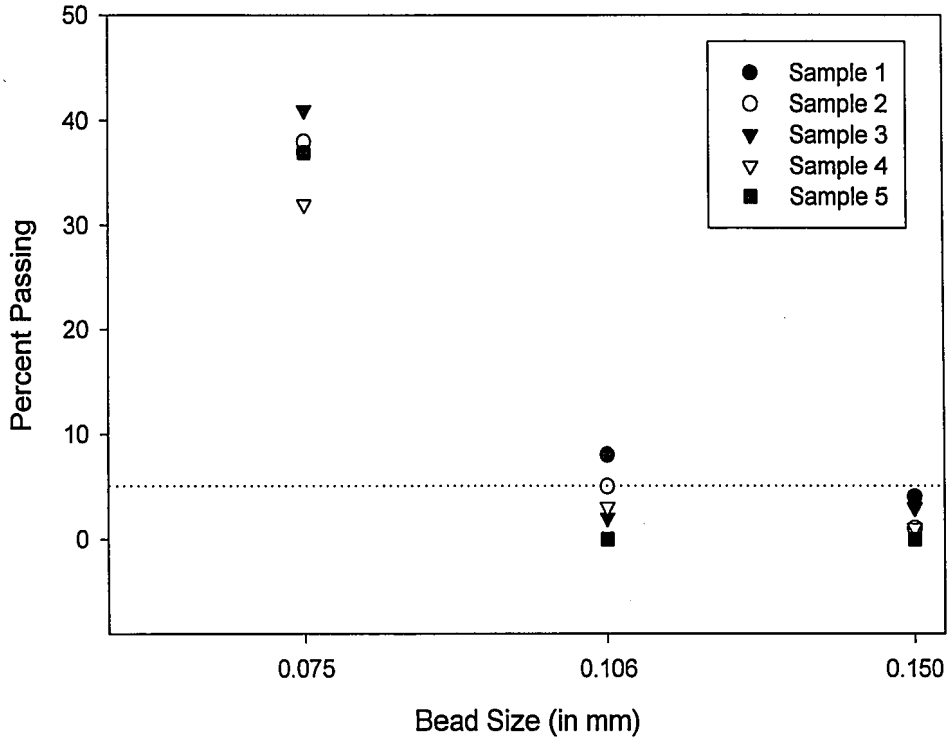

Figure E.10 Apparent Opening Size Plot for C at 3% Strain

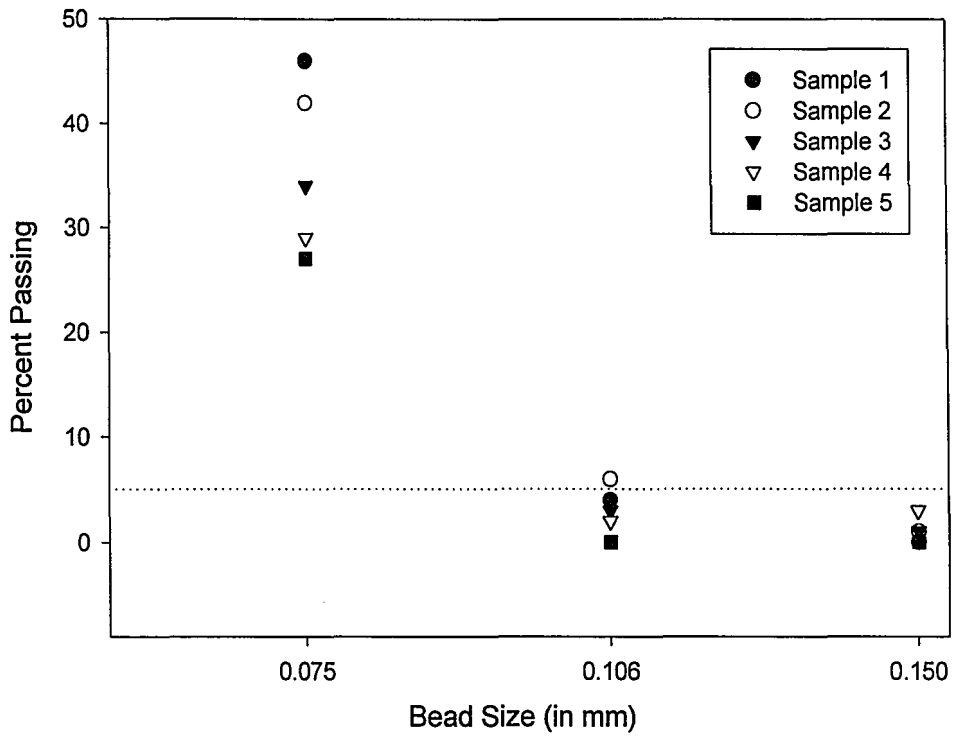

Figure E.11 Apparent Opening Size Plot for C at 6% Strain

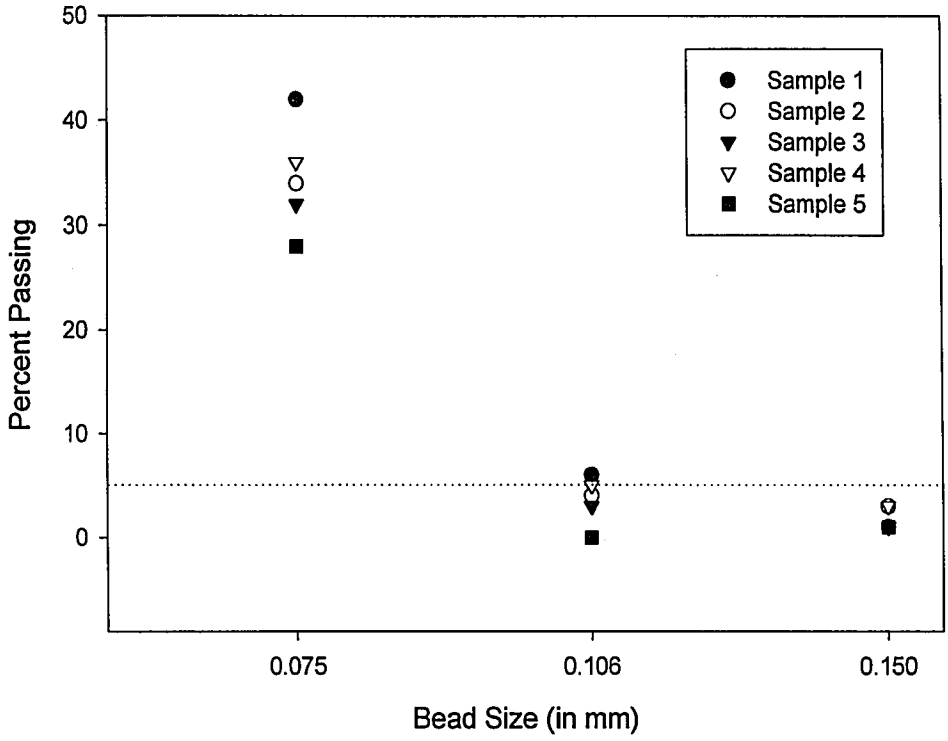

Figure E.12 Apparent Opening Size Plot for C at 9% Strain

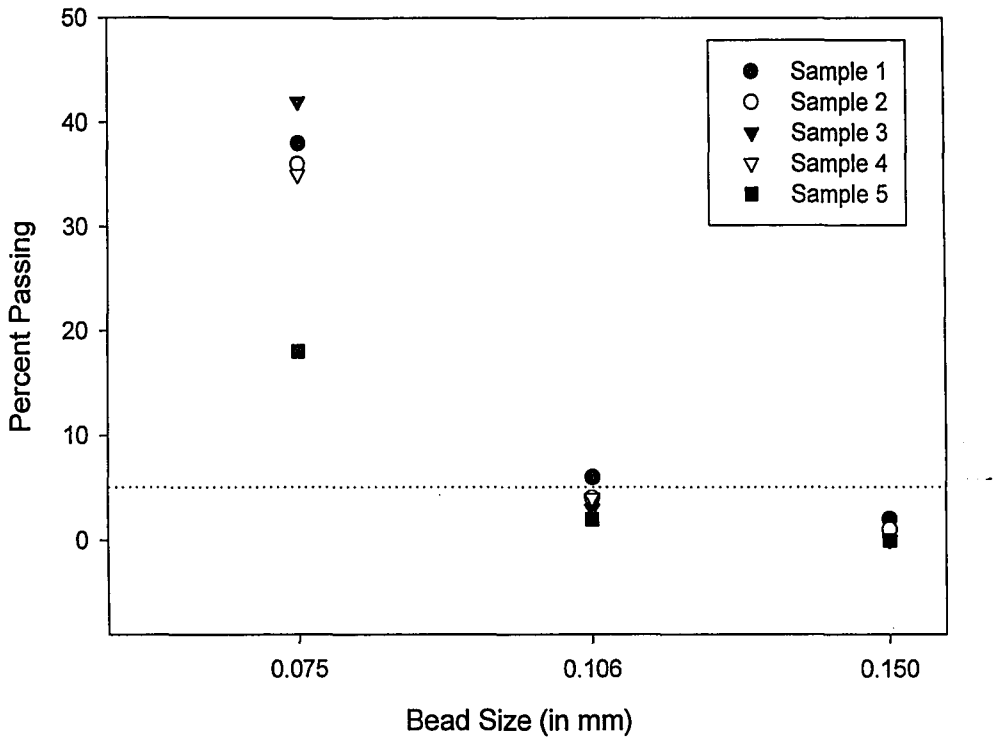

Figure E.13 Apparent Opening Size Plot for D at 0% Strain

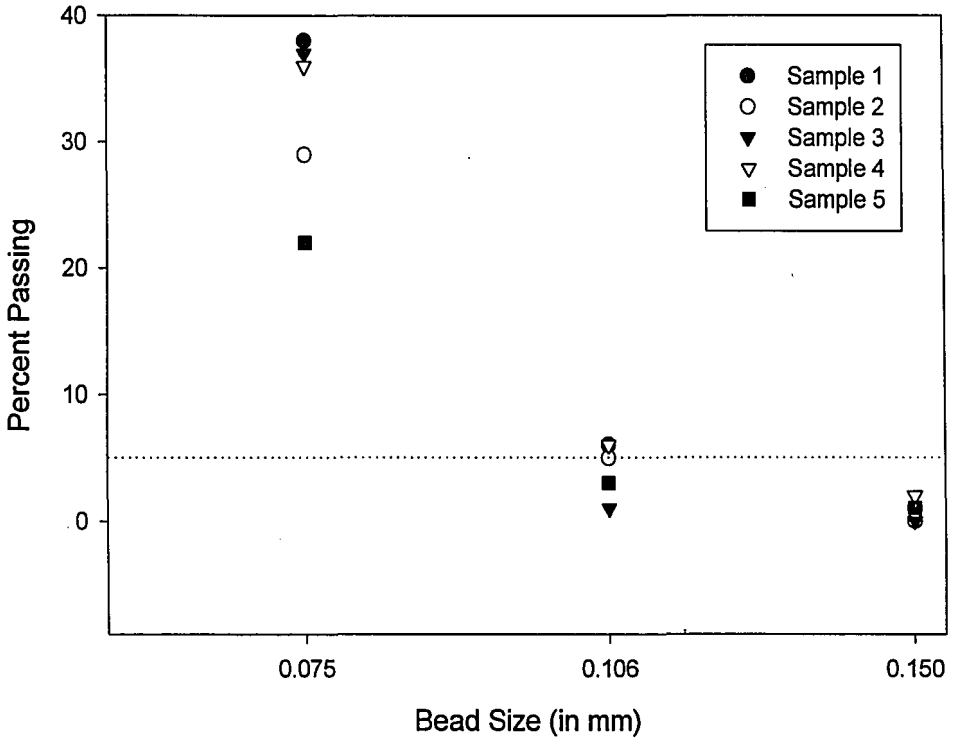

Figure E.14 Apparent Opening Size Plot for D at 3% Strain

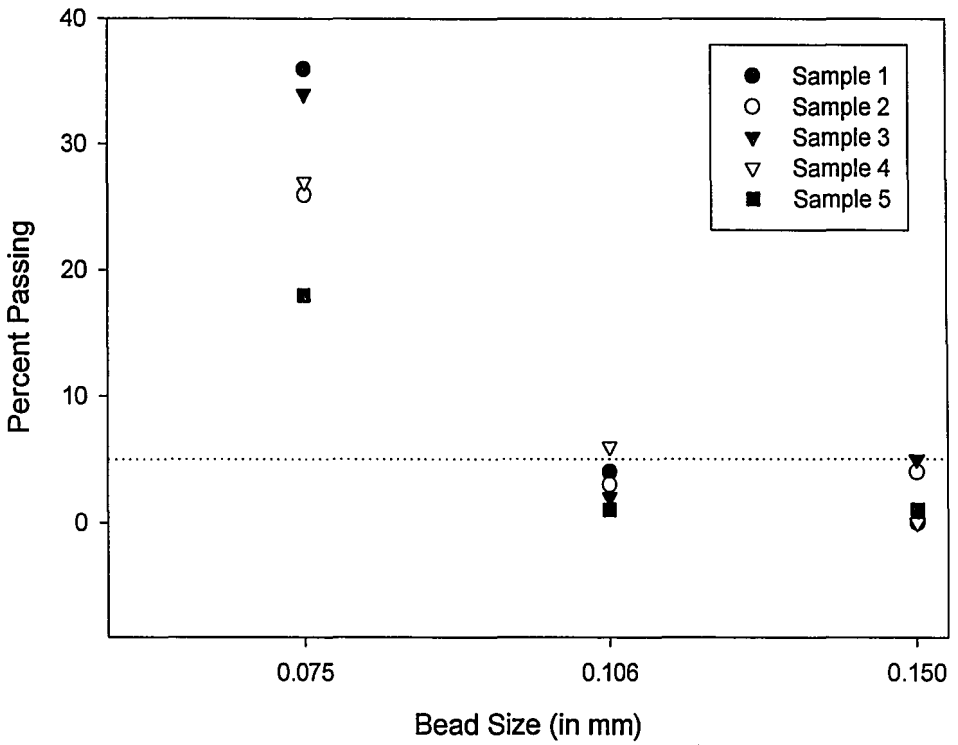

Figure E.15 Apparent Opening Size Plot for D at 6% Strain

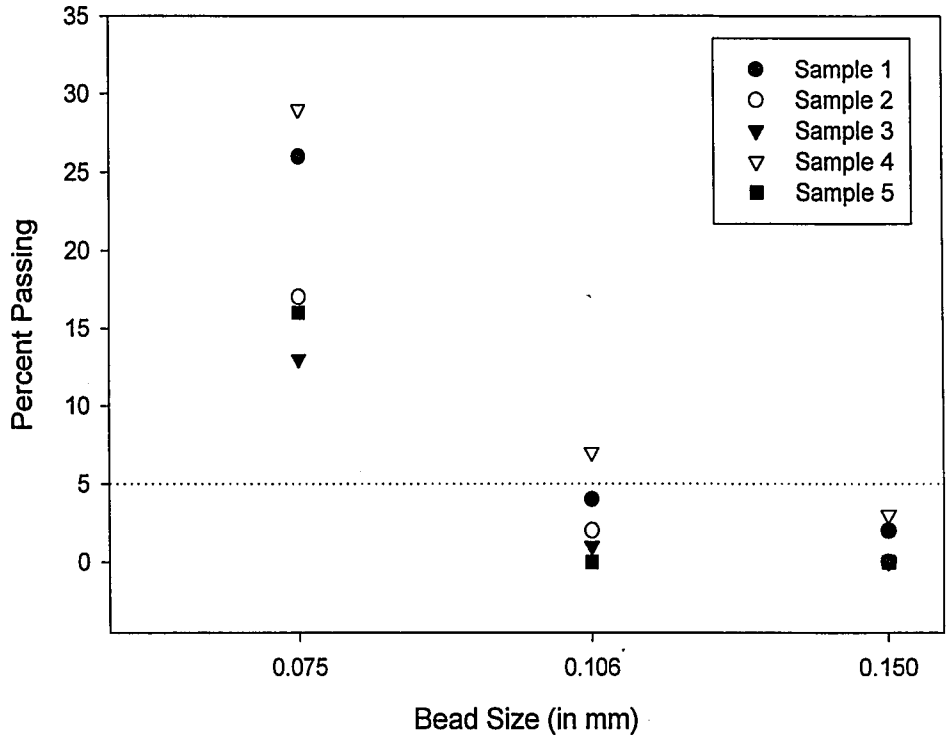

Figure E.16 Apparent Opening Size Plot for D at 9% Strain

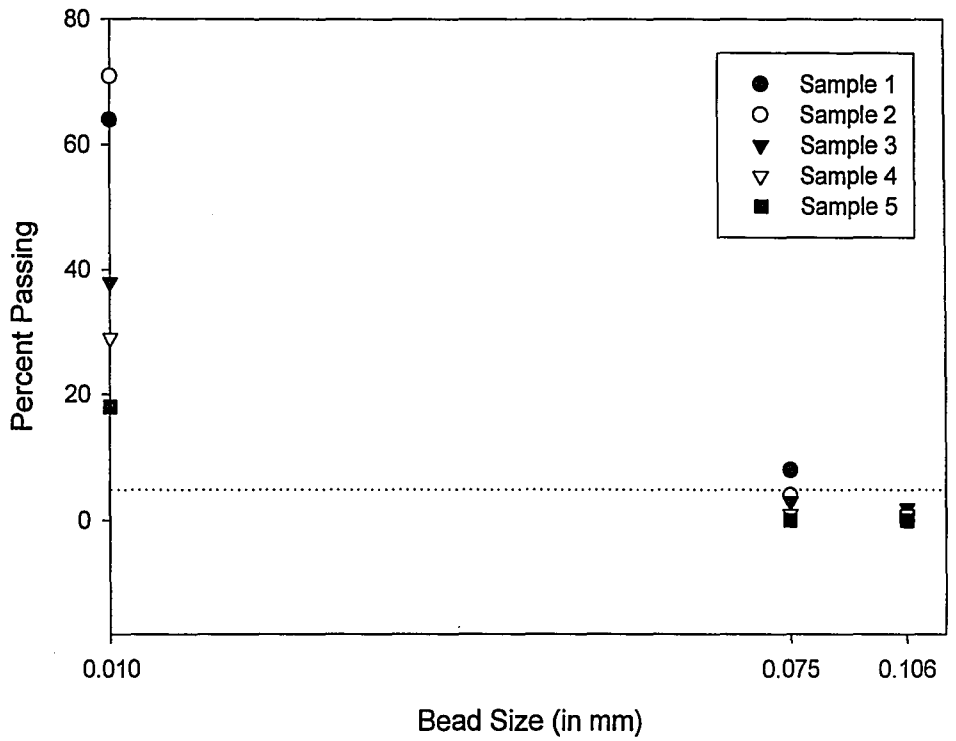

Figure E.17 Apparent Opening Size Plot for E at 0% Strain

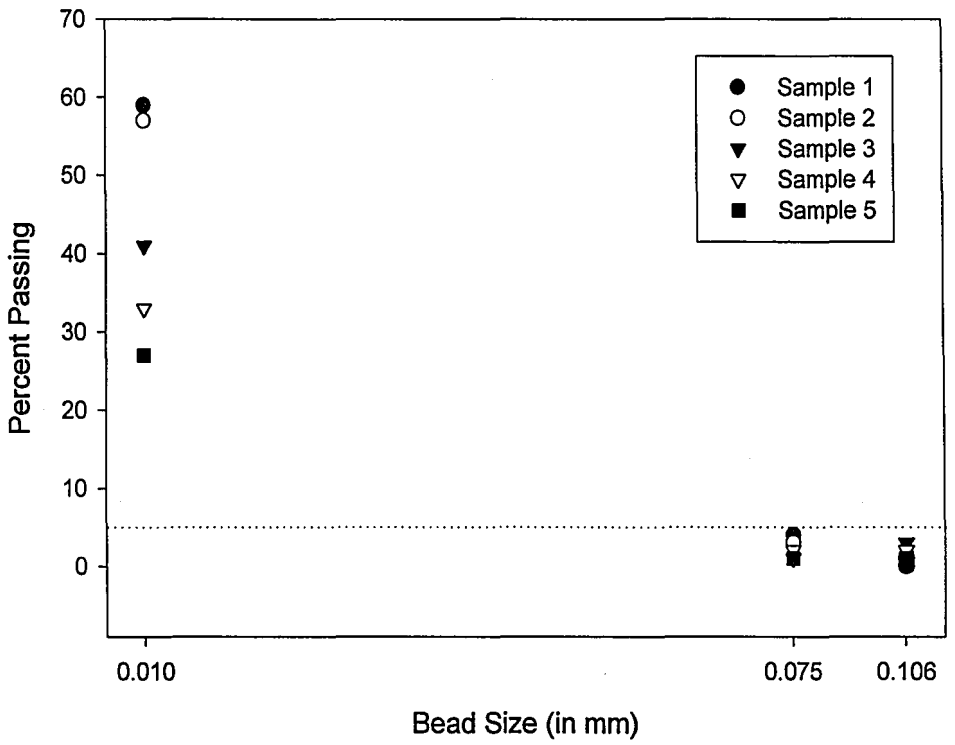

Figure E.18 Apparent Opening Size Plot for E at 3% Strain

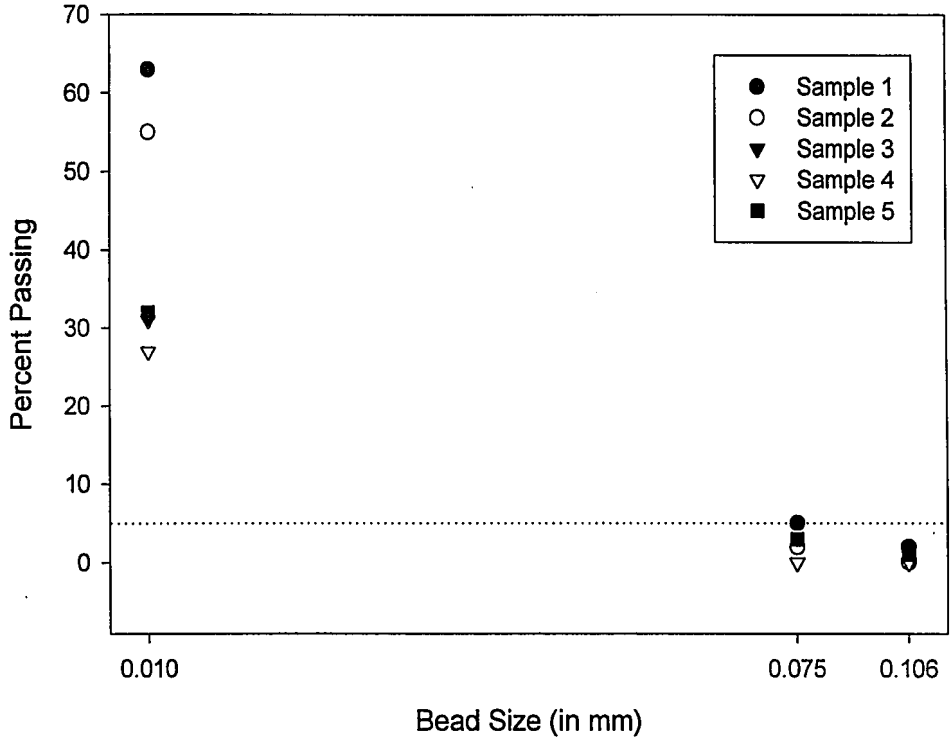

Figure E.19 Apparent Opening Size Plot for E at 6% Strain

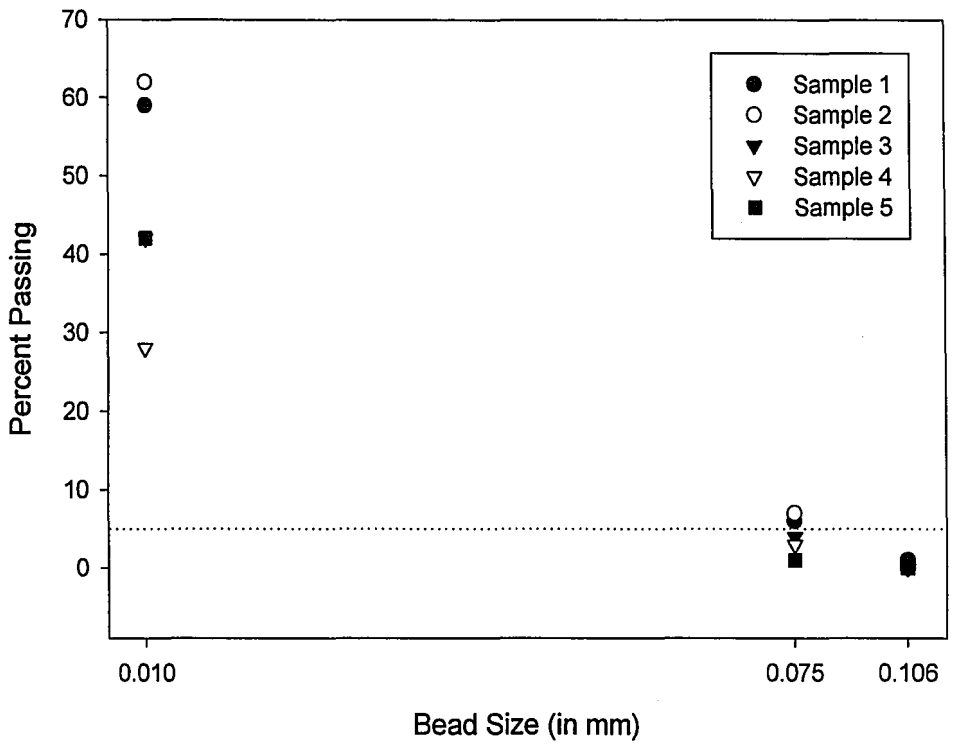

Figure E.20 Apparent Opening Size Plot for E at 9% Strain

APPENDIX F. Filtration Tests under Strain.

Table F.1 Filtration Tests at 10 psi (69 kPA) and 0% Strain

Sample Number	Initial Water Content (%)	Final Water Content (%)	Initial TS (mg/l)	Filtrate TSS (mg/l)	Filtering Efficiency (%)
A					
1	203.5	111.4	491390.9	213.5	99.957
2	203.5	120.6	491390.9	165.4	99.966
3	203.5	113.5	49130.9	198.7	99.596
A + B					
1	201.6	116.3	496031.7	118.3	99.976
2	201.6	111.2	496031.7	116.2	99.977
3	201.6	117.6	496031.7	119.2	99.976
A + C					
1	202.2	108.6	494559.8	63.5	99.987
2	202.2	112.6	494559.8	64.2	99.987
3	202.2	131.2	494559.8	46.8	99.991
A + D					
1	180.5	118.4	554016.6	30.4	99.995
2	180.5	114.2	554016.6	42.5	99.992
3	180.5	126.3	554016.6	26.8	99.995
A + E					
1	182.3	134.2	548546.4	38.5	99.993
2	182.3	119.5	548546.4	29.8	99.995
3	182.3	117.0	548546.4	39.6	99.993

Table F.2 Filtration Tests at 10 psi (69 kPA) and 3% Strain

Sample Number	Initial Water Content (%)	Final Water Content (%)	Initial TS (mg/l)	Filtrate TSS (mg/l)	Filtering Efficiency (%)
A					
1	186.5	135.6	536193.0	202.5	99.962
2	186.5	114.7	536193.0	224.6	99.958
3	186.5	135.8	536193.0	199.3	99.963
A + B					
1	203.6	118.5	491159.1	120.5	99.975
2	203.6	115.2	491159.1	121.5	99.975
3	203.6	111.5	491159.1	119.3	99.976
A + C					
1	196.8	113.5	508130.1	68.2	99.987
2	196.8	132.1	508130.1	66.4	99.987
3	196.8	118.0	508130.1	59.3	99.988
A + D					
1	194.6	115.8	513874.6	44.6	99.991
2	194.6	116.2	513874.6	48.2	99.991
3	194.6	113.5	513874.6	34.1	99.993
A + E					
1	201.4	121.0	496524.3	40.5	99.992
2	201.4	116.4	496524.3	42.8	99.991
3	201.4	118.3	496524.3	32.7	99.993

Table F.3 Filtration Tests at 10 psi (69 kPA) and 6% Strain

Sample Number	Initial Water Content (%)	Final Water Content (%)	Initial TS (mg/l)	Filtrate TSS (mg/l)	Filtering Efficiency (%)
A					
1	196.4	118.2	509165.0	228.6	99.955
2	196.4	116.7	509165.0	230.5	99.955
3	196.4	121.6	509165.0	194.6	99.962
A + B					
1	208.2	114.5	480307.4	130.2	99.973
2	208.2	115.9	480307.4	118.6	99.975
3	208.2	134.2	480307.4	140.3	99.971
A + C					
1	203.6	128.6	491159.1	75.8	99.985
2	203.6	119.9	491159.1	72.6	99.985
3	203.6	114.0	491159.1	82.4	99.983
A + D					
1	214.8	123.8	465549.3	55.6	99.988
2	214.8	130.8	465549.3	43.8	99.991
3	214.8	156.2	465549.3	62.1	99.987
A + E					
1	210.5	109.5	475059.4	54.2	99.989
2	210.5	118.7	475059.4	42.5	99.991
3	210.5	124.9	475059.4	35.4	99.993

Table F.4 Filtration Tests at 10 psi (69 kPA) and 9% Strain

Sample Number	Initial Water Content (%)	Final Water Content (%)	Initial TS (mg/l)	Filtrate TSS (mg/l)	Filtering Efficiency (%)
A					
1	210.2	133.4	475737.4	226.8	99.952
2	210.2	126.8	475737.4	240.5	99.949
3	210.2	134.8	475737.4	254.6	99.946
A + B					
1	206.0	126.8	485436.9	142.5	99.971
2	206.0	120.4	485436.9	125.6	99.974
3	206.0	116.4	485436.9	128.3	99.974
A + C					
1	187.6	128.7	533049.0	76.2	99.986
2	187.6	131.5	533049.0	83.4	99.984
3	187.6	126.4	533049.0	79.7	99.985
A + D					
1	183.2	110.5	545851.5	34.6	99.994
2	183.2	126.6	545851.5	32.8	99.994
3	183.2	135.4	545851.5	41.3	99.992
A + E					
1	198.6	118.7	503524.7	25.6	99.995
2	198.6	111.1	503524.7	34.5	99.993
3	198.6	132.0	503524.7	23.8	99.995

Table F.5 Filtration Tests at 20 psi (138 kPA) and 0% Strain

Sample Number	Initial Water Content (%)	Final Water Content (%)	Initial TS (mg/l)	Filtrate TSS (mg/l)	Filtering Efficiency (%)
A					
1	198.6	110.9	503524.7	256.8	99.949
2	198.6	109.6	503524.7	268.4	99.947
3	198.6	112.5	503524.7	222.1	99.956
A + B					
1	212.1	115.7	471475.7	132.5	99.972
2	212.1	132.1	471475.7	128.9	99.973
3	212.1	126.4	471475.7	139.6	99.970
A + C					
1	208.4	115.4	479846.4	82.6	99.983
2	208.4	111.6	479846.4	81.9	99.983
3	208.4	121.0	479846.4	64.7	99.987
A + D					
1	206.5	101.3	484261.5	36.4	99.992
2	206.5	121.8	484261.5	48.7	99.990
3	206.5	116.5	484261.5	32.5	99.993
A + E					
1	199.3	110.5	501756.1	43.5	99.991
2	199.3	112.8	501756.1	32.1	99.994
3	199.3	106.4	501756.1	36.7	99.993

Table F.6 Filtration Tests at 20 psi (138 kPA) and 3% Strain

Sample Number	Initial Water Content (%)	Final Water Content (%)	Initial TS (mg/l)	Filtrate TSS (mg/l)	Filtering Efficiency (%)
A					
1	211.3	118.6	473260.8	279.5	99.941
2	211.3	121.2	473260.8	296.3	99.937
3	211.3	116.4	473260.8	234.8	99.950
A + B					
1	215.6	121.3	463821.9	141.6	99.969
2	215.6	128.7	463821.9	125.8	99.973
3	215.6	134.2	463821.9	135.7	99.971
A + C					
1	209.7	113.3	476871.7	82.7	99.983
2	209.7	112.7	476871.7	79.5	99.983
3	209.7	106.5	476871.7	86.3	99.982
A + D					
1	199.6	108.7	501002.0	42.5	99.992
2	199.6	131.2	501002.0	33.6	99.993
3	199.6	121.3	501002.0	25.4	99.995
A + E					
1	197.5	121.1	506329.1	18.3	99.996
2	197.5	118.1	506329.1	42.2	99.992
3	197.5	102.6	506329.1	34.6	99.993

Table F.7 Filtration Tests at 20 psi (138 kPA) and 6% Strain

Sample Number	Initial Water Content (%)	Final Water Content (%)	Initial TS (mg/l)	Filtrate TSS (mg/l)	Filtering Efficiency (%)
A					
1	186.7	110.2	535618.6	302.1	99.944
2	186.7	106.7	535618.6	296.8	99.945
3	186.7	99.5	535618.6	287.2	99.946
A + B					
1	179.3	110.8	557724.5	155.2	99.972
2	179.3	121.6	557724.5	132.1	99.976
3	179.3	111.8	557724.5	125.6	99.977
A + C					
1	211.1	115.3	473709.1	65.8	99.986
2	211.1	117.7	473709.1	92.2	99.981
3	211.1	99.6	473709.1	75.2	99.984
A + D					
1	206.3	111.1	484731.0	32.2	99.993
2	206.3	120.0	484731.0	21.8	99.996
3	206.3	131.1	484731.0	18.5	99.996
A + E					
1	209.5	116.2	477327.0	13.2	99.997
2	209.5	144.2	477327.0	10.8	99.998
3	209.5	106.3	477327.0	26.7	99.994

Table F.8 Filtration Tests at 20 psi (138 kPA) and 9% Strain

Sample Number	Initial Water Content (%)	Final Water Content (%)	Initial TS (mg/l)	Filtrate TSS (mg/l)	Filtering Efficiency (%)
A					
1	198.2	106.2	504540.9	299.7	99.941
2	198.2	110.2	504540.9	321.0	99.936
3	198.2	121.8	504540.9	301.5	99.940
A + B					
1	208.9	114.3	4786997.9	162.2	99.966
2	208.9	118.6	4786997.9	146.5	99.969
3	208.9	106.2	4786997.9	171.3	99.964
A + C					
1	211.5	97.2	472813.2	89.2	99.981
2	211.5	110.5	472813.2	93.2	99.980
3	211.5	111.1	472813.2	62.5	99.987
A + D					
1	214.6	121.5	465983.2	54.2	99.988
2	214.6	108.7	465983.2	43.2	99.991
3	214.6	114.5	465983.2	38.8	99.992
A + E					
1	193.9	111.5	515729.8	62.2	99.988
2	193.9	116.3	515729.8	71.4	99.986
3	193.9	117.1	515729.8	78.7	99.985

VITA

Charles Ochola was born on December 30th, 1969 to Selina and Harrison Ochola. He has four brothers Isaac, Donald, Edward, Peter, and one sister Ruth.

He received his Bachelor of Science in Physics from East Stroudsburg University in 1994. In September 1995 he enrolled at Lehigh University where he completed his Master of Science in Civil and Environmental Engineering in June 1997.

Charles is currently pursuing his Ph.D. in Geo-environmental Engineering at Lehigh University.

END

OF

TITLE